UNIVERSITÀ DEGLI STUDI DI SIENA

Scuola di Dottorato in Scienze della Terra - Preistoria

Sezione di Scienze della Terra

Ciclo XXIV

Mineralogy of sediments from AND-2A drill core (McMurdo Sound, Antarctica)

Tesi di dottorato di
Francesco Iacoviello

Tutore
Prof.ssa Isabella Turbanti Memmi
Dipartimento di Scienze della Terra
Università degli Studi di Siena

Co-tutore
Dr.ssa Giovanna Giorgetti
Dipartimento di Scienze della Terra
Università degli Studi di Siena

ANNO 2012

"The scientific man does not aim at an immediate result. He does not expect that his advanced ideas will be readily taken up. His work is like that of the planter — for the future. His duty is to lay the foundation for those who are to come, and point the way. He lives and labors and hopes."

"L'uomo di scienza non mira ad un risultato immediato. Egli non si aspetta che le sue idee avanzate verranno assimilate rapidamente. Il suo lavoro è come quello di un piantatore — per il futuro. Il suo compito è quello di porre le basi per coloro che verranno, e di indicare il cammino. Egli vive e lavora e spera."

Nikola Tesla

Abstract

The present study deals with a combined clay-heavy mineral analysis of marine sediments recovered in 2007 in the McMurdo Sound region (Ross Sea, Antarctica) during the ANtarctic DRILLing Program (ANDRILL) - Southern McMurdo Sound Project. The main objectives are to: 1) study how clay minerals reflect paleoclimatic conditions, in particular the Mid-Miocene Climatic Optimum, 2) investigate how heavy mineral assemblages reflect different source rocks and hence different provenance areas 3) study the ice sheet development in East-Antarctica in the last 20 Ma.

The AND-2A drill core recovered several stratigraphic intervals that span from Early Miocene to Pleistocene and it collected a variety of terrigenous clastic lithologies. The clay mineral assemblages of the 1138,54 m thick sedimentary succession have been analyzed through X-Ray Diffraction (XRD) analyses on clay fraction, Field Emission Scanning Electron Microscopy (FESEM), Scanning Electron Microscopy (SEM) observations and SEM-EDS microanalyses on smectite particles. SEM observations and SEM-EDS microanalyses were carried out on heavy mineral samples starting from 650 mbsf. In the upper sedimentary sections (36 - 440 mbsf, 0.7 - 16.5 Ma) smectites are interpreted to be predominantly detrital, whereas in the lower portion of the core (440 -1123.20 mbsf, 18.5 - 20.2 Ma) authigenic smectites are the most common feature. The predominance of illite**,** the abundance of chlorite and the nature of smectites in the upper part of the core indicate physical weathering under cold and dry climate and dominant provenance for the clay minerals from the Transantarctic Mountains. Smectites in the lower section are considered mostly authigenic and they are probably the result of early diagenetic processes being formed from the alteration of volcanic material and/or through precipitation from fluids of a possible hydrothermal origin. The heavy mineral analysis shows that the sediments are a

mix of detritus dominated by McMurdo Volcanic Group (MVG) sources most likely located in the present-day Mount Morning area (Proto-Mount Morning) with minor contribution from Transantarctic Mountains (TAM) rocks located west of the drill site. The clay and heavy mineral records of the lower 650 mbsf indicate that an ice sheet similar in size to modern ice sheet was periodically present between 17.6 and 19.3 Ma and between 20.1 and 20.2 Ma.

The clay and heavy mineral records of AND-2A drill core have increased our understanding of the timing and spatial distribution of ice sheet growth and decay in the McMurdo Sound region during Early Miocene (15.9 - 20.2 Ma) and the Miocene Climate Optimum (ca. 15 - 17 Ma). The present study has demonstrated that the occurrence of authigenic clay minerals may conduct to incorrect paleoclimatic interpretations. Therefore, detailed clay mineral analyses, possibly integrated with heavy mineral study, are necessary for reconstructing sediment provenance and consequently ice-sheet dynamics.

Riassunto

Il presente studio riguarda un'analisi combinata dei minerali argillosi e pesanti dei sedimenti marini recuperati nel 2007 nella regione del McMurdo Sound (Mare di Ross, Antartide) durante il progetto ANtarctic DRILLing Program (ANDRILL) - Southern McMurdo Sound. I principali obbiettivi sono quelli di: 1) studiare come i minerali argillosi riflettono le condizioni paleoclimatiche; 2) investigare come le associazioni di minerali pesanti riflettono le differenti rocce sorgenti e quindi le diverse aree di provenienza; 3)

studiare il comportamento della calotta glaciale nell'Antartide Orientale durante gli ultimi 20 milioni di anni. La perforazione AND-2A ha recuperato numerosi intervalli stratigrafici che spaziano dal Miocene medio al Pleistocene e ha collezionato una varietà di litologie terrigene clastiche. Le associazioni di minerali argillosi della successione sedimentaria spessa 1138,54 m sono state analizzate mediante diffrattometria a raggi X (XRD) sulla frazione argillosa, attraverso osservazioni in microscopia elettronica a scansione ad emissione di campo (FESEM) e microscopia elettronica a scansione (SEM) e microanalisi SEM-EDS sulle particelle di smectite. Delle osservazioni al SEM e microanalisi SEM-EDS sono state effettuate sui minerali pesanti a partire da 650 m di profondità. Nelle sezioni sedimentarie superiori (36 - 440 mbsf, 0.7 - 16.5 Ma) le smectiti sono interpretate come prevalentemente detritiche, mentre nella porzione inferiore della perforazione (440 - 1123.20 mbsf, 18.5 - 20.2 Ma) le smectiti autigene sono la caratteristica più comune. La predominanza dell'illite, l'abbondanza della clorite e la natura delle smectiti nella parte superiore della perforazione indicano un'alterazione di carattere fisico in climi freddi e asciutti e la provenienza dominante dei minerali argillosi dalle Montagne Transantartiche. Le smectiti nella sezione inferiore sono considerate principalmente autigene e sono verosimilmente il risultato di processi di diagenesi precoce essendosi formate dall'alterazione di materiale vulcanico e/o attraverso la precipitazione da fluidi di possibile origine idrotermale. L'analisi dei minerali pesanti dimostra che i sedimenti sono un insieme di detrito dominato da rocce sorgenti del McMurdo Volcanic Group (MVG) verosimilmente ubicate nell'area dell'attuale Mount Morning (Proto-Mount Morning), con un contributo inferiore dalle rocce delle Montagne Transantartiche (TAM) situate ad ovest del sito di perforazione. I record dei minerali argillosi e dei minerali pesanti degli ultimi 650 m della perforazione indicano che una calotta glaciale simile nelle dimensioni all'attuale calotta glaciale era periodicamente presente tra 17.6 e 19.3 Ma e tra 20.1 e 20.2

Ma. I record dei minerali argillosi e di quelli pesanti hanno migliorato la nostra conoscenza della distribuzione spaziale e temporale della crescita e della diminuzione della calotta glaciale nella regione del McMurdo Sound durante il Miocene Inferiore (15.9 - 20.2 Ma) e durante l'Optimum climatico miocenico (ca. 15 - 17 Ma). Il presente studio ha dimostrato che la presenza di minerali argillosi autigeni può condurre ad incorrette interpretazioni paleoclimatiche. Per questo motivo sono necessarie delle analisi dettagliate sui minerali argillosi, possibilmente integrate con uno studio dei minerali pesanti, per ricostruire la provenienza dei sedimenti e di conseguenza le dinamiche della calotta glaciale.

Contents

1. Introduction

The East Antarctic Ice Sheet (EAIS) and the West Antarctic Ice Sheet (WAIS) are important components of the global climate system because of their high albedo and influence on sea level variations, on sea ice formation and, not least, on ocean circulation. Stable isotope and sea level records suggest that the polar ice sheets represent ca. 70 meters of sea-level equivalents and that changes in ice volume have controlled global sea level throughout the past ca. 35 Ma (Zachos *et al.*, 2001; Miller *et al.*, 2005). The Middle Miocene Climate Transition has recorded a major shift in Earth's climate evolution, characterized by one of the three large Cenozoic increases in $\delta^{18}O$, resulting from a combination of global cooling and ice growth in Antarctica (Zachos *et al.*, 2001). Modeling studies conducted by DeConto & Pollard (2003) show that Antarctic ice growth is controlled by atmospheric pCO_2, and pCO_2 reached a maximum, with higher than present-day levels, in the Middle Miocene (Tripati *et al.*, 2009). Recording changes in Antarctic ice volume through these climate transitions is essential for understanding future responses to the rising pCO_2.

Multiple Miocene oxygen isotope events, named Mi1 - Mi7, have been identified by other authors and have been correlated to Antarctic glacial events (Miller *et al.*, 1991) with ice volumes periodically larger than today (Pekar & DeConto, 2006). Anyway, stable isotope records present some restrictions since they are controlled by many factors besides ice volume (e.g. water temperature and salinity). Moreover, reconstructions of sea-level variation on passive continental margins are influenced by global geodynamics and not only by regional tectonics (Bamber *et al.*, 2009).

Consequently, the comprehension and interpretation of global change records in ocean requires to know how much ice was present during different Earth history periods and in

particular where the ice was situated.

Until lately, the Early and Middle Miocene glacial record of the Antarctic continental margin was partial due to the presence of hiatuses in drill holes, probably caused by glacial erosion on the Antarctic continental shelf (Hambrey & Barrett, 1993; Barrett, 2007). The time of formation of a quasi-permanent ice sheet in East Antarctica during this time has been a subject of great debate. Some authors have proposed that the East Antarctic Ice Sheet became a stable ice sheet in the Middle Miocene (ca. 14 Ma) (Sugden & Denton, 2004), while on the other hand other authors opted for a glacial setting in which periods of warming resulted in periodic changes to more dynamic wet-based glacial conditions, with a transition to a more permanent dry-based polar ice sheet as late as ca. 3 Ma (Harwood & Webb, 1998; Rebesco *et al.*, 2006). Lewis *et al.* (2007), relying on a geomorphological study in the Dry Valleys, have suggested that wet-based glacial conditions prevailed in East Antarctica during the Miocene climatic optimum (15 - 17 Ma), followed by a transition to dry-based glacial conditions prior to 14 Ma.

During 2007 the Antarctic Geological Drilling Program (ANDRILL), drilled a 1138.54 - meters deep drill-hole (AND-2A) in southern McMurdo Sound (Ross Sea). The recovered strata range in age from Early Miocene to Pleistocene and include an expanded Lower and Middle Miocene section, not previously recovered from the Antarctic continental shelf (Passchier *et al.*, 2012). The AND-2A record allows, for the first time, to identify changes in ice extent at an ice-proximal site during a critical period in the Antarctic glacial history. The AND-2A drill-hole is located in the Northern Victoria Land basin, a portion of the West Antarctic Rift System. The primary sources for sediments supplied to the drill-site since 20 Ma are the nearby Transantarctic Mountains and the Cenozoic volcanic centers in McMurdo Sound. The mineralogy of glacial and glaciomarine sediments deposited on the Antarctic continental margin is a powerful tool to understand the subglacial and

glaciomarine processes which occur in subglacial, ice shelf, and open ocean environments. Physical weathering on continents produce peculiar mineral associations which reflect the composition of the source rocks. Clay mineral variations in Antarctic marine sediments directly indicate changes of the source areas and indirectly reflect the glacial dynamics on the continent (Ehrmann *et al*., 1992; Petschick *et al*., 1996; Ehrmann, 1998 a-b; Hillenbrand & Ehrmann, 2005; Ehrmann *et al*., 2005; Damiani *et al*., 2006; Franke & Ehrmann, 2010).

Moreover, heavy minerals are excellent source rock indicators since they are less common and more diagnostic than most light minerals. As a result, heavy mineral investigation can be successfully employed to identify different source areas and to reconstruct the ice sheets dynamics (Ehrmann & Polozek, 1999; Neumann, 2001; Damiani & Giorgetti, 2008; Giorgetti *et al.,* 2009; Hauptvogel & Passchier, 2012).

The aim of this research project is to reconstruct the ice dynamics in the Southern McMurdo Sound region (western Ross Sea) through an integrated clay and heavy mineral study of Lower Miocene-to Quaternary sediments.

Clay mineral assemblages have been analyzed throughout the core, and a detailed Scanning Electron Microscopy (SEM) and Field Emission Scanning Electron Microscopy (FESEM) survey have been necessary in order to discriminate between authigenic and detrital smectites.

In very old sedimentary sequences such as AND-2A, clay minerals can be affected by early diagenesis processes and fluid circulation and therefore especially in the lower sections of drill cores authigenic clay minerals can occur. Since only detrital minerals mirror the nature of the source areas, starting from 650 mbsf, heavy minerals have been studied in order to compare their down-core trend with clay minerals variation.

2. Core setting

During 2007, the Southern McMurdo Sound (SMS) Project recovered a 1138.54 meters long drill core (AND-2A) from thick floating sea ice platform (~ 8.5 meters thick) over approximately 350 meters of water (Fig.1). The coordinates of the drilling site are the following: 77°45.488S; 165°16.613E.

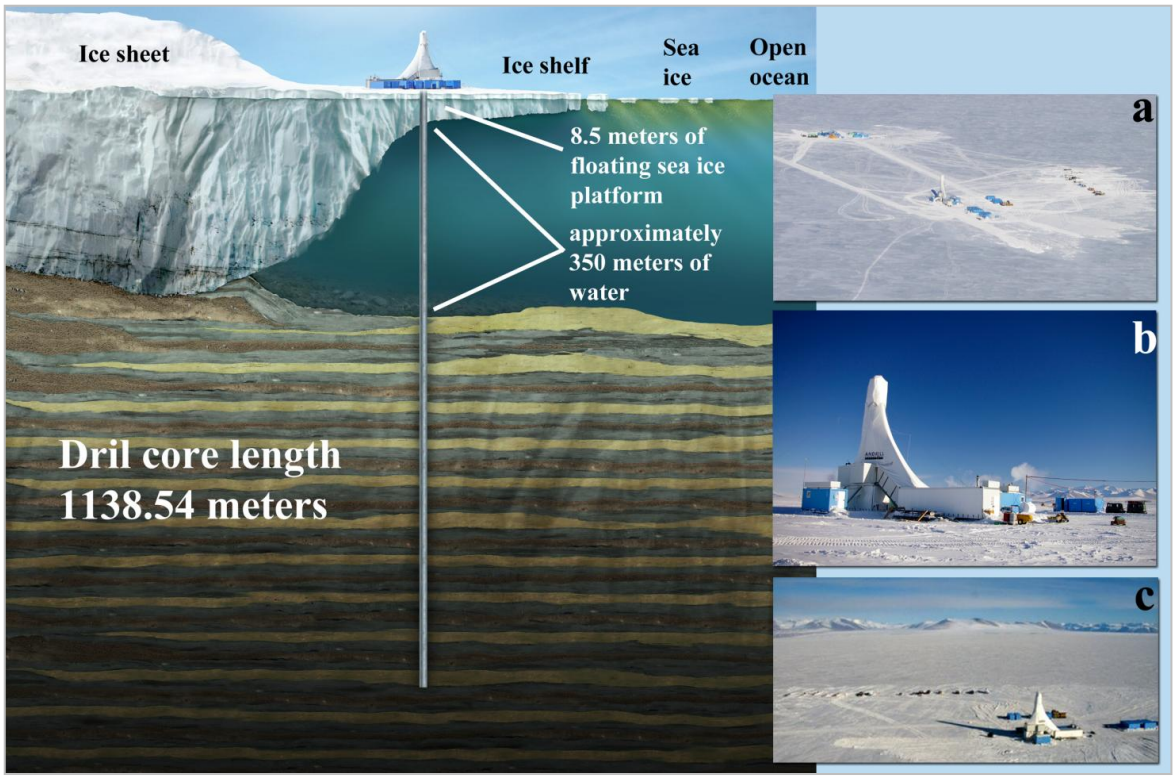

Fig.1. Schematic view of the AND-2A drill site; **a**, **b** and **c** represent different view of the drilling site.

The SMS AND-2A drill-site is located in the South-Western sector of McMurdo Sound (Fig.2), a key-area at the intersection between various components of the West Antarctic Rift System, including the Victoria Land Basin (a structural half-graben, approximately 350 km-long), the Transantarctic Mountains (TAM, a 4-km high mountain range) and

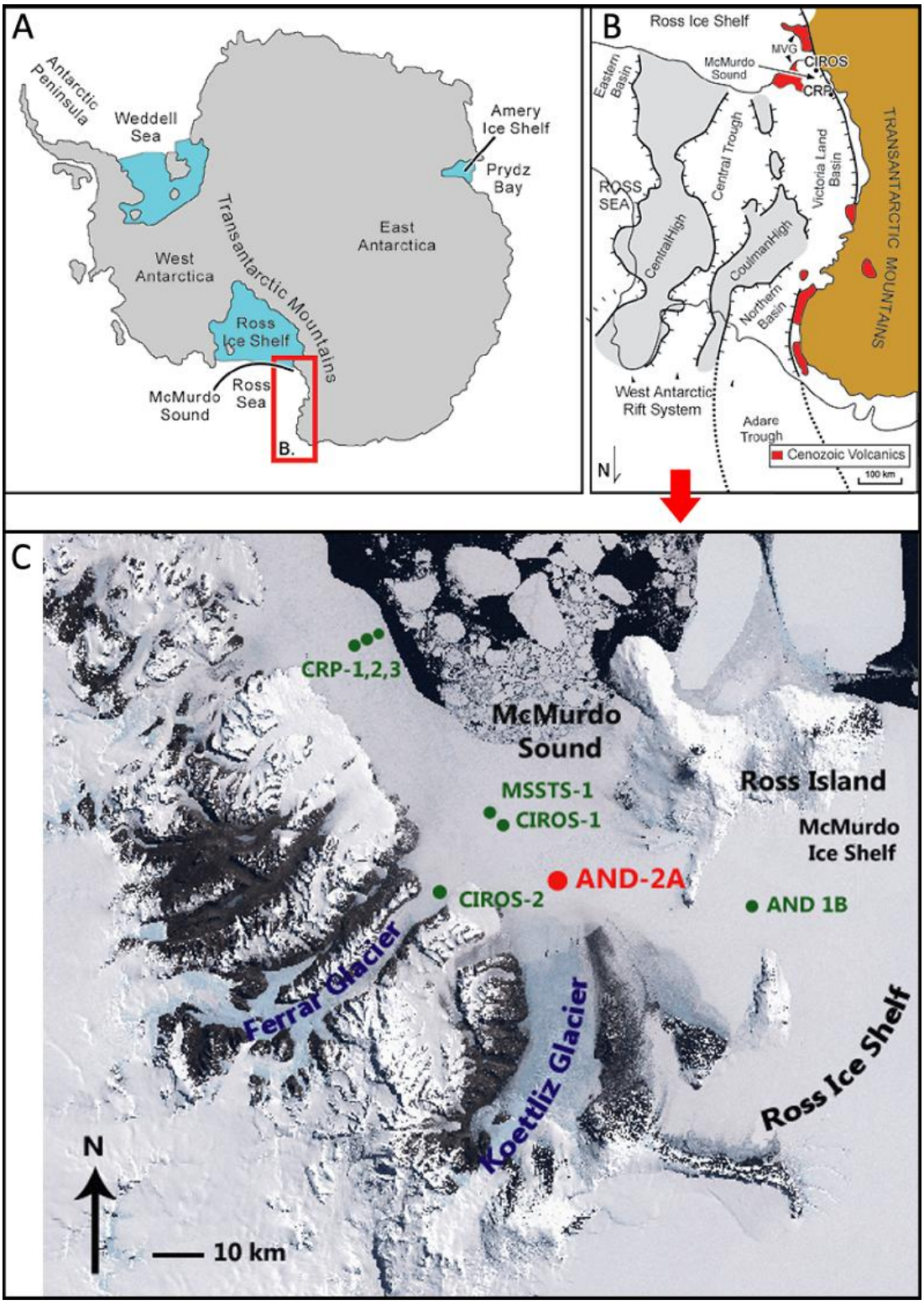

Fig. 2. A) Location of McMurdo Sound in western Ross Sea close to the north western corner of the Ross Sea Ice Shelf and the Transantarctic Mountains. B) Shows the regional tectonic setting. C) Satellite image of the McMurdo Sound, showing the location of AND-2A drill site (red dot) and previous stratigraphic drill holes (MSSTS, CIROS, CRP and AND 1-B). Landsat Image Mosaic of Antarctica (LIMA) images provided by United States Geological Survey (USGS), National Science Foundation (NSF) National Aeronautics and Space Administration (NASA) and British Antarctic Survey (BAS).

the Erebus Volcanic Province, part of the Cenozoic McMurdo Volcanic Group (Barrett, 1979; Wilson, 1999).

Furthermore, the region is influenced by three significant elements of the Antarctic cryospheric system: the East Antarctic Ice Sheet (EAIS), Ross Ice Shelf (RIS), West Antarctic Ice Sheet (WAIS), and Ross Embayment sea-ice (Fig. 2A and 2B). The subsidence associated with rifting and volcanic loading has allowed Early Cenozoic to Quaternary stratigraphic accommodation space adjacent to the rising TAM (Fielding, 2006). The combination of a high sediment supply from TAM and the accommodation space provided by rifting and subsidence of the VLB has allowed the region to help protecting the sediments from the erosive effects of glaciers that often removed other Antarctic ice-proximal records. Upper Eocene sediments are the oldest post-Paleozoic sediments recovered until today by stratigraphic drilling along the western margin of the basin as documented by the CIROS-1 drillcore (e.g., Wilson *et al*., 1998).

These Eocene strata unconformably overlie Devonian sediments of the Taylor Group (Davey *et al*., 2001). The terrigenous components of sediments recovered at the SMS Project AND-2A site are derived from either the segment of the TAM located between main outlet glaciers of the EAIS (Ferrar Glacier - Mulock Glacier regions) (Panter *et al*., 2008-2009) or several volcanic centers of the Late Neogene McMurdo Volcanic Province, which are distributed around the Southern McMurdo Sound.

The southern McMurdo Sound is bounded to the west by a sector of the TAM, and largely uplifted starting at ca. 55 Ma as a consequence of the West Antarctic Rift System evolution (Fitzgerald, 2002). On the contrary, the southern and eastern sides are characterized by the presence of extensive volcanic edifices, belonging to the Cenozoic alkalic McMurdo Volcanic Group - Erebus Volcanic Province (Gunn & Warren, 1962; Kyle, 1990; Fig. 3).

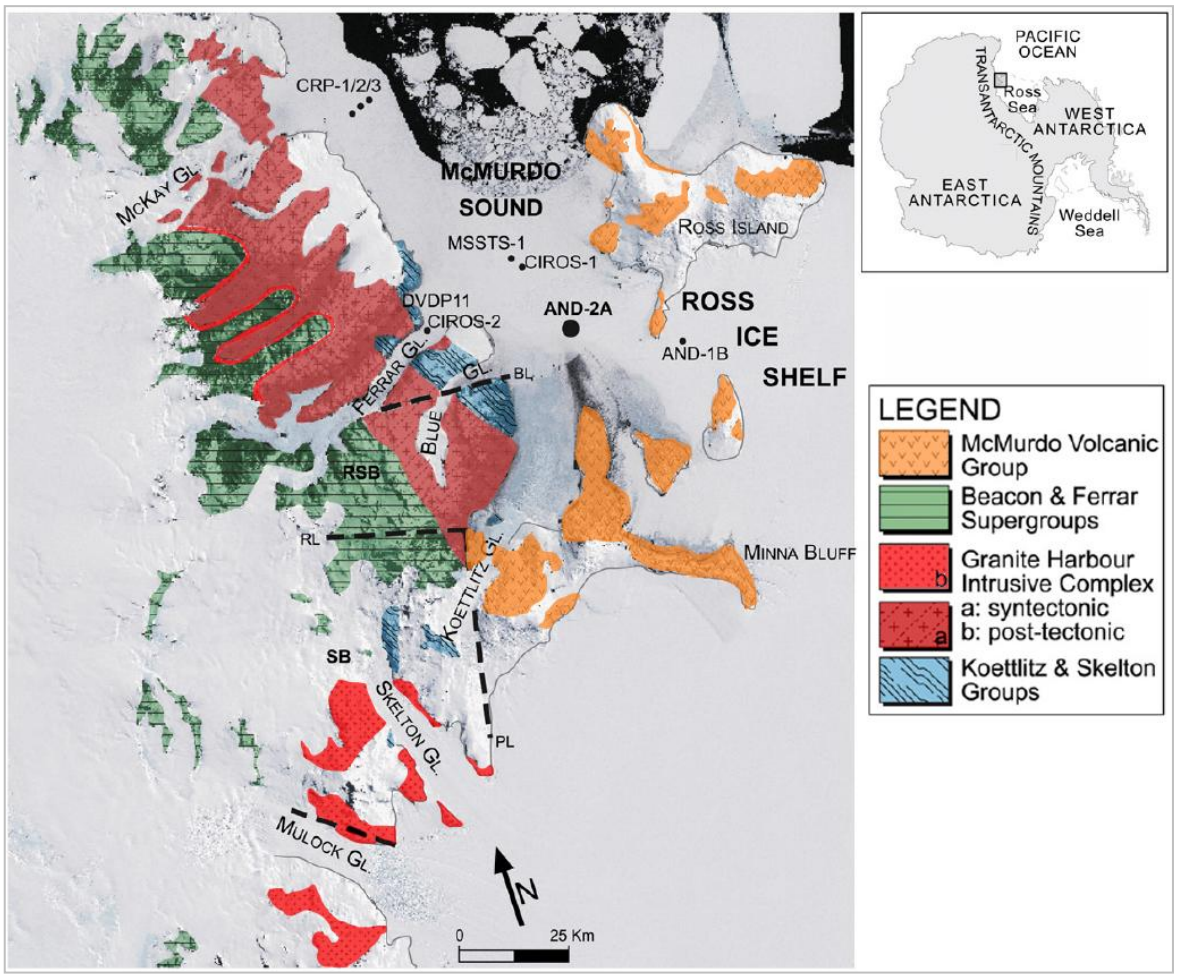

Fig. 3. Geological sketch map of the southern Victoria Land (modified after Warren, 1969 overlapped on a present-day satellite image (LIMA image provided at the http://lima.usgs.gov/ web site). Major inland faults and tectonic blocks are reported (Wilson, 1999; abbreviations BL, RL and PL are Blue, Radian and Pyramid lineaments, RSB and SB are Royal Society and Skelton blocks, respectively). Locations of AND-2A drill site and previous drill holes (DVDP, MSSTS, CIROS, CRP, and AND-1B) are shown.

The Transantarctic Mountains are constituted by a Late Precambrian to Early Palaeozoic crystalline basement which formed during the Ross Orogeny and mainly outcrops along the coast, overlain by a cover complex situated in the inner part of the on-shore region (Fig. 3; Gunn & Warren, 1962).

In southern Victoria Land, the basement complex is composed by metamorphic rocks of Koettlitz Group (medium - to high metamorphic grade), exposed between the Ferrar and Koettlitz glaciers, and by the Skelton Group (low - grade metasedimentary rocks), mainly

limited to the area near the Skelton Glacier (Cook & Craw, 2002). The metamorphic groups are intruded by numerous plutons (Cambrian - Early Ordovician Granite Harbour Intrusive Complex; Gunn & Warren, 1962), ranging in composition from granites to gabbros, and smaller dykes of porphyries. Kukri Peneplain is the consequence of pluton emplacement and successive uplift and erosion, representing the substratum for the deposition of the sedimentary succession of the Devonian to Triassic Beacon Supergroup (McKelvey *et al*., 1977).

During the Jurassic, both crystalline basement and sedimentary cover were intruded by large doleritic sills and dykes of the Ferrar Supergroup, as a consequence of Gondwana break-up (Elliott, 1992; Marsh, 2004; Bedard *et al*., 2007; Zavala *et al*., 2011).

The Erebus Volcanic Province of the McMurdo Volcanic Group constitutes the youngest rocks outcropping in this region (Kyle, 1990). The large alkaline volcanic activity occurred in Cenozoic time during two main phases, the first one (19 to ca. 10 Ma) with dominant trachytic rocks and the more important second one (last 10 Ma) characterized by basanitic to phonolitic compositions.

However, indirect evidences of an older volcanism (Oligocene), have been found within sediments of the Ross Sea Victoria Land Basin recovered by the CIROS-1 and the CRP-2A drill cores (Sandroni & Talarico, 2004; Smellie, 2000).

The distribution of volcanic centers was controlled by two sub-orthogonal lineament sets (NNE and WNW trending; Wilson, 1999) which developed during the Cenozoic (starting at ca. 55 Ma and lasting until middle-Miocene time; Fitzgerald, 2002) as a consequence of the West Antarctic Rift System evolution.

The AND-2A drill core recovered a sedimentary sequence with 98% recovery within an Early Miocene to Quaternary succession punctuated by several disconformities (Harwood *et al*., 2009).

This core contains a range of lithologies, including:

- terrigenous clastic diamictites,
- conglomerate and breccias,
- volcanic lavas,
- diatomites,
- sandstones and mudrocks,
- pyroclastic and reworked volcanic sedimentary rocks.

The succession is divided in fourteen lithostratigraphic units (LSUs, Fig.4, Tab.1, Fielding *et al*., 2008-2009, 2011).

According to Fielding *et al*. (2008-2009) and Fielding *et al.* (2011) thirteen lithofacies have been recognized. They range from diatomites and bioturbated, fossil-bearing mudrocks (that represent most ice distal setting) through interlaminated sandstone-mudrock facies and sandstone with varying dispersed gravel components, to diamictite and conglomerate (that represent most ice-proximal environments). Furthermore, also lava, volcanic breccia and volcanic sedimentary rocks representing extrusion, fallout and reworking of material from basaltic volcanic activity have been identified.

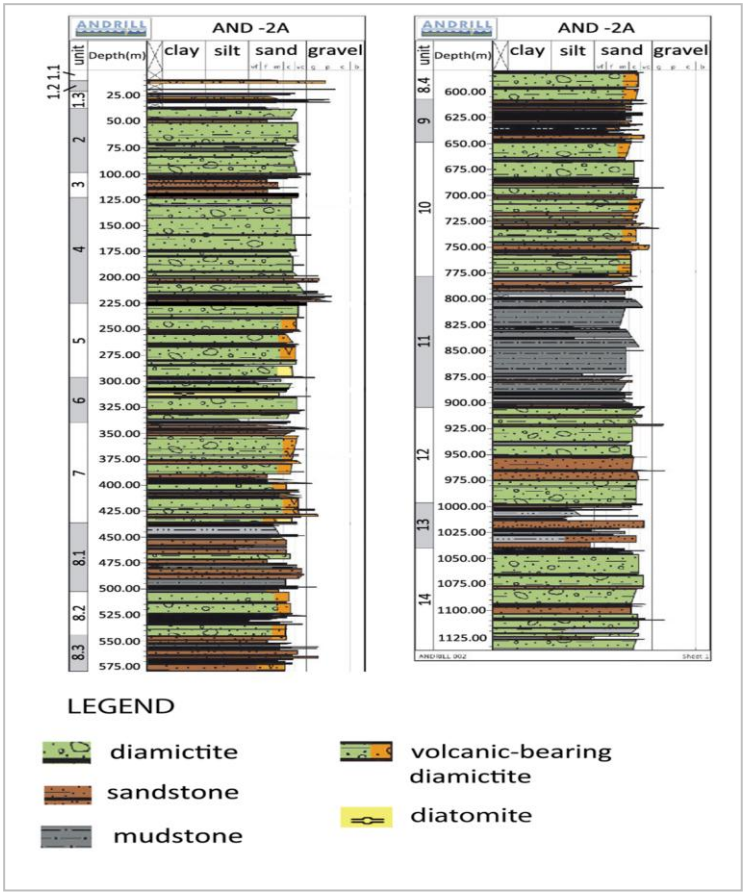

Fig. 4. Summary logs of AND-2A drill core. The grey and white intervals on the left side indicate lithostratigraphic units as defined in Tab. 1.

LSU	*Depth - top (m)*	*Depth - base (m)*	*Unit Thickness (m)*	*Lithology*
1,1	0	10.22	10.22	Mixed volcanic rocks and sedimentary rocks
1,2	12.22	20.57	10.35	Volcanic: basaltic lava & monomictic lava breccia
1,3	20.57	37.07	16.5	Volcanic sedimentary rocks
2	37.07	98.47	61.4	Diamictite with minor sandstone, conglomerate and clayey siltstone
3	98.47	122.86	24.39	Planar bedded sandstone and conglomerate
4	122.86	224.82	101.96	Diamictite with minor sandstone, conglomerate and siltstone
5	224.82	296.34	71.52	Diamictite with biogenic silica, sandstone and minor conglomerate & siltstone
6	296.34	339.92	43.58	Diamictite, diatomite, conglomerate, fine-grained sandstone, siltstone, and claystone
7	339.92	436.18	96.26	Volcanic-bearing diamictite and sandstone
8,1	436.18	502.69	65.51	Volcanic-bearing mudstone, with sandstone and diamictite
8,2	502.69	544.47	41.78	Volcanic-bearing diamictite, mudstone, and sandstone
8,3	544.47	579.33	34.86	Volcanic-bearing sandstone, conglomerate, mudstone, and diamictite
8,4	579.33	607.35	28.02	Volcanic-bearing diamictite, siltstone, sandstone, and conglomerate
9	607.35	648.74	41.39	Volcanic-bearing sandstone, siltstone, and minor diamictite
10	648.74	778.34	129.6	Volcanic-bearing diamictite, sandstone, and sandy mudstone
11	778.34	904.66	126.32	Sandy siltstone with dispersed clasts and sandstone with/without dispersed clasts
12	904.66	996.69	92.03	Clast-rich and clast-poor diamictite, muddy sandstone with dispersed clasts, and minor mudstone with dispersed clasts
13	996,69	1040.28	43.59	Fine siltstone, coarse siltstone, and very fine-grained sandstone with dispersed clasts and rare diamictite
14	1040.28	1138.54	98.26	Diamictite, sandstone, and siltstone

Tab. 1. Summary of the lithostratrigraphic units (LSUs) defined within the AND-2A drill core.

According to Passchier *et al*., (2011) three types of facies associations (Fig.5.1) can be recognized with significantly different paleoclimatic interpretations:

1) A diamictite-dominated facies association which represents glacially dominated depositional environments, including subglacial environments, with only brief intervals where ice free coasts existed, and time periods when the ice sheet was periodically more extended than the modern ice-sheet.
2) A stratified diamictite and mudstone facies association which includes facies characteristic of open marine to iceberg influenced depositional environments, and it is more compatible with a very dynamic ice-sheet, with a grounding line south of the modern position.
3) A mudstone-dominated facies association which generally lacks diamictites, and it was produced in hemipelagic depositional environment influenced by ice.

Age intervals are based on a combination of ^{40}Ar - ^{39}Ar geochronology of volcanic material, diatom, and foram biostratigraphy, magnetostratigraphy, and Sr-isotope chronology of shell material (Acton *et al*., 2008-2009, modified after ANDRILL SMS Science Team, 2010; Di Vincenzo *et al*. 2010; Fig. 5.2). ^{40}Ar - ^{39}Ar ages indicate that in the investigated core section the age model has generally a good precision with errors of ^{40}Ar - ^{39}Ar ages in the range between 0.15 and 0.40 Ma (Di Vincenzo *et al*. 2010).

The major diagenetic processes include calcite replacement of fine-grained matrix, calcite cementation in primary pore space and late-stage fractures, as well as pyrite cementation, hydration, and zeolitisation of volcanic glass fragments (Fielding *et al*., 2008-2009).

1

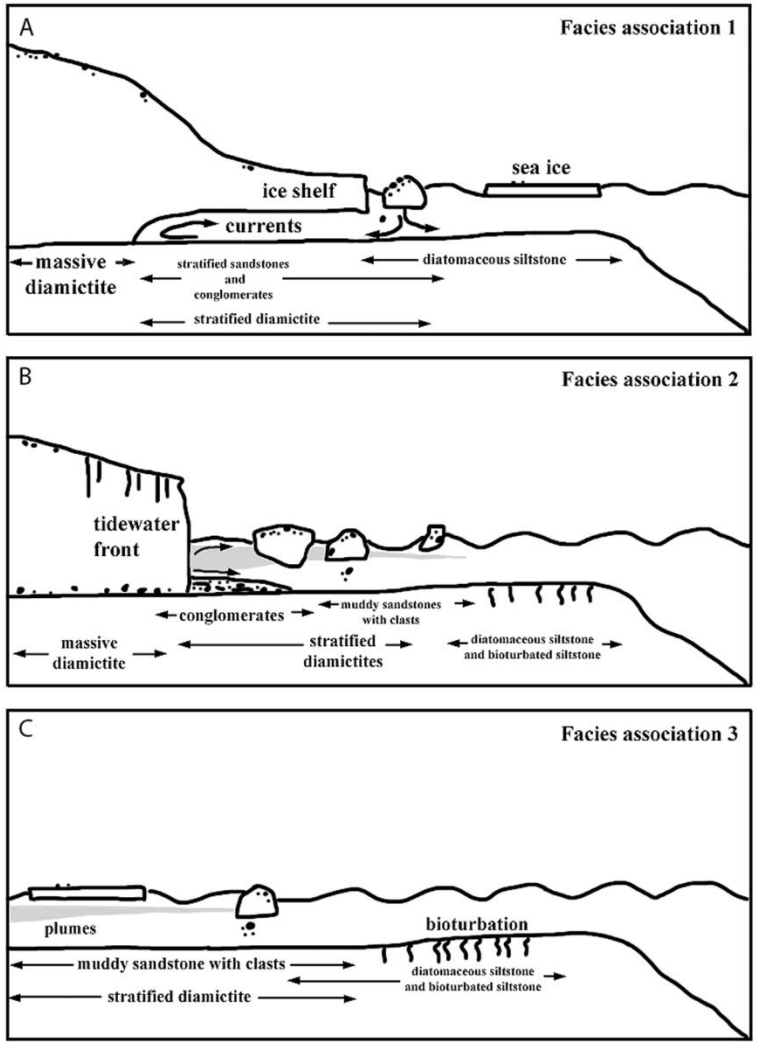
A
Facies association 1
sea ice
ice shelf
currents
massive diamictite
stratified sandstones and conglomerates
diatomaceous siltstone
stratified diamictite
B
Facies association 2
tidewater front
conglomerates
muddy sandstones with clasts
massive diamictite
stratified diamictites
diatomaceous siltstone and bioturbated siltstone
C
Facies association 3
plumes
bioturbation
muddy sandstone with clasts
diatomaceous siltstone and bioturbated siltstone
stratified diamictite

2

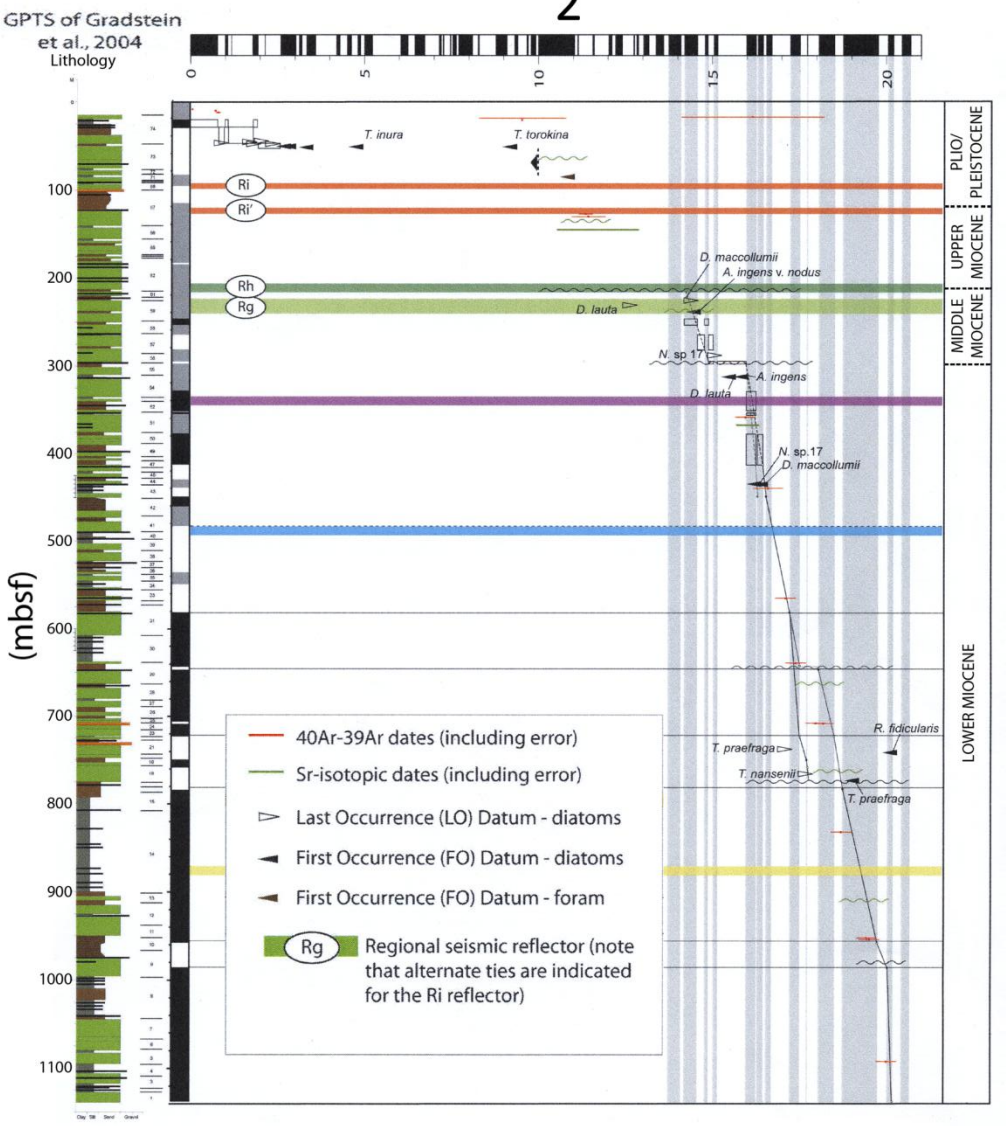
GPTS of Gradstein et al., 2004
Lithology
0
5
10
15
20
(mbsf)
100
200
300
400
500
600
700
800
900
1000
1100
T. inura
T. torokina
Ri
Ri'
Rh
Rg
D. maccollumii
A. ingens v. nodus
D. lauta
N. sp 17
A. ingens
D. lauta
N. sp.17
D. maccollumii
T. praefraga
T. nanseniit
T. praefraga
R. fidicularis
PLIO/ PLEISTOCENE
UPPER MIOCENE
MIDDLE MIOCENE
LOWER MIOCENE
40Ar-39Ar dates (including error)
Sr-isotopic dates (including error)
Last Occurrence (LO) Datum - diatoms
First Occurrence (FO) Datum - diatoms
First Occurrence (FO) Datum - foram
Rg
Regional seismic reflector (note that alternate ties are indicated for the Ri reflector)

Diagenetic calcite occurs throughout the core section. Calcite occurs in the following forms, in decreasing order of occurrence: microcrystalline, microgranular, blocky, fibrous, and spheroidal. The microcrystalline calcite occurs chiefly as dispersed crystals that replace the fine-grained matrix of the host rock. The coarser forms, microgranular and blocky calcite, are often dispersed in the matrix, but can also form rims around sand grains. In some sandstones, these phases fill the primary intergranular pore space. Late-stage fractures are commonly filled with blocky cement or fibrous calcite.

Pyrite is nearly absent above ca. 440 mbsf, but becomes common to abundant at greater depths (Fielding *et al.*, 2008-2009). In some intervals, disseminated pyrite imparts a black color to the sediments and obscures primary sedimentary features. This type of pyrite is most abundant in the following stratigraphic intervals: ca. 555 - 597 mbsf (LSUs 8.3 and 8.4), ca. 775 - 828 mbsf (LSU 11.1), ca. 958 - 1011 mbsf (LSUs 12.1 and 13.1), and below ca. 1040 mbsf (LSU 14.1). Although all lithofacies are affected to some degree, the black spotting is most common in finer lithologies like mudstones. Within these intervals, pyrite is present as cement within the pore space of skeletal grains and replaces volcanic glass. Below ca. 444 mbsf, coarser pyrite occurs alone or in association with calcite and other minerals within late-stage fractures.

Fig. 5. (*previous page*) 1) Facies model for the three facies associations (modified after Passchier *et al*., 2011). A: Facies associations near marine-based polar ice sheet. B: Facies associations near marine based temperate outlet glaciers. C: Facies associations in the marine environment near temperate ice sheet with a terrestrial terminus. 2) Age model for AND-2A drill core (ANDRILL SMS Science team, 2010). The preliminary magnetic polarity stratigraphy is plotted to the top of the Age vs Depth diagram. The magnetozones are black = normal polarity, white = reversed polarity, and grey = uncertain polarity. The schematic summary lithologic column is plotted on the left. Age are reported in millions of years (Ma). Depth is expressed in meters below sea floor (mbsf).

3. Materials and methods

3.1. Clay mineral analysis

A total of 169 sediment samples was analyzed, starting from 36 mbsf to 1123.20 mbsf. Sediment samples for XRD analysis were selected in order to achieve a constant sample spacing along the whole drill core. Sample spacing was approximatively 6 m.

Sediment samples for SEM and FESEM investigations were selected on the basis of clay mineral percentage distribution. In order to achieve a coherent investigation, sample from the different lithologies (diamictites, sandstones, mudstones and volcanic-bearing diamictites) and with varying smectite content were chosen (high, medium, low).

Sediment samples were prepared following the subsequent methodology to analyze clay minerals through X-Ray Diffraction (XRD). For each sample, 10 cm^3 of sediment were gently disaggregated in deionized water, firstly through magnetic stirrer for 30 minutes and secondly through ultrasonic bath for 5 minutes. Afterwards, sediment samples were sieved through a 63 μm sieve.

Since we are analyzing marine sediments, we needed to remove soluble salts (i.e. halite, NaCl) present in the samples. The soluble salts are easily removable through repeated washing cycles with deionized water, using a centrifuge, operating at 2900 rounds per minute (RPM) for 10 minutes.

The most used method for clay fraction separation is to disperse clay in the water and to divide them on the basis of their size by settling procedure, following Stoke's law.

$$\mathbf{V_T = [g(d_p - d_1)D^2] / 18\eta}$$

with:

$\mathbf{V_T}$ = settling velocity of particles

g = gravitational acceleration (m/sec^2)

$\mathbf{d_p - d_1}$ = difference of density between particle and liquid

$\mathbf{D^2}$ = diameter of particle (cm)

$\boldsymbol{\eta}$ = viscosity of the liquid at specific temperature

Taking into account that *velocity* = *distance/time*, Stoke's law can be re-written:

$$\mathbf{t = 18\eta h / [g(d_p - d_1)D^2]}$$

This equation establishes the time **t**, in seconds, that a particle takes to fall from a given height **h**, express in centimeters. In this case, **h** corresponds to the height of the settling cylinder used for clay fraction separation. It is now possible to calculate clay fraction's settling time in water, at determined height of the water column and at given temperatures.

Texturally-oriented samples were used to facilitate clay minerals' identification through X-Ray Diffraction technique. The obtained basal reflections at low diffraction angles are characteristic of clay minerals. Clay mineral reflections, even if they do not interfere with other mineral reflections, can show partial peak overlapping one each-other.

In case of diagnostic peak overlapping, further sample treatments are needed. Those treatments, in fact, acting on crystal structure, cause variations in the basal spacing of clay minerals, and a consequent shift of the diffraction peaks.

In the studied samples, glycolation and magnesium saturation were the treatment used to differentiate clay minerals. Some clay minerals adsorb anions and cations and hold them in an exchangeable state (Moore & Reynolds, 1997). Samples were saturated with

magnesium, that brings to the formation of a stable complex of two water molecules between smectite layers and increases the basal spacing (d) (001) to around 14 Å. Saturation technique consists in treating the clay minerals with a 1 N solution of magnesium chloride ($MgCl_2$). Between 10 and 30 ml of a 50% $MgCl_2$ solution was added to the clay suspension in order to charge the clay minerals. Subsequently, excess ions were removed by double centrifugation with distilled water, and the samples were dried at a temperature of 60°C (Ehrmann *et al.*, 1992a; Petschick *et al*., 1996).

Glycolation is needed to modify smectite basal spacing (Bradley, 1945; Novich & Martin, 1983). This treatment allows to discriminate smectites from chlorites; the second ones, in fact are not affected by this treatment and keep their basal spacing to 14 Å. Ethylene glycol solvation was achieved exposing the sample, mounted on a glass slide, to the vapor of the reagent for at least 8 hours at 60°C, in a large desiccator put in an oven (Moore & Reynolds, 1997).

XRD measurements were conducted on 169 sediment samples with an automated Philips PW1710 powder diffraction control system, coupled with a PW1820 generator, using CuKa radiation (40 kV, 20 mA). Each texturally oriented sample was analyzed between 4° 2θ and 40° 2θ, with a step size of 0.02° 2θ, in the air-dry state and after ethylene glycol solvation.

Chlorite has a basal series of diffraction peaks at 7 Å (002) superimposed or nearly superimposed on the members of the kaolinite *00l* series (001). Most kaolinites have the 002 peak at 24.9°2θ, and common chlorites have their 004 reflection at ~ 25.1°2θ.

For this reason, in addition, a slow scan, between 23°2θ and 25.5°2θ, with a step size of 0.005°2θ, was performed on the ethylene-glycolated samples to achieve a better resolution of the chlorite (004) - kaolinite (002) twin peak at ~ 25°2θ (Fig. 6).

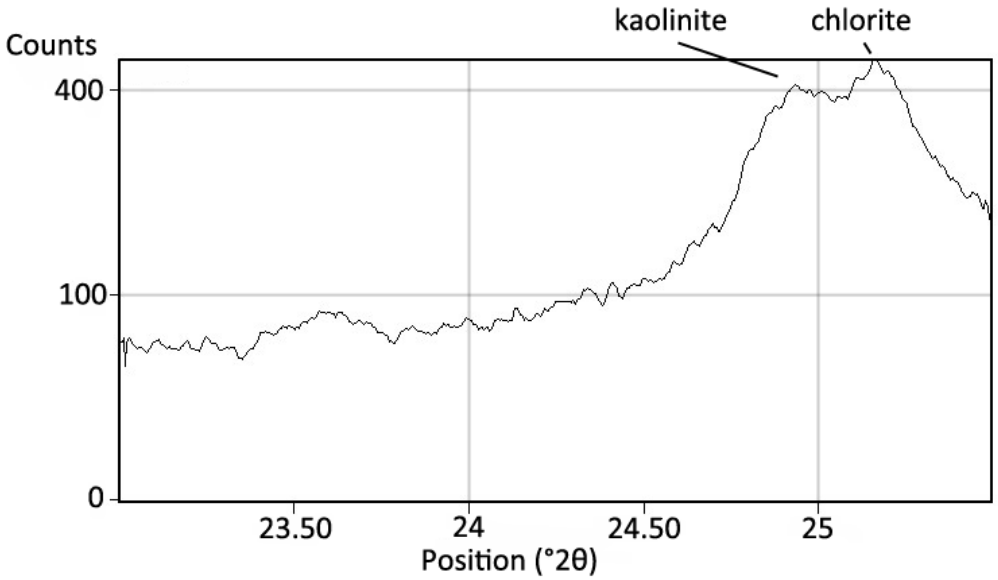

Fig. 6. X-Ray diffractogram of an analyzed sample, between 23° 2θ and 25.5°2θ (CuKα), with a step size of 0.05°2θ. In this case kaolinite peak is at 24.93°2θ while chlorite peak is at 25.16°2θ.

Diffractograms were processed using the "MacDiff" software (Petschick, 2001, free on line).

This software automatically calculates area and intensity peak values. Abundance of the principal clay minerals (smectite, illite, chlorite and kaolinite) was semi-quantitatively estimated by calculating the peak areas of their main basal reflections in the glycolated state: smectite at 17 Å, illite at 10 and 5 Å, chlorite at 14.2, 7, 3.54 Å and kaolinite at 7 and 3.57 Å (Petschick *et al*., 1996).

The terms smectite, illite, kaolinite and chlorite are used as a general expression for the respective mineral groups. The term illite was introduced by Grim *et al*. (1937) to refer to very little mica-like mineral, commonly found in argillaceous sediments. A more restrictive definition was given by Środoń & Eberl (1984) who referred to an Al-K mica-like, non-expanding, dioctahedral mineral, occurring in the clay fraction.

The relative clay mineral contents of smectite, illite, kaolinite and chlorite were determined using ratios of integrated peak areas of their basal reflections, weighted by empirically estimated factors (Biscaye, 1965; Brindley & Brown, 1980; Ehrmann *et al*., 1992a;

Diekmann *et al*., 1996; Vogt *et al*., 2001). Accordingly the smectite 17 Å peak area is multiplied by 1, the 10 Å illite peak area by 4 and both kaolinite and chlorite proportions of their 7 Å peak by 2.

The 7 Å peak, common to both kaolinite and chlorite, was divided between the two in proportion to the fraction of each mineral in the total area under the resolved 3.5 Å kaolinite-chlorite doublet.

Clay mineral percentage standard deviations were calculated using results of ten diffractograms obtained from one single oriented sample. Standard deviations vary for the four minerals in the following way: smectite ± 0.4 ; illite ± 1.5 %; chlorite ± 0.9 %; kaolinite ± 1.1 % (Tab. 2).

Number of diffractograms	% Smectite	% Illite	% Chlorite	% Kaolinite
1	7.6	50.4	20.1	21.9
2	7.8	47.3	21.7	23.3
3	7.8	45.9	21.6	24.7
4	8.3	48.4	21.8	21.5
5	8.2	48.1	22.1	21.6
6	7.5	49.0	21.2	22.3
7	7.6	48.8	19.5	24.1
8	8.1	47.3	21.5	23.1
9	8.8	45.2	22.6	23.4
10	7.8	47.4	21.9	22.9
Mean	**8.0**	**47.8**	**21.4**	**22.9**
Standard Deviation	**0.4**	**1.5**	**0.9**	**1.1**

Tab. 2. Clay mineral percentages calculated running 10 diffractograms on the same glass slide. Mean and standard deviation are also shown.

The grade of lattice order and the crystallite size of clay minerals is usually referred to as crystallinity and the measurements were made by calculating the IB (Integral Breadth) of the glycolated 17 Å smectite peak (Klug & Alexander, 1974; Diekmann *et al*., 1996; Petschick *et al*., 1996; Ehrmann, 1997).

High values indicate poor crystallinities, whereas low values indicate good crystallinities.

Categories for crystallinities were determined taking into account the IB range for smectite (Diekmann *et al*., 1996).

Categories for smectite crystallinities are: very well crystalline (IB < 1.0 Δ2°θ), well crystalline (1.0 – 1.5 Δ2°θ), moderately crystalline (1.5 – 2.0 Δ2°θ) and poorly crystalline (IB > 2.0 Δ2°θ).

Scanning Electron Microscopy (SEM) observations and chemical microanalysis were carried out on 32 selected, polished thin sections using a Philips® XL30 device operated at 20 kV and equipped with an EDAX energy-dispersive (EDS) X-Ray spectrometer (Dipartimento di Scienze della Terra, University of Siena, Italy).

Field Emission Scanning Electron Microscopy (FESEM) investigations were performed on ten rock chip selected samples by a LEO (Carl Zeiss) 1530 GEMINI (Centro de Instrumentación Científica, CIC, University of Granada, Spain) operated at 10Kv and equipped with an Oxford INCA 200 microanalysis system. FESEM allows higher magnification (up to 900 kx) compared to traditional SEM and thus yields a better resolution of clay particles micromorphologies.

3.2. Heavy mineral analysis

A total of 32 heavy mineral samples were analyzed starting from 650.00 mbsf to 1123.20 mbsf.

Samples for SEM analysis were selected in order to achieve a coherent sample spacing along the whole investigated section. Sample spacing was approximatively 15 m.

The heavy mineral separation from the sand fraction (between 63 μm and 2 mm) was carried out in a centrifuge operated at 2900 RPM for 10 minutes, using a sodium

polytungstate solution with a density of 2.90 g cm^{-3} (Callahan, 1987). After centrifugation, the bottom part of plastic funnels containing heavy mineral fraction was frozen through immersion in liquid nitrogen (N_20) so that it did not mix with the light fraction when funnel is emptied. Afterwards, heavy minerals were carefully washed with deionized water and dried on various type of paper filter.

Then heavy minerals from each sample were mounted on a glass slide, carbon coated and viewed using the previously dscribed SEM-EDS (Philips XL30 SEM) equipped with an energy dispersive X-ray detection system (EDAX).

Following the method proposed by Hanan & Totten (1996), each mineral was determined through chemical analyses collected by EDS and mineral shape, obtained by back scattered electron imaging. The grain morphology allows to establish the crystallinity versus glassy nature of the grains; the chemical analyses allows to determine the mineral composition, making it possible to refine the distinction among pyroxenes (Fe-Mg pyroxenes, diospide, titanoaugites), amphiboles, oxides.

The abundance of each mineral was calculated as a percentage of the total grains (n=200) counted for each samples. Errors were estimated from repeated measurements (n=3) on three separates of the same sample and they are always lower than 6 %. Semi-quantitative chemical analyses for each mineral species have been obtained; although the errors are higher than the errors for analyses obtained on a polished mineral surface, the analyses can be compared and they are representative of compositions for each mineral species.

4. Results

4.1. Clay minerals

A large part of the clay minerals accumulating in the ocean close to continents is derived from the adjacent land masses. They were provided by physical or chemical weathering processes on a variety of lithologies. The clay mineral types and the proportions of the individual clay minerals in marine sediments hence depend on the climatic conditions on land and on the nature of the source rocks (Ehrmann *et al*., 1992a-b).

The distribution of different clay minerals in the actual ocean sediments shows a latitudinal zonation that strongly mirrors the pedogenic zonation and climatic conditions on the adjacent continental land masses (Biscaye, 1965; Griffin *et al*., 1968).

Consequently, clay mineral assemblages in marine sedimentary sequences are useful tools for reconstructing the paleoclimatic conditions through time (Chamley, 1989). However, the small size of the clay minerals makes them inclined to erosion, transport and redistribution by different media, such as wind transport, fluvial transport, as well as transport and erosion by bottom currents or gravitational sediment movements (Ehrmann *et al.* 1992a). Thus, clay minerals may also be useful tools for deciphering and reconstructing sedimentary processes.

The type and grade of alteration regulate the relative percentage of different clay minerals; transport and sedimentation may determine a selective enrichment of different mineralogical phases depending on their grain size (Ehrmann *et al*., 1992a).

Antarctica represents a very complex environment and climate changes generate strong erosion events as well as sediment transport and deposition mechanisms that are directly

influenced by expansions and retreats of ice cover. For this reason clay minerals present in the marine sedimentary successions were considered useful tools to investigate the provenance area of the deposited material (Carroll, 1970; Moriarty, 1977; Petschick *et al.*, 1996;), to reconstruct paleoenvironmental and paleoclimatic conditions (Darby, 1975; Ehrmann & Mackensen, 1992; Ehrmann, 1998a-b; Ehrmann, 2005) and paleoceanographic evolution (Ehrmann *et al.*, 1992a-b; Diekmann *et al.*, 1996, 1999).

Clay minerals used for this kind of reconstructions are: smectite, illite, chlorite and kaolinite.

Illite and chlorite are detrital clay minerals, products of physical weathering and glacial scour. They are, therefore, the typical clay minerals of the high latitudes. They are derived, particularly, from crystalline rocks, such as those that are widespread in East Antarctica.

Chlorite is a characteristic mineral for low-grade, chlorite-bearing metamorphic and basic source rocks, but it is not resistant to chemical weathering and transport.

Illite tends to be derived from more acidic rocks and is relatively resistant (Biscaye, 1965; Griffin *et al*., 1968). Together with kaolinite, chlorite and smectite, illite is in fact one of the four major constituents of argillaceous sedimentary rocks.

Kaolinite and smectite, in contrast, are products of chemical weathering. High concentrations of kaolinite are normally restricted to moist temperate to tropical regions, where long-continued and intense hydrolysis, especially of granitic source rocks and lateritic soil formation occurs.

Kaolinite cannot form under polar conditions. However, because this mineral is very resistant, reworked kaolinite from older sediments may also be found in polar environments (Chamley, 1989; Ehrmann *et al*., 1992a).

Smectite normally forms by hydrolysis under warm-humid and cold-dry climatic conditions (Chamley, 1989), in environments characterized by very slow movement of

water. In general, smectite formation in the recent Antarctic environment is only a secondary process. Evidence of smectite formation has been reported from a few soils in Antarctica (Claridge, 1965; Claridge & Campbell, 1989; Chamley, 1989). Some Antarctic tills also contain smectite (Bardin *et al*., 1979; Bardin, 1982). In quaternary antarctic sedimentary sequences smectite concentration is chiefly controlled by lithologic source and by transport mechanisms. High smectite concentrations have been reported from glaciomarine sediments in areas with Mesozoic basalts in the hinterland (Ehrmann *et al*., 1992a), showing that basalts can provide considerable amounts of smectite under a polar climate.

4.1.1. Clay mineral distribution

The most abundant clay minerals in sediments of AND-2A drill core are illite and smectite. Illite content ranges between 0 and 91 % and it is negatively correlated (R^2 = - 0.93) with smectite content (which ranges between 1 and 100%). Chlorite content is seldom higher than 30 % and kaolinite is absent or present only in traces (< 4 %). All analyses are shown in Table 1A in Appendix.

Figure 7 shows the down-core clay mineral variations. Due to these variations it was possible to distinguish 3 units. In Unit I (36 - 225 mbsf, 0.7 - 15 Ma) smectite and illite are quite constant (average of 35 and 41%, respectively) and chlorite shows large fluctuations. In Unit II (225 - 440 mbsf, 15 - 16.5 Ma) smectite content decreases (average of 9%) and illite content increases (average of 72%), while chlorite content slightly decreases and shows lower fluctuations.

Unit III (440 - 1123 mbsf, 16.5 - 20.2 Ma) is characterized by high smectite-illite

fluctuations, while chlorite displays moderate fluctuations with an average value of 14%. These results are coherent with those reported by Franke & Ehrmann (2010) for the same AND-2A drill-core, although with differences in clay mineral percentages.

For all samples, correlation coefficient (r) between all clay minerals from investigated sediment samples was calculated and results are shown in Table 3.

Smectite - Illite	-0.96
Smectite - Kaolinite	-0.08
Smectite - Chlorite	-0.65
Illite - Kaolinite	0.08
Illite - Chlorite	0.42
Kaolinite - Chlorite	-0.05

Tab. 3. Correlation coefficient calculated between all clay minerals present in the investigated sediment samples.

As aforementioned, smectite and illite show a strong negative correlation (r = - 0.96). Smectite and chlorite show a negative correlation, even if not so strong as the smectite - illite correlation.

Smectite mean IB value for the whole drill core is 1 (Fig. 8). In Unit I and Unit II smectite IB displays relatively higher value, respectively 1.17 and 1.29. In Unit III smectite IB shows relatively lower values and the mean value is 0.91.

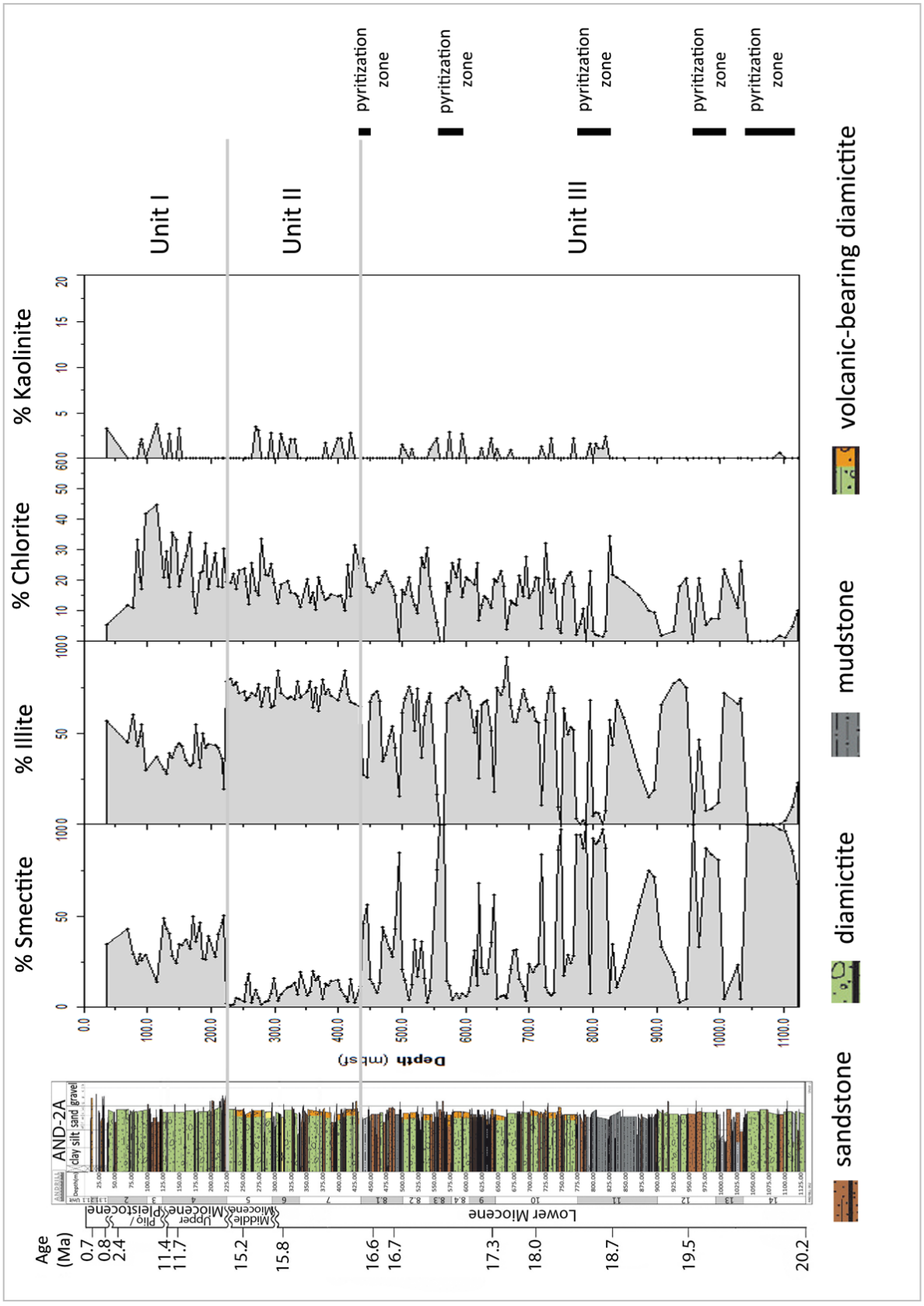

Fig. 7. Down-core variations of clay mineral contents in AND-2A drill core. A lithological core log is reported (Fielding *et al.*, 2008-2009). Gray horizontal lines indicate unit boundaries. mbsf: meters below sea floor. Zone of pyritization as indicated by Fielding *et al.*, (2008-2009) are also reported.

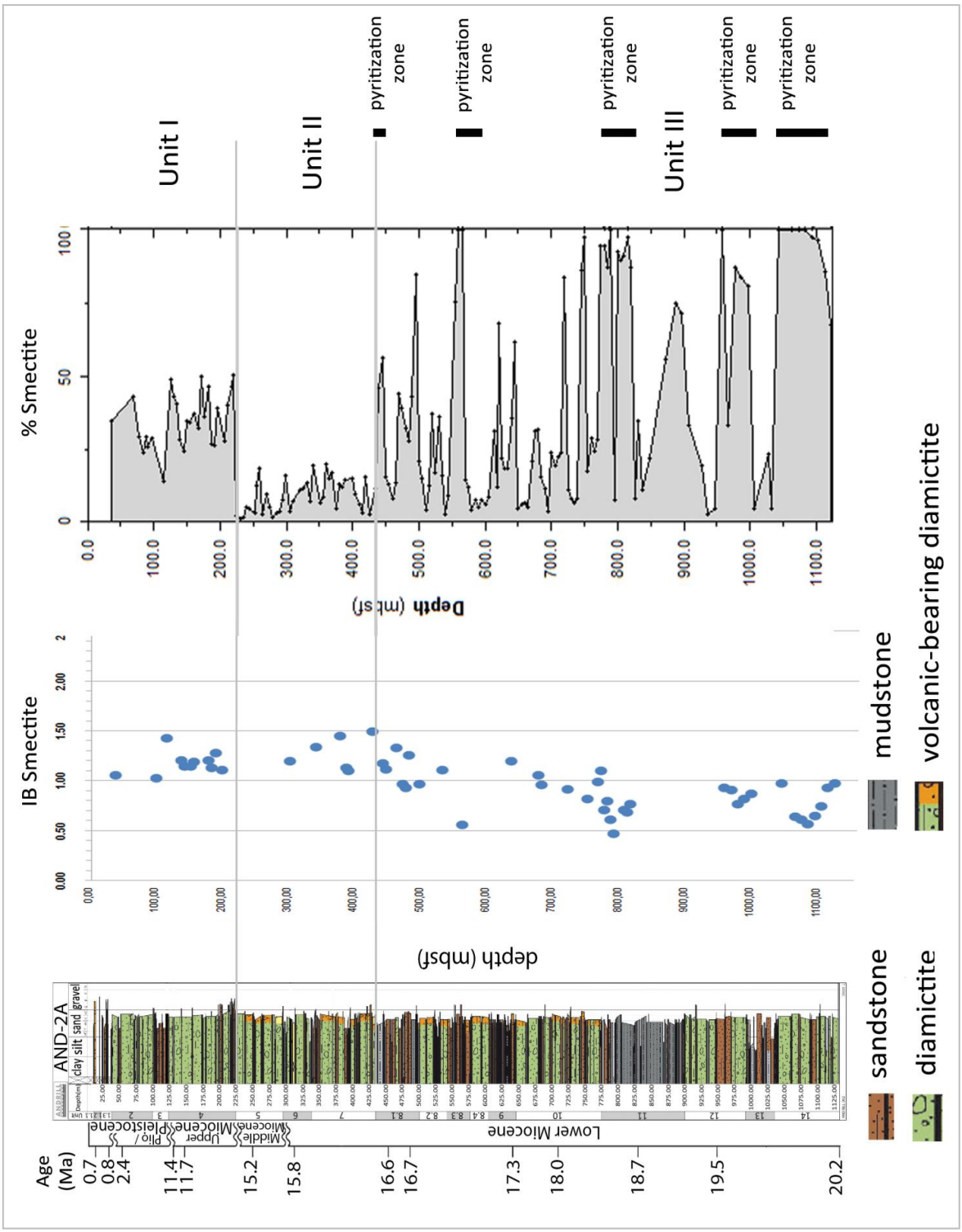

Fig. 8. Down-core variations of smectite crystallinity indexes in AND-2A drill core. A lithological core log is reported (Fielding *et al*., 2008-2009). Gray horizontal lines indicate unit boundaries. mbsf: meters below sea floor. Zone of pyritization as indicated by Fielding *et al*. (2008-2009) are also reported. Categories for smectite crystallinity are: very well crystalline (IB < 1.0 Δ2°θ), well crystalline (1.0 - 1.5 Δ2°θ), moderately crystalline (1.5 - 2.0 Δ2°θ) and poorly crystalline (IB > 2.0 Δ2°θ).

4.1.2. Smectite morphology and composition

SEM and FESEM observations on the clay mineral fraction showed that the smectites of AND-2A sediments display both hairy and honeycomb structures (Vitali *et al.*, 1999; Ehrmann *et al.*, 2005; Fesharaki *et al.*, 2007) as well as flaky shapes; such forms have also been recognized in CRP-1, 2, 3 core and in other records from the Ross Sea (Setti *et al.*, 1997, 1998, 2000; Ehrmann, 2000, 2001; Ehrmann *et al.*, 2003). Flaky shapes are considered of detrital origin and are mostly typical of alkaline smectites or beidellites, being these forms usually found in soils. Hairy and honeycomb smectites frequently occur in marine sediments. Because of their morphology, hairy and honeycomb shapes are fragile and have been considered to be authigenic (Chamley, 1989; Vitali *et al.*, 1999; de la Fuente *et al.*, 2000; Ehrmann *et al.*, 2005, Fesharaki *et al.*, 2007). We defined authigenic smectites those crystals that coat grains, that replace other minerals or grow over them and that showed hairy shape or honeycomb structures. Detrital smectites are more difficult to identify, because they do not show such peculiar features. However, we defined detrital smectites, those crystals in the fine-grained matrix, showing no textural relation with glass or other volcanic fragments and that present platy morphologies.

Figures 9A and 9B show both detrital and authigenic smectites from sample 124.97 mbsf (Unit I). Figure 9A displays authigenic smectites that completely replace a glass shard. In the upper portion of the image detrital smectites are also present. Figure 9B shows a FESEM-SE view of the same sample; a flaky structure typical of detrital origin is well recognizable. A platy morphology of smectites is clearly observable and some crystallites show rounded edge shape. Such structures are very similar to other ones interpreted by Ehrmann *et al.* (2005) as detrital.

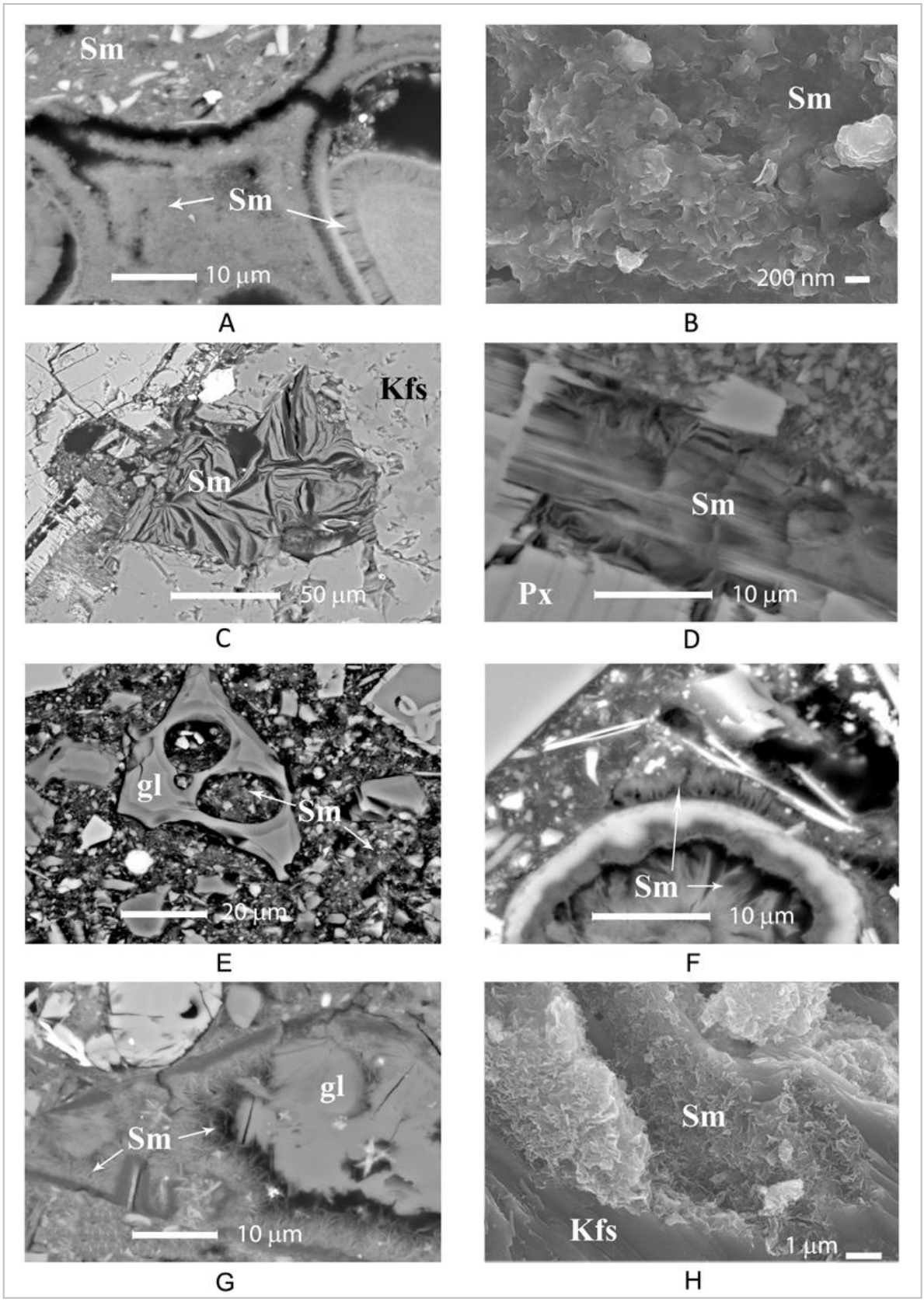
Sm
Sm
10 µm
A
Sm
200 nm
B
Kfs
Sm
50 µm
C
Sm
Px
10 µm
D
gl
Sm
20 µm
E
Sm
10 µm
F
gl
Sm
10 µm
G
Sm
Kfs
1 µm
H

Figures 9C and 9D show authigenic smectites from sample 315,00 mbsf (Unit II). We observed crystals of K-feldspars (9C) and pyroxenes (9D) that constitute the parent material for authigenic smectites. This fact is in agreement with experimental studies by Drief *et al*. (2001) who demonstrated that the alteration mechanism and the sequence of feldspar transformation into clays are controlled by dissolution-reprecipitation processes. These authors also showed that the chemical nature of the newly formed smectite is determined by the composition of the parent mineral. Detrital smectites usually constitute the matrix of the sediments (Fig. 9E). On the contrary, authigenic smectites occur as coating on detrital grain or develop in pore cavities (Fig. 9F).

Figures 9G and 9H display authigenic smectites from Unit III, respectively from sample 775.00 and 1113.02. Figure 9G shows hairy shape smectites replacing a highly altered glass shard. FESEM investigations emphasize smectite features that are clearly different from those observed in figure 9B. In particular, we observed a feldspar grain with a typical honey-comb shape (Fig. 9H), characteristic feature of newly-formed smectites: in contrast to flaky feature typical of detrital smectites, honeycomb shapes show warped edges and a very delicate structure. Our morphologic investigations are very similar to those performed by Fesharaki *et al*. (2007): these authors recognized partial dissolution of feldspars with honeycomb smectite of montmorillonitic composition grown on them.

Fig. 9. (*Previous page).* SEM and FESEM images of authigenic and detrital smectite from Unit I, II and III. SEM-BSE image A shows a glass shard completely replaced by authigenic smectite (Sm, white arrows); in the upper part of the image detrital smectites (Sm) is shown (sample 124.97 mbsf, Unit I). B shows a FESEM-SE image of detrital smectites (Sm) from sample 124.97 mbsf (Unit I). C shows a SEM-BSE image displaying smectite assemblages (Sm) of neoformation origin from sample 315.00 mbsf (Unit II). D (SEM-BSE) shows neoformation smectite replacing a pyroxene (Px) in sample 315.00 mbsf (Unit II). Mineral abbreviations after Kretz (1983). SEM-BSE image E displays detrital smectite assemblage (Sm, white arrows), in sample 695.95 mbsf. F (SEM-BSE) shows a hairy shape feature characteristic of authigenic smectites (Sm, white arrows) in sample 749.99 mbsf. G (SEM-BSE) displays a partial replacement of a glass shard by newly formed smectite (Sm, white arrows) in sample 775.00 mbsf. H shows a FESEM-SE image displaying honeycomb structure characteristic of authigenic smectite (Sm) from sample 1113.02 mbsf. Mineral abbreviations after Kretz (1983), except gl: glass.

In Tables 4A and 4B chemical compositions of smectites in AND-2A drill core are reported. Authigenic or detrital origin has been assigned to the analyzed smectite taking into account their morphologic features. In polished thin section authigenic smectites are well recognizable because they occur as radial rims around grains or with a filamentous shape (hairy shape). A combined SEM-FESEM observation was needed to ascertain quite clearly the detrital nature of the smectites.

The composition of smectites is extremely variable, ranging from Al-rich smectites to Mg-Fe-rich smectites. In each unit, smectites are characterized by the presence of aluminum in both tetrahedral and octahedral sites and by variable substitution of Fe^{3+} and Mg for octahedral Al. Fe was assumed to be all ferric, since Fe^{2+} in smectite oxidizes very quickly when exposed to the atmosphere (Decarreau & Bonnin, 1986).

In figure 10 the octahedral composition (Al^{VI} - Mg^{VI} - Fe^{VI} diagram) of smectite was plotted with respect to the three units. The usual smectite grain size is smaller than the spatial resolution of analyses in SEM, therefore most of the analyses probably represent more the composition of a smectitic area than that of an individual smectite grain. In spite of this fact, in each unit, two distinct compositional trends can be recognized: detrital smectites show an Al-richer composition, close to the montmorillonite-beidellite field; authigenic smectites have higher Fe-Mg content and intermediate compositions between the saponite and nontronite field. Some authigenic smectites on feldspar grains show relatively higher Al-rich composition close to montmorillinitic-beidellitic composition.

Some of the analyses presented on Table 4A and 4B show high interlayer charge and/or low Si content. Such chemical characteristics could be a consequence of contamination by illite or chlorite due to the size of the analyzed area in relation to the small grain size of smectite, but they also could represent illite or illite/smectite interstratified minerals.

n.	depth (mbsf)	Tetrahedral sheet		Octahedral sheet				Interlayer				Habit	Unit
		Si	Al^{IV}	Al^{VI}	Mg^{VI}	Fe^{3+}	Σ oct.	K	Ca	Na	int. charge		
1	68.01	3.61	0.39	0.70	0.91	0.67	2.28	0.13	0.06	0.14	0.39	AUT	I
2		3.61	0.39	0.73	1.00	0.57	2.30	0.10	0.07	0.11	0.35	AUT	
3	78.05	3.68	0.32	0.69	0.65	0.69	2.03	0.15	0.09	0.12	0.45	AUT	I
4		3.38	0.62	0.63	0.99	1.07	2.69	0.09	0.01	0.10	0.21	AUT	
5	88.01	3.67	0.33	0.79	0.49	0.70	1.98	0.38	0.17	0.12	0.84	DET	I
6		3.66	0.34	0.72	0.45	0.82	1.99	0.43	0.24	0.06	0.97	DET	
7	98.00	3.64	0.36	0.77	0.58	0.60	1.96	0.32	0.18	0.10	0.78	DET	I
8		3.69	0.31	0.82	0.55	0.59	1.97	0.37	0.22	0.19	1.00	DET	
9	124.97	3.77	0.23	0.94	0.48	0.56	1.98	0.33	0.07	0.36	0.83	DET	I
10		3.71	0.29	0.64	0.77	0.93	2.33	0.11	0.02	0.13	0.28	AUT	
11	140.07	3.84	0.16	0.85	0.53	0.59	1.97	0.32	0.11	0.23	0.77	DET	I
12		3.87	0.13	0.85	0.58	0.55	1.98	0.31	0.08	0.21	0.68	DET	
13	145.00	3.84	0.16	0.92	0.49	0.57	1.98	0.24	0.16	0.18	0.74	DET	I
14		3.70	0.30	0.69	0.69	0.62	2.00	0.16	0.09	0.24	0.58	AUT	
15	181.99	3.39	0.61	0.34	0.96	1.08	2.37	0.08	0.61	0.22	1.52	AUT	I
16		3.76	0.24	0.76	0.56	0.63	1.96	0.22	0.16	0.31	0.85	DET	
17	202.00	3.72	0.28	1.31	0.38	0.31	2.00	0.32	0.04	0.12	0.52	DET	I
18		3.84	0.16	0.64	0.74	0.84	2.22	0.16	0.07	0.12	0.42	AUT	
19	212.00	3.74	0.26	0.83	0.53	0.60	1.97	0.39	0.08	0.20	0.75	DET	I
20		3.74	0.26	0.90	0.49	0.56	1.95	0.42	0.17	0.28	1.04	DET	
21	225.01	3.50	0.50	0.37	0.90	0.92	2.19	0.20	0.25	0.25	0.95	AUT	II
22		3.75	0.25	0.97	0.64	0.38	1.99	0.28	0.10	0.19	0.67	DET	
23	280.01	3.72	0.28	0.55	0.56	0.87	1.99	0.21	0.36	0.14	1.07	AUT	II
24	299.50	3.70	0.30	0.80	0.58	0.57	1.96	0.27	0.21	0.26	0.95	DET	II
25		3.88	0.12	0.91	0.50	0.56	1.98	0.31	0.10	0.21	0.72	DET	
26	315.02	3.82	0.18	0.62	0.54	1.02	2.18	0.09	0.07	0.21	0.44	AUT	II
27		3.43	0.57	0.46	1.14	0.84	2.44	0.05	0.29	0.10	0.73	AUT	
28	370.01	3.78	0.22	0.79	0.69	0.50	1.98	0.25	0.25	0.34	1.09	DET	II
29		3.81	0.19	0.87	0.65	0.51	2.03	0.18	0.27	0.28	1.00	DET	
30	388.00	3.84	0.16	0.59	0.57	0.81	1.97	0.21	0.17	0.30	0.85	AUT	II
31		3.72	0.28	0.80	0.49	0.71	1.99	0.23	0.31	0.39	1.24	DET	
32	415.02	3.65	0.35	0.19	1.28	1.01	2.47	0.06	0.08	0.16	0.38	AUT	II
33		3.82	0.18	0.72	0.60	0.64	1.96	0.20	0.16	0.18	0.70	DET	
34	425.02	3.71	0.29	0.31	1.02	0.93	2.26	0.12	0.27	0.10	0.76	AUT	II
35		3.74	0.26	1.00	0.57	0.44	2.00	0.32	0.14	0.17	0.77	DET	

Tab. 4A. EDS microanalyses have been used to calculate the structural formulae of smectites on the basis of $O_{10}(OH)_2$.

n.	depth (mbsf)	Tetrahedral sheet		Octahedral sheet				Interlayer				Habit	Unit
		Si	Al^{IV}	Al^{VI}	Mg^{VI}	Fe^{3+}	Σ oct.	K	Ca	Na	int. charge		
36	439.52	3.25	0.75	0.25	1.15	1.06	2.46	0.19	0.34	0.07	0.94	AUT	III
37	540.00	3.65	0.35	0.91	0.62	0.53	2.06	0.21	0.34	0.24	1.13	DET	III
38	605.02	3.24	0.76	0.09	1.09	1.50	2.68	0.19	0.34	0.21	1.08	AUT	III
39	765.00	3.34	0.66	0.16	1.04	1.45	2.64	0.05	0.04	0.15	0.28	AUT	III
40		3.87	0.13	0.86	0.62	0.42	1.90	0.23	0.10	0.28	0.71	DET	
41	775.00	3.69	0.31	0.27	1.48	1.00	2.75	0.10	0.03	0.15	0.31	AUT	III
42		3.78	0.22	0.59	0.83	0.68	2.10	0.24	0.22	0.18	0.86	DET	
43	805.00	3.53	0.47	0.03	1.63	0.95	2.61	0.03	0.01	0.08	0.13	AUT	III
44		3.52	0.48	0.05	1.65	0.98	2.69	0.06	0.07	0.07	0.27	AUT	
45	815.00	3.39	0.61	0.04	1.31	1.34	2.68	0.12	0.09	0.17	0.47	AUT	III
46		3.72	0.28	0.59	0.78	0.69	2.05	0.20	0.07	0.34	0.68	DET	
47	897.01	3.31	0.69	0.32	1.04	1.06	2.41	0.03	0.31	0.12	0.77	AUT	III
48		3.88	0.12	0.90	0.82	0.47	2.19	0.06	0.04	0.12	0.26	DET	
49	927.28	3.84	0.16	0.92	0.58	0.53	2.03	0.29	0.14	0.15	0.72	DET	III
50		3.80	0.20	1.07	0.43	0.59	2.09	0.31	0.05	0.16	0.57	DET	
51	967.03	3.42	0.58	0.20	1.22	1.03	2.45	0.14	0.31	0.09	0.85	AUT	III
52		3.69	0.31	0.70	0.63	0.68	2.01	0.46	0.14	0.10	0.84	DET	
53	1043.02	3.31	0.69	0.84	0.59	0.56	1.99	0.02	0.65	0.29	1.61	DET	III
54		3.54	0.46	0.33	1.18	0.93	2.44	0.04	0.23	0.05	0.55	AUT	
55	1063.00	3.26	0.74	0.12	1.50	1.12	2.75	0.10	0.12	0.05	0.39	AUT	III
56		3.77	0.23	0.54	1.02	0.64	2.20	0.13	0.10	0.14	0.47	DET	
57	1113.02	3.69	0.31	0.64	0.93	0.75	2.32	0.04	0.08	0.14	0.34	AUT	III
58		3.78	0.22	0.79	0.57	0.65	2.01	0.12	0.16	0.08	0.52	DET	

Tab. 4B. EDS microanalyses have been used to calculate the structural formulae of smectites on the basis of $O_{10}(OH)_2$.

Furthermore, as aforementioned, detrital smectites were identified in the fine-grained matrix, and contamination by Ca, Na or K from other phases present in the matrix (e.g. small calcite grains, plagioclases and K-feldspars) can occur. This could explain why some of the detrital smectite analyses show interlayer charge > 1.

Figure 11 shows a frequency histogram of octahedral site occupancy of detrital and authigenic smectites. Detrital smectites belong predominantly to class 1.90 - 2.09, thus confirming the dioctahedral nature of this phyllosilicate. On the contrary, authigenic smectites show a more variable behavior and most of the values fall into class 2.50 - 2.69, our data probably represent analyses of intimately mixed species (Abad *et al.*, 2003; Jiménez-Millán *et al.*, 2008), therefore representing mixed compositions with a predominant trioctahedral character.

Authigenic smectites have intermediate composition, between dioctahedral and trioctahedral field and a minor number of analyses clearly corresponding to dioctahedral compositions. The limit between the detrital and authigenic smectitic areas seems to fall in the class 2.10 - 2.29.

Figure 12 shows the evolution of the chemical composition of smectites with depth. An increase of the trioctahedral character from top to the bottom of the sequence can be recognized by the higher Mg content and particularly by the increase of the octahedral site occupancy. The change in Fe content is less patent, for which the chemical change with depth affect more the saponitic than the nontronitic component. The most significant change in smectite composition occurs in the range between 400 and 600 mbsf (Fig.15).

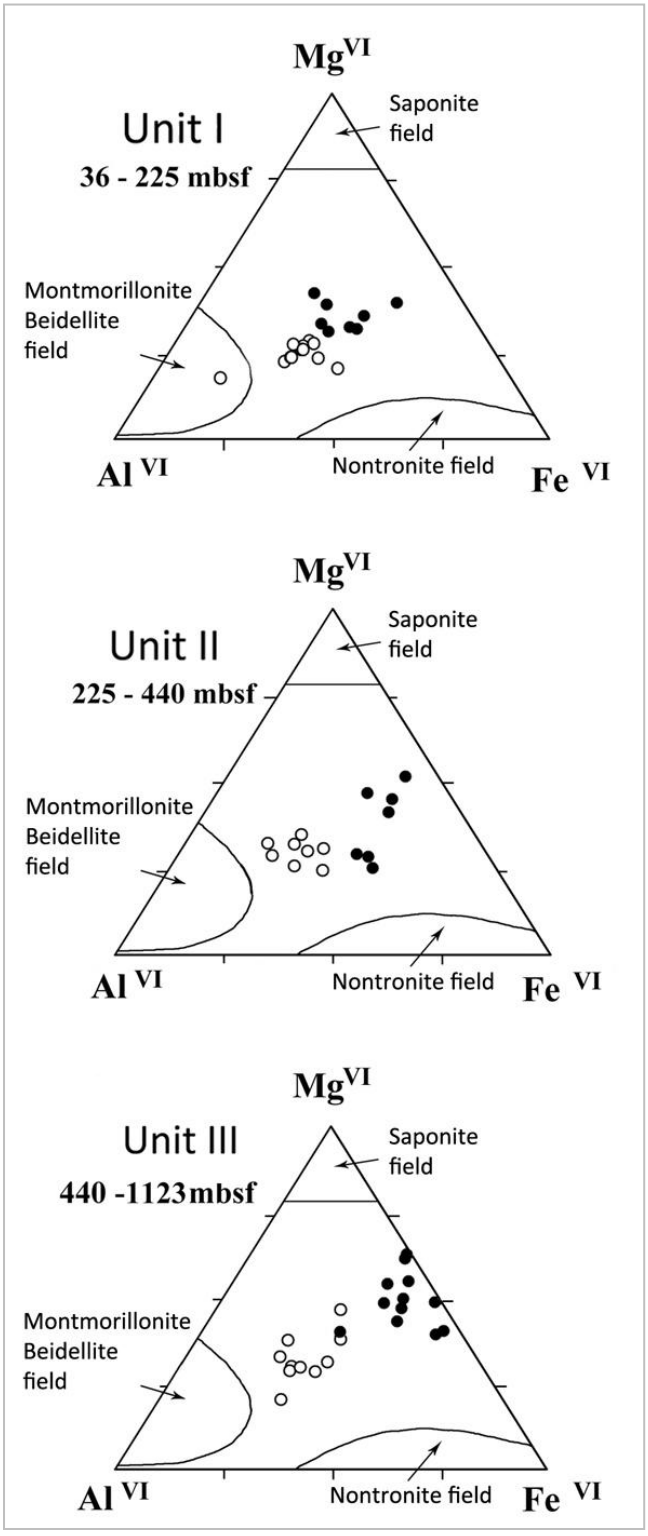

Fig. 10. Ternary Al^{VI} - Mg^{VI} - Fe^{VI} diagram of octahedral site composition of the smectites from different units (black circles indicate authigenic smectites, while white circles display detrital smectites). The montmorillonite-beidellite field usually includes detrital smectites, while saponite and nontronite field comprises authigenic phases.

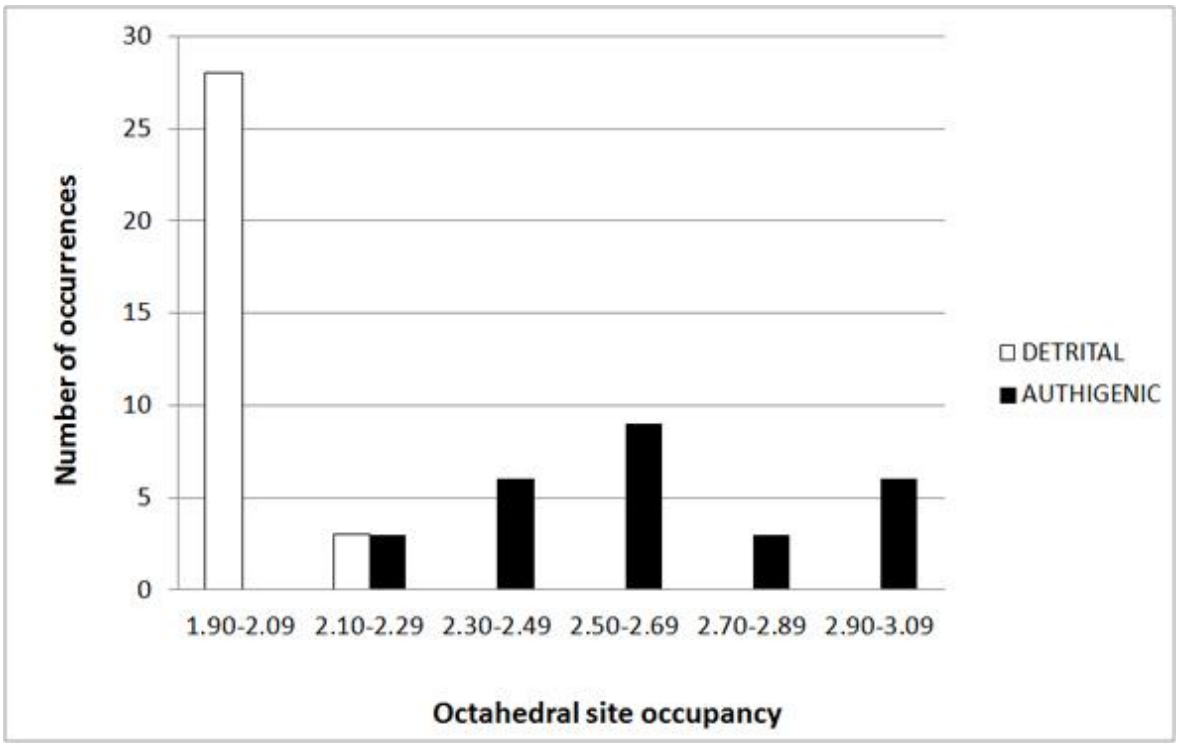

Fig. 11. Frequency histogram of octahedral site occupancy of detrital and authigenic smectites.

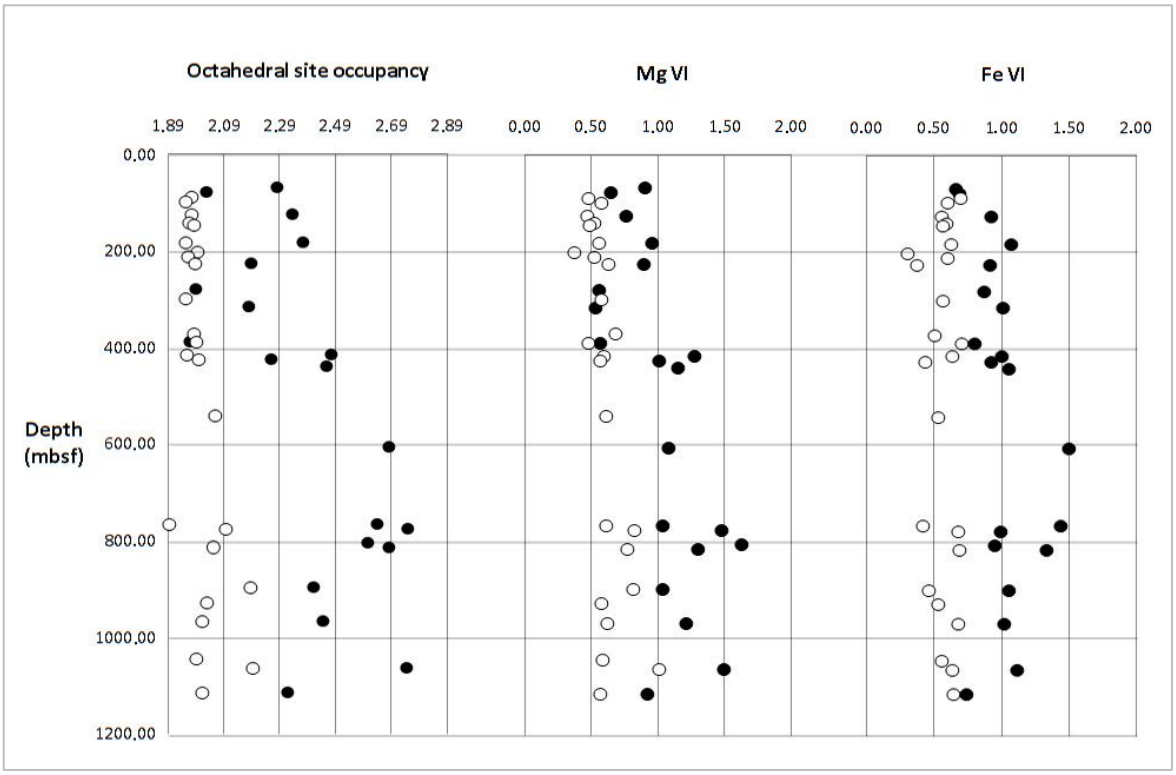

Fig. 12. Plot of the chemical composition of smectites with depth (black circles indicate authigenic smectites, while white circles display detrital smectites).

4.2. Heavy minerals

The mineralogy of glacial and glaciomarine sediments deposited on the Antarctic continental margin is a powerful tool to understand the subglacial and glaciomarine processes which occur in subglacial, ice shelf, and open ocean environments.

Heavy mineral analysis is one of the most sensitive and used techniques in the determination of sandstone provenance. In fact, heavy mineral data provide constraints on the mineralogical nature of the source rocks. One of the main advantages of heavy mineral analysis is that these kind of minerals are resistant to chemical and physical alteration, as well as to transport and therefore a wide variety of detrital heavy minerals has been found in sandstones (Morton & Hallsworth, 1999).

The study of heavy minerals is one of the most common mineralogical method employed to characterize marine sediments and to obtain information on sediment provenance areas which might allow us to identify sedimentary processes that depend on environmental and climatic conditions (Morton, 1985; Rimington *et al*., 2000).

The heavy-mineral composition of glacial sediments has long been of interest in both ore exploration (Zeschke, 1961; Brundin & Bergstrom, 1977; McClenaghan *et al*., 2000; McClenaghan, 2005) and glacial studies. Glacial studies include subjects such as till provenance, till stratigraphy, and the processes which involve erosion and transport of glacial debris (Dreimanis & Vagners, 1972; Peuraniemi, 1990; Shilts, 1996; Passchier, 2007). More recently, the heavy-mineral composition in deposits on the margins of large continental ice-sheets has received attention because of its potential in reconstructing ice-sheet drainage patterns and ice-sheet dynamics (Gravenor, 1979; Passchier, 2001; Damiani & Giorgetti, 2008; Giorgetti *et al*., 2009; Hauptvogel & Passchier, 2011). Studies of the behaviour of continental ice-sheets are important because of the global effects of changes

in ice-sheet volume. Knowledge of the location and timing of major ice drainage paths is fundamental for reconstructing former continental ice-sheets (Stokes & Clark, 2001). The main controls on ice-flow patterns are the position of snow-accumulation areas and subglacial topography. During glaciation of a continent, the main snow-accumulation areas change in response to climatic and glaciological effects. However, these properties alone usually indicate the youngest drainage stage of an ice-sheet and preclude interpretations of changing sediment transport paths during past glaciation. Compositional analyses of tills reflect the pathways of glacial dispersal and the sequence of erosional events. Nevertheless bulk geochemical analyses have become a common practice in discerning till provenance due to the availability of inexpensive analytical techniques (McClenaghan *et al*., 2000), a study of the sand and gravel-sized fraction of till is necessary to identify all the sediment sources (Shilts, 1996; Morton & Hallsworth, 1999).

Heavy-mineral assemblages in glacial sediments are controlled by three main factors (Passchier, 2007): (1) the composition of the source rock, (2) the mechanical resistance of minerals to crushing and abrasion during glacial transport, and (3) dissolution caused by diagenesis and chemical weathering at different stages of glacial-interglacial sedimentation (Dreimanis & Vagners, 1972; Gravenor, 1979). Microscopic analyses of heavy-mineral assemblages are usually carried out on the sand fraction, where the effects of mechanical and chemical processes on the heavy-mineral composition are best identified. However, the subdivision of components in a till during glacial transport causes some minerals, for example phyllosilicates, to be underrepresented in the heavy-mineral separates.

Heavy mineral assemblages in Antarctic marine sediments can be successfully used to identify different source areas and to reconstruct the dynamics of ice sheets (Ehrmann & Polozek, 1999; Polozek, 2000; Neumann, 2001; Passchier, 2001; Damiani & Giorgetti, 2008; Giorgetti *et al*., 2009; Hauptvogel & Passchier, 2012).

4.2.1. Heavy minerals composition and down-core distribution

The heavy mineral assemblage in sediments from AND-2A drill core is dominated by pyroxenes (augite, titanaugite, aegirine, orthopyroxene and hedenbergite) spinels and ilmenites, whereas amphiboles, carbonates and chemically stable minerals (such as zircon, tourmaline, garnet, rutile and epidote), usually common in sediments (Morton & Hallsworth, 1999), are present only in minor amount (Tab. 5A and 5B). The chemical compositions of the main silicates are presented in table 6.

Six types of pyroxenes have been recognized on the basis of their chemical composition (Tab. 6).

Clinopyroxene 1 corresponds to low-Ca augite that falls in the chemical composition field of Ferrar Province (Fig. 13). Augites (Tab. 6, Fig. 13) usually show a rounded/sub-rounded shapes and clearly visible cleavage planes (Fig. 14B). Clinopyroxene 2 and titanaugite (Tab. 6, Fig. 13) show very similar composition except for the different amount of both Ti and Al and fall in the McMurdo Volcanic Province field (Fig. 13). Clinopyroxene 2 shows a chemical composition of diopside. Titanaugite and clinopyroxene 2 are the most abundant phases and occur as very irregular crystal with visible hacksaw terminations (Fig. 14A and 14C, respectively). Due to their chemical and morphological similarities these two types of pyroxenes have been put in the same group called *MVG (McMurdo Volcanic Group) clinopyroxene*.

Hedenbergites (Tab. 6, Fig. 13) usually display euhedral crystals (Fig. 14D).

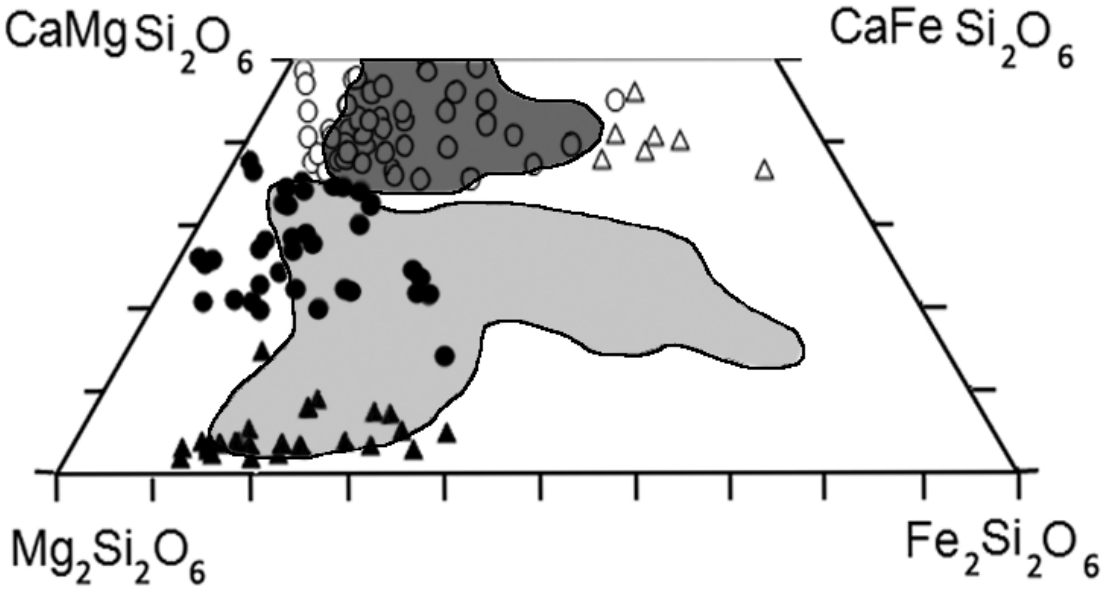

Fig. 13. Chemical compositions of pyroxenes from the AND-2A samples. Fields representing chemical composition of pyroxenes from the McMurdo Volcanic Province (after Gamble *et al*., 1986) (dark grey) and from the Ferrar Province (after Haban & Elliot, 1985) (light grey). Open circles: Titanaugite from the MGV and clinopyroxene 2; Black circles: clinopyroxenes 1 from the Ferrar Group; black triangles: Orthopyroxene from the Ferrar Group; White triangles: hedenbergite from the Granite Harbor Intrusive Complex.

Aegirines were not plotted on the quadrilateral of pyroxenes since their composition is sodic and a different plot is needed. They generally show a good cleavage (Fig. 14E).

Orthopyroxene group (Tab. 6, Fig. 13) comprises Mg-rich pyroxene, including pigeonites. Orthopyroxenes usually show an elongated shape with visible cleavage (Fig. 14F).

Three types of amphiboles have been distinguished: hornblende, kaersutite and ortoamphibole gedrite (Tab. 6, Fig. 14K and 14L).

Apatite grains occur with two kind of morphology: apatite 1 (angular apatite) shows euhedral crystal with visible crystal faces (Fig. 14G) whereas apatite 2 (rounded apatite) shows sub-rounded-shaped crystals with fracture plates (Fig. 14H).

Spinels and ilmenites are quite common phases and occur as sub-euhedral crystals (Fig. 14I).

Garnet grains have a chemical composition varying from the almandine member to spessartine and grossular (Tab. 6). They usually occur with sub-rounded shapes and smooth edges (Fig. 14J).

An aluminosilicate (Al_2SiO_5) has been also recognized. Carbonate grains with different composition have been identified: a carbonate with only Ca and a carbonate grain with dolomitic composition. They have been put in the same group called *carbonate*.

Figure 15 shows the down-core variation of the main heavy mineral phases observed in the core.

MVG clinopyroxenes show the highest percentage as well as the highest down-core variation. In sample 1027.02 mbsf MVG clinopyroxenes are not present, whilst sample 1043.00 mbsf shows the highest percentage (83 %). MVG clinopyroxenes are particularly abundant starting from ~ 700 mbsf down-core, they show high oscillations between 887 mbsf and 1043 mbsf, displaying the highest percentages in the lower part of the core starting from 1043 mbsf.

Augites and orthopyroxenes occur throughout the core and are particularly abundant in the upper part of the investigated succession (650 - 770 mbsf) and between 890 - 1043 mbsf. The percentages of MVG clinopyroxenes and augites anti-correlate, as well as MVG clinopyroxenes and orthopyroxenes. On the contrary, augites and orthopyroxenes show a similar behaviour.

Spinels, ilmenites, apatites 1 (angular) and aegirine co-vary and they are particularly abundant between 770 mbsf and 890 mbsf, with higher percentage oscillation between 890 mbsf and 1043 mbsf. Spinels and ilmenite display a very similar trend.

Kaersutites and aenigmatites do not occur in high amount as well as they do not show a defined trend down-core.

Depth (mbsf)	Sample															
	649.99	**655.45**	**674.97**	**695.95**	**705.02**	**719.99**	**735.02**	**749.99**	**770.00**	**775.00**	**794.99**	**805.00**	**820.02**	**830.01**	**849.01**	**871.53**
MVG Clinopyroxene	11	9	22	52	45	39	52	54	27	28	30	26	40	41	53	34
Kaersutite	0	0	0	0	4	0	0	0	1	5	0	0	0	5	0	0
Spinels	4	0	4	0	5	17	6	7	2	25	13	16	20	22	8	15
Ilmenite	2	4	0	6	1	8	4	7	7	6	16	18	8	4	8	10
Apatite 1	0	0	0	1	0	0	0	0	0	0	7	3	0	0	0	0
Aegirine	1	0	0	0	1	0	1	0	0	4	5	10	10	1	0	8
Aenigmatite	0	0	0	0	0	0	0	3	0	0	0	0	0	1	0	0
Hornblende	0	0	0	0	1	2	0	0	1	0	0	8	2	1	3	2
Augite	4	1	24	7	4	13	2	1	21	15	13	15	5	5	3	5
Orthopyroxene	37	36	27	31	20	12	18	10	26	4	0	0	5	5	5	3
Garnet	8	4	1	0	2	1	6	0	9	1	2	0	0	1	0	0
Biotite	5	15	1	1	0	1	4	1	3	5	2	0	3	0	3	10
Al-silicate	0	0	0	0	0	0	1	0	1	0	0	0	0	0	0	0
Apatite 2	2	0	1	0	0	0	1	0	0	0	7	0	2	0	0	0
Zircon	1	0	0	0	2	1	1	0	0	0	0	2	0	0	0	0
Rutile	0	0	0	0	1	1	2	0	0	0	0	0	0	0	0	0
Carbonate	0	25	9	2	9	1	1	12	0	0	5	0	0	0	8	5
Sphene	3	3	6	0	1	0	1	0	0	0	0	2	0	4	0	3
Orthoamphibole	16	0	1	0	4	3	0	3	2	2	0	0	3	0	5	3
Tourmaline	1	0	0	0	0	0	0	0	0	0	0	0	0	0	0	0
Epidote	6	1	4	0	1	1	0	0	0	0	0	0	0	0	0	0
Hedenbergite	0	0	0	0	1	0	1	0	0	3	0	0	2	10	8	0

Tab. 5A. Percentage counts of heavy minerals for the first 16 samples in the lower 650 m of AND-2A.

Depth (mbsf)	Sample															
	887.57	**907.00**	**927.28**	**937.01**	**947.07**	**967.03**	**977.01**	**987.13**	**996.41**	**1007.00**	**1027.02**	**1033.00**	**1043.00**	**1073.00**	**1083.00**	**1123.20**
MVG Clinopyroxene	20	8	5	9	61	31	20	44	24	5	0	14	87	53	61	42
Kaersutite	0	4	0	0	0	8	1	0	12	0	0	0	0	0	0	0
Spinels	22	20	8	9	11	1	4	13	3	9	0	0	2	9	5	0
Ilmenite	21	12	5	6	3	7	14	3	12	6	0	4	0	25	9	3
Apatite 1	7	0	3	1	0	0	1	4	3	0	0	0	0	2	4	0
Aegirine	6	0	0	4	0	0	1	4	0	0	0	0	2	2	5	0
Aenigmatite	0	0	0	0	0	0	0	0	1	0	0	0	0	0	0	0
Hornblende	0	0	0	0	0	10	9	8	6	0	0	0	4	0	0	15
Augite	6	0	17	12	3	7	10	9	4	5	0	0	2	5	10	7
Orthopyroxene	4	0	8	9	0	0	1	0	1	12	0	0	4	0	0	0
Garnet	6	4	14	12	3	17	4	8	11	26	57	3	0	2	3	8
Biotite	4	23	4	11	0	6	2	0	1	11	4	52	0	2	0	0
Al-silicate	0	0	0	0	0	0	0	0	0	4	0	0	0	0	0	2
Apatite 2	3	4	4	6	0	2	5	1	5	7	0	3	0	2	0	7
Zircon	0	3	1	2	0	1	2	2	0	0	0	1	0	0	0	0
Rutile	0	1	0	0	0	0	1	2	0	0	0	1	0	0	0	0
Carbonate	0	0	26	16	17	0	4	0	8	10	0	0	0	0	0	2
Sphene	1	3	3	2	3	0	6	0	0	5	0	4	0	0	4	3
Orthoamphibole	0	16	0	0	0	8	12	2	8	0	25	16	0	0	0	8
Tourmaline	1	1	0	0	0	3	0	0	3	0	14	0	0	0	0	0
Epidote	0	1	3	0	0	0	5	2	0	0	0	0	0	0	0	3
Hedenbergite	0	0	0	0	0	0	0	0	0	0	0	0	0	0	1	0

Tab. 5B. Percentage counts of heavy minerals for the last 16 samples in the lower 650 m of AND-2A.

Mineral	Data type	Na_2O	MgO	Al_2O_3	SiO_2	K_2O	CaO	TiO_2	Cr_2O_3	Mn	Fe
Clinopyroxene 1	Average	0.98	17.76	3.04	53.29	0.23	14.98	0.32	0.24	0.34	8.84
	STDEV	0.36	2.97	1.90	1.74	0.31	4.22	0.13	0.17	0.21	5.28
Clinopyroxene 2	Average	0.86	13.74	1.64	52.32	0.09	23.16	0.23	0.39	0.50	7.10
	STDEV	0.30	2.80	0.77	1.70	0.08	1.53	0.19	0.20	0.18	3.04
Titanaugite	Average	1.05	13.94	6.33	47.79	0.05	20.48	2.27	0.20	0.23	7.66
	STDEV	0.30	1.28	1.23	1.56	0.05	1.60	0.74	0.12	0.14	1.13
Orthopyroxene	Average	1.21	23.83	2.49	55.18	0.21	2.48	0.27	0.22	0.48	13.65
	STDEV	0.53	4.18	1.04	2.24	0.12	1.01	0.09	0.14	0.10	4.40
Aegirine	Average	14.85	1.50	2.08	55.94	0.15	0.75	1.84	0.11	1.06	21.71
	STDEV	1.38	0.62	0.85	1.79	0.12	0.69	0.90	0.04	0.53	1.56
Hedenbergite	Average	1.60	3.06	1.13	47.52	0.12	18.94	0.61	0.16	1.48	25.39
	STDEV	0.53	1.56	0.16	2.50	0.04	1.77	0.16	0.11	0.20	3.87
Hornblende	Average	1.67	12.40	12.27	48.50	0.74	11.74	1.04	0.24	0.55	10.84
	STDEV	0.12	0.91	2.10	1.29	0.35	3.46	0.74	0.21	0.04	4.13
Kaersutite	Average	2.15	9.16	13.18	42.52	2.13	8.82	3.23	0.10	0.46	18.24
	STDEV	0.78	2.27	2.49	4.26	1.49	4.08	1.21	0.09	0.21	5.26
Garnet	Average	0.69	1.02	19.34	40.38	0.02	32.47	0.85	0.29	0.34	4.63
	STDEV	0.45	0.61	3.05	1.39	0.03	0.42	0.91	0.08	0.02	2.14
Garnet	Average	0.79	8.38	22.62	41.54	0.07	1.48	0.14	0.19	0.86	23.96
	STDEV	0.78	2.86	0.50	0.92	0.04	0.71	0.08	0.08	0.46	3.93
Garnet	Average	0.55	4.55	21.76	39.58	0.10	1.05	0.17	0.26	17.47	14.55
	STDEV	0.45	0.19	0.40	1.41	0.02	0.12	0.02	0.02	3.66	2.55
Gedrite	Average	0.97	8.65	21.94	40.55	0.17	2.66	0.20	0.21	0.92	23.71
	STDEV	0.50	2.36	0.92	1.84	0.03	2.91	0.10	0.12	0.34	3.72

Tab. 6. Average chemical compositions of abundant heavy minerals as determined by SEM-EDS analysis. Averages are based on several grains from different locations in the AND-2A drill core.

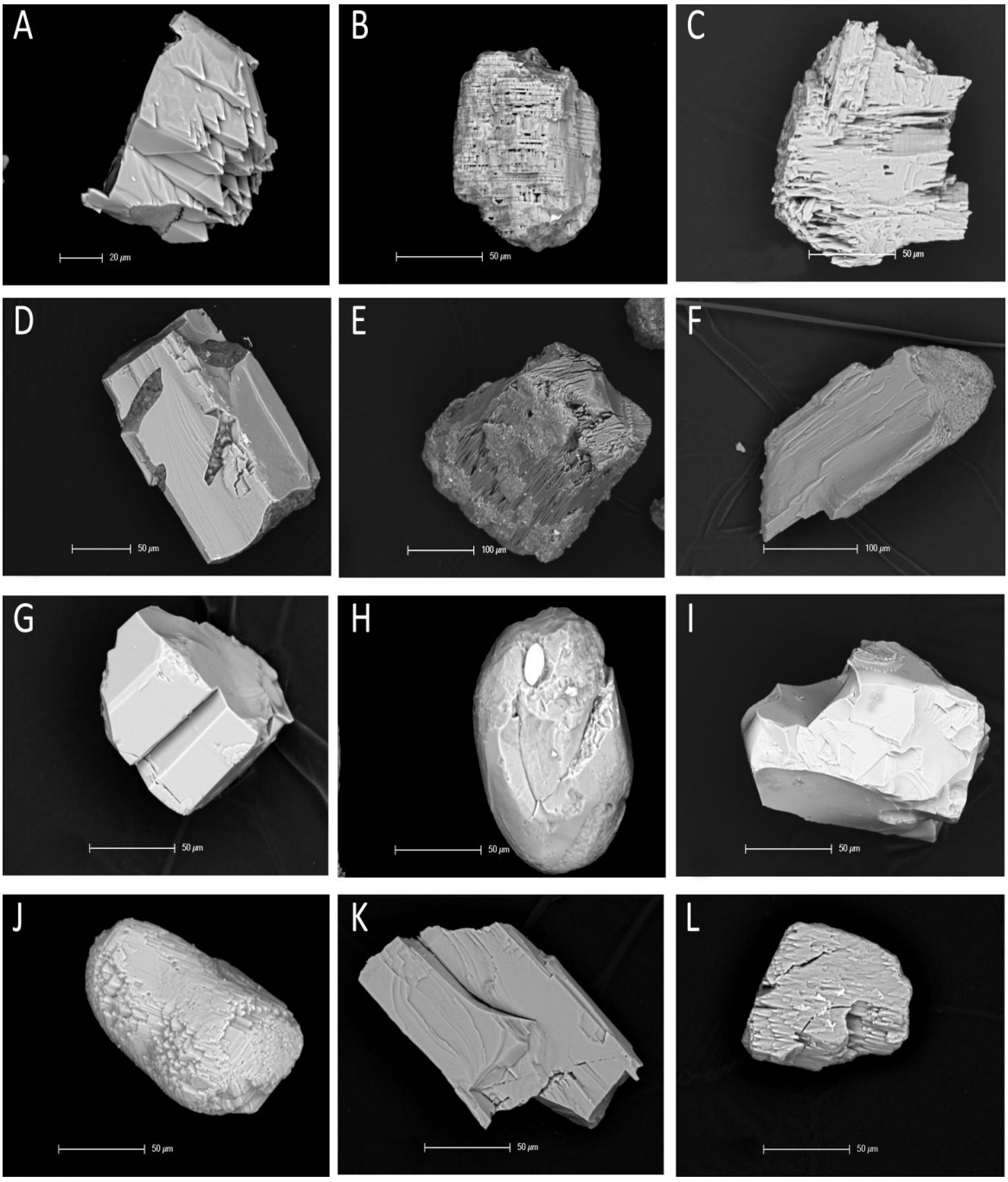

Fig. 14. SEM backscatter image of the most common heavy minerals in AND-2A drill core.
A) titanaugite with hacksaw terminations from sample 987.13 mbsf. B) clinopyroxene 1 with visible cleavage at 987.13 mbsf. C) clynopiroxene 2 with no visible cleavage and hacksaw termination at 705.02 mbsf. D) hedenbergite grain at 820.02 mbsf. E) aegirine at 820.02 mbsf. F) orthopyroxene grain at 655.45 mbsf. G) angular apatite (apatite 1) grain at 996.41 mbsf. H) rounded apatite (apatite 2) grain at 987.13 mbsf. I) spinel at 820.02 mbsf. J) subrounded garnet grain at 907.00 mbsf. K) hornblende grain at 967.03 mbsf. L) kaersutite from sample 967.03 mbsf.

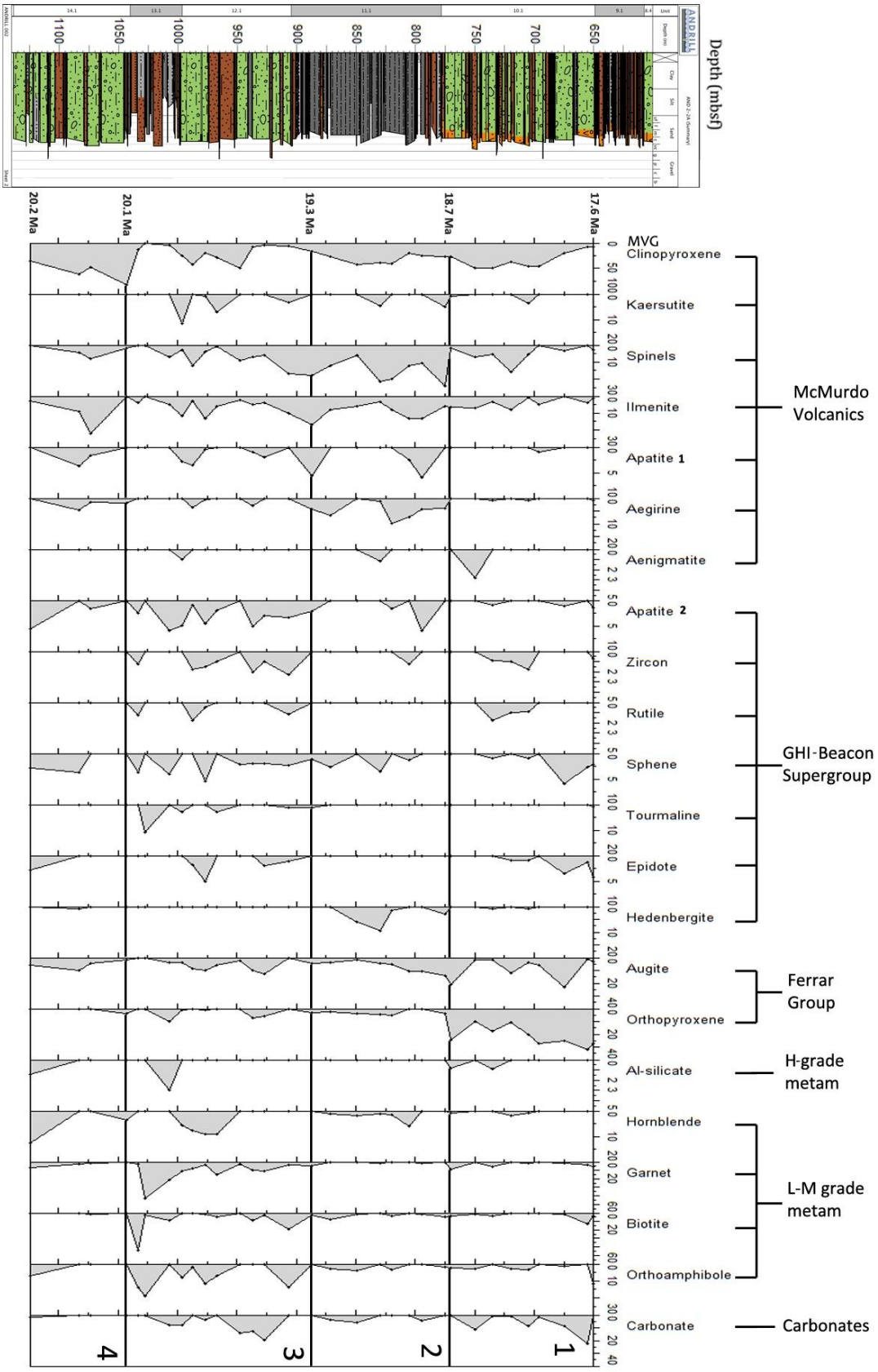

Fig. 15. Down-core variation of the main heavy mineral phases present in AND-2A drill core. Groups of sediment provenance are taken from Hauptvogel & Passchier (2012). GHI indicates Granite Harbour Intrusive.

Rutiles and zircons are quite abundant in interval 700 - 750 mbsf and between 890 and 1043 mbsf, and they show a similar down-core trend. Sphenes and epidotes show a very similar behavior since they are present in the upper part of the investigate succession, between 650 and 700 mbsf, show high oscillations in the interval 890-1043 mbsf, and are present again starting from ~ 1075 mbsf.

Garnets are quite abundant especially in the interval between 890 and 1043 mbsf and they show the highest percentage at 1027 mbsf (43 %). Garnets and MVG Clinopyroxenes seem to show a negative trend.

Biotites and orthoamphibole show a similar down-core variation. They occur throughout the core and are particularly abundant in the interval between 890 and 1043 mbsf.

Carbonates are very abundant in the interval between 650 and 770 mbsf and in the interval between 890 and 1043 mbsf. They display a negative trend with MVG clinopyroxenes.

Al-silicates show very low percentages. Nonetheless, they are present in the interval between 730 and 770 mbsf, in sample 1007.00 mbsf, and in the lower part of the investigate succession at 1123.20 mbsf.

5. Discussion and conclusions

5.1. Clay minerals

The clay mineral assemblage of sediments from AND-2A drill core is dominated by smectite and illite, with minor chlorite and traces of kaolinite. Smectite and illite show the highest oscillations. Relying on clay mineral variations, it was possible to subdivide the sediment core in three Units named I to III from top to bottom.

In Unit I smectite and illite are quite constant and chlorite shows large fluctuations. In Unit II smectite content decreases and illite content increases, while chlorite content slightly decreases and shows lower fluctuations. Unit III is characterized by high smectite-illite fluctuation, while chlorite displays moderate fluctuations.

In marine sediments clay mineral assemblages are strongly controlled by source rock compositions, physical - chemical weathering, transport and depositional mechanisms (Biscaye, 1965; Ehrmann *et al*., 1992a; Diekmann *et al*., 1996). Source areas and weathering type control the different clay mineral assemblages, while transport and sedimentation mechanisms may cause a selective enrichment of the different mineralogical phases. Consequently, clay minerals from Antarctic marine sediments have been interpreted to reflect changes in source areas as tracers of paleo-ice stream directions (Petschick *et al*., 1996), to check weathering styles with respect to paleoclimatic changes (Ehrmann & Mackensen, 1992; Ehrmann, 1998a), and for paleoceanographic reconstructions (Diekmann *et al*., 1996).

Detrital smectites are normally the result of chemical weathering under warm and humid climatic conditions in areas with very slowly moving water and contrasting dry and wet seasons (Chamley, 1989). Under a cold climate with predominant physical weathering,

high smectite concentrations commonly indicate a source area that is characterized by volcanic rocks (Ehrmann *et al*., 1992b; Ehrmann, 1998). High smectite concentrations have been reported from glaciomarine sediments in areas with basalt in the hinterland (Ehrmann *et al*., 1992a), showing that basalt can provide considerable amounts of smectite under a glacial climate. In AND-2A core, detrital smectites most likely derive from McMurdo Volcanic Group rocks located south to the drill site. Illite and chlorite are typical clay minerals of high latitudes indicating the predominance of physical weathering. They generally form by weathering of crystalline rocks, such as those cropping out in the Transantarctic Mountains (Fig. 3). Although illite tends to be derived from acidic crystalline rocks (Biscaye, 1965; Griffin *et al*., 1968), the sediments of the Beacon Supergroup also contain illite and therefore they may represent possible source rocks (Ehrmann *et al*., 2005). Illite cannot form in situ in the marine environment (Griffin *et al*., 1968).

Among these four clay minerals, smectite is the only one that can occur either as detrital or authigenic. The occurrence of authigenic smectites may conduct to incorrect palaeoclimatic interpretations. Therefore differentiating between detrital and authigenic phases is of utmost importance in order to avoid errors in paleoclimatic interpretation.

Recent studies on clay minerals in the sequences collected near Cape Roberts have attempted to discriminate detrital and authigenic clay minerals (Setti *et al*., 2001, 2004; Wise *et al.* 2001; Ehrmann *et al*., 2005; Giorgetti *et al*., 2007). Authigenic clay minerals may provide indications of post-sedimentary processes and geochemical conditions (Chamley, 1989; Weaver, 1989; Setti *et al*., 2004; Ehrmann *et al*., 2005). Franke & Ehrmann (2010) performed a semi-quantitative analysis of the clay mineral assemblages in sediments from ANDRILL AND-2A drill core, but they did not focus on a detailed and systematic observation of authigenic and detrital smectites and on their chemistry.

Wise *et al*. (2001) and Giorgetti *et al*. (2007) performed textural investigations on authigenic smectites from CRP-3 Project and found out a mechanism of fluid circulation for the formation of authigenic smectites. In particular, Giorgetti *et al.* (2007) found out that authigenic clay assemblages do not change down-core, but they do vary in chemically different rocks, i.e. newly formed dioctahedral smectites occur in sediments, whereas newly formed trioctahedral smectites are dominant in mafic rocks. Chamley (1989) has reported that Mg and Fe-Mg smectite are the main clay minerals derived from submarine alteration of volcanic rocks. As aforementioned, volcanic material is persistent throughout the AND-2A core and is the dominant clast type (> 50%) in nine of the 14 lithostratigraphic units (Panter *et al*., 2008-2009). AND-2A fresh glass is mafic, strongly Si-undersaturated and very similar to mafic-intermediate EVP (Erebus Volcanic Province) whole rock data (Nyland *et al*., 2011). Most of the lava clasts from LSU 1 are mafic and Si-undersaturated, whole-rock compositions vary from basanite to tephrite and hawaiite.

Franke & Ehrmann (2010) have compared the smectite concentrations with the number of volcanic clasts in the sediments from the same drilling-core studied here. In some intervals, smectite peaks correlate with high numbers of volcanic clasts and they may be interpreted as resulting from productive volcanic activity and/or high influx of volcanic erosional products from the south. However, in other intervals, smectite peaks correlate with low numbers of volcanic clasts. In these intervals, the high smectite contents are evidently not caused by volcanic activity and/or erosion of volcanic material. The occurrence of authigenic smectites associated with other newly-formed minerals (calcite, framboidal pyrite) in the intervals indicates that the high smectite contents were probably caused by diagenetic processes. Previous investigations of submarine diagenesis in volcaniclastic successions from Ocean Drilling Program Leg 126, similar to that investigated by ANDRILL SMS project, demonstrate that the main alteration processes are the formation

of hydrous secondary minerals such as phyllosilicates, zeolites, calcite precipitation and the hydration of volcanic glass (Marsaglia & Tazaki, 1992; Gifkins *et al*., 2005).

In the upper part of the sedimentary sequence, corresponding to Unit I (36 - 225 mbsf) and Unit II (225 - 440 mbsf) smectites are both detrital and authigenic: the detrital ones display a chemistry close to montmorillonite and beidellite field, showing a flaky structure, generally considered of detrital origin (Setti *et al*., 2000; Ehrmann *et al*., 2005).

In the lower part of the drilling core, Unit III (440 - 1123 mbsf), detrital and authigenic smectites are also recognized and they display the same morphologic features of smectites from Unit I and II, while the chemistry of both detrital and authigenic smectites changes starting from ca. 440 mbsf (Fig. 12). The most of the authigenic smectites show a Mg-Fe-rich composition associated to hairy shape and honeycomb feature, regarded to be of neoformation origin (Chamley, 1989; Buatier *et al*., 2002). The change with depth of the alteration products is characteristic of a diffuse hydrothermal ore complex indicating proximity to active volcanic complexes. This explanation is also corroborated by a high geothermal gradient inferred from the high down-hole temperatures. Detrital and authigenic smectitic crystals from Unit III show slightly lower content of Al and the chemical composition of authigenic smectite is closer to saponite-nontronite series, which implies that the proportion of Mg-rich and Fe-rich smectites in the analysed areas has increased in relation to the proportion of beidellite-montmorillonite. However, composition of honeycomb authigenic smectites grown on feldspar grains (i.e. 1113.02 mbsf) is Al-richer, and this feature depends on the aluminous chemical nature of the parent material (Drief *et al*., 2001).

The increase in Mg and Fe with respect to Al may be explained by an important increment of volcanic material alteration related to early diagenesis processes in the lower part of the core. Evidences for the early diagenesis hypothesis can be found in the presence of fracture

filled by authigenic smectites (Fig. 16A), and iron sulfide (pyrite) formation of diagenetic origin (Fig. 16B).

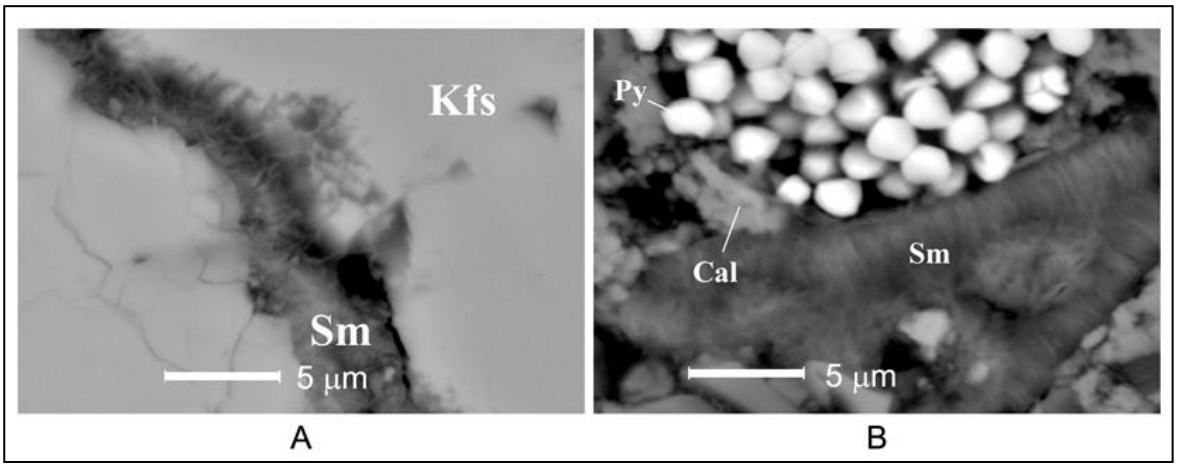

Fig. 16. A) SEM-BSE image showing a fracture in a K-feldspar grain (Kfs) filled by hairy shape smectite (Sm) of authigenic origin in sample 775.00 (Unit III). Mineral abbreviations after Kretz (1983). B) SEM-BSE image of sample 825.80 (Unit III) showing a newly-formed hairy shape smectite (Sm) in association with framboidal pyrite (Py) and authigenic calcite (Cal). Mineral abbreviations after Kretz (1983).

Pyrite is a common mineral product of early diagenesis in organic-rich sediments. It results from the reaction of sulfide (produced via bacterial sulfate reduction, Berner, 1970, 1980). Fielding *et al*. (2008-2009) found out that pyrite is nearly absent above 430 mbsf, but it becomes common to abundant at greater depths. In some intervals (555 - 597 mbsf; 775 - 828 mbsf; 958 - 1011 mbsf and below 1043 mbsf) pyrite imparts a black color to the sediments and obscures primary sedimentary features. In addition, below ca. 440 mbsf a coarser form of pyrite occurs alone or in association with calcite within late-stage fractures. SEM investigations allowed us to identify pyrite in association with newly-formed smectite and calcite (Fig. 16B) and these findings confirmed what has been observed by Fielding *et al*. (2008-2009). It is noteworthy to highlight that the higher smectite contents occur in the zone of pyritization (Fig. 7) described by Fielding *et al*. (2008-2009). In these intervals authigenic smectite close to saponitic-nontronitic composition are also predominant, thus confirming a possible correlation with volcanic material alteration coupled with early diagenetic processes. Moreover, smectite crystallinity shows lower

values (higher crystallinity) in correspondence with pyritization intervals (Fig. 8) thus confirming the possible role of circulation of fluid in altering volcanic material.

The upper part of the investigated sedimentary succession (Unit I and Unit II) is characterized by the lower amount of diagenetic processes, as testified by the low percentage of diagenetic calcite (Fielding *et al*., 2008-2009) and the absence of diagenetic pyrite. In these two Units, illite and chlorite, which are detrital clay minerals, reach the highest content. These features indicate the dominant detrital nature of these sediments and the absence of diagenesis in the upper part of the core.

Another significant change in the behavior of the smectite/illite ratio along the stratigraphic column is that Units I and II present a quite stable ratio, generally with relatively low smectite content and higher illite content; on the contrary, in Units III the changes in the ratio are abrupt from sample to sample. Furthermore, in Units III the samples with low smectite content present clay mineral content values very similar to those of Units I and II whereas some other samples, randomly distributed along the Unit III, show smectite content three or four times higher than the former, reaching in some cases values of 100%. Do Campo *et al*. (2010) described a similar scenario for the beginning of the volcanic activity in the Palaeogene Andean foreland of Northwestern Argentina. Through SEM textural images, mineral composition and smectite chemical data, they demonstrated that the samples showing anomalously high smectite content represented episodes of volcanic input to the basin. The rest of the samples showed a low smectite content of detrital origin. In a similar way, we interpret that in all the samples showing low smectite content, the detrital origin of smectite is the predominant one and the peaks showing major smectite content in Units III correspond to some influence of volcanic activity.

Smectites in AND-2A drill core show very high composition variability, with frequent analyses well in the compositional gap between di- and tri-octahedral smectites, which

supports the fact that authigenic and detrital phases are both present and intimately mixed. Some of the smectite analyses show high interlayer charge and/or low Si content; these chemical characteristics could represent illite/smectite interstratified minerals. Even if a detailed transmission electron microscopy (TEM) study would be required to confirm or rule out such interstratification, their presence in the McMurdo sediments is probable. Metamorphic rocks are exposed in the Transantarctic Mountains, including low-grade metasedimentary rocks of the Skelton Group in the area near the Skelton Glacier (Cook & Craw, 2002). Such rocks could have supplied to the sedimentary basin illite-smectite interstratified minerals, a typical component of very-low grade metamorphic rocks. Furthermore, we have to take into account the possibility of analytical contamination by Ca, Na and K coming from other mineralogical phases. In the whole AND-2A drill core, in fact, both calcite and feldspars are widespread from the top to the bottom of the succession (Fig. 16).

Although authigenic smectite occur throughout the core, smectites in Unit I and II are predominantly detrital and they formed through weathering of volcanogenic source rocks. Detrital smectites are essentially di-octahedral Fe-Al members of the beidellite-montmorillonite-nontronite series. The most probable source for detrital smectites are the eruptive centers located at the south of the drill core.

Newly formed smectites in the central and in the lower part (Unit III) of the sequence are richer in Mg and Fe and poorer in Al, and their compositional fields are closer to saponite and nontronite field. The presence of authigenic smectites in central and lower part of the sequence was presumably attributed to chemical alteration of volcanic rock fragments and glass shards coupled with early diagenetic processes.

5.2. Heavy minerals

As aforementioned, the presence of authigenic smectites in central and lower part of the investigated sedimentary succession do not provide a robust proxy for palaeoenvironmental and palaeoclimatic conditions. Between 400 and 650 mbsf the most significant change in chemical composition of smectites occurs (Fig. 12). This interval represents a crucial point in the palaeoenvironmental and palaeoclimatic interpretations of the Early Miocene sedimentary succession of the McMurdo Sound Area. In order to better reconstruct the sediment provenance, a detailed heavy mineral analysis below 650 mbsf was performed.

5.2.1. Heavy mineral sources

Heavy mineral assemblages in sediments can be related to their source rocks through both their chemical composition via SEM-EDS and optical characteristics (Ehrmann & Polozek, 1999; Passchier, 2001; Damiani & Giorgetti, 2008; Hauptvogel & Passchier, 2012) and they can be used to identify changes in source regions (Gwyn & Dreimanis, 1979; Passchier, 2007; Damiani & Giorgetti, 2008; Giorgetti *et al*., 2009; Hauptvogel & Passchier, 2012). In order to establish the main source rocks of heavy mineral assemblages, we have based our provenance reconstructions on sediment sources identified by previous authors who analyzed the upper 650 meters of AND 2A drill core (Hauptvogel & Passchier, 2012). In such way, the different heavy minerals recognized in the lower 650 mbsf of AND-2A core can be related to six main source rocks (Tab. 7): (1) McMurdo Volcanic Group rocks are located directly to the south of the drill-site (Fig. 17), (2) Ferrar

Group, (3) high-grade metamorphic basement rocks, as well as (4) Carbonates are located in the upland regions of the Transantarctic Mountains (Fig. 17), (5) Granite Harbour Intrusives-Beacon Supergroup, and (6) low to medium grade metamorphic rocks are exposed along the coast of the Transantarctic Mountains (Fig. 17).

Source rock	Heavy mineral assemblages
McMurdo Volcanic Group	MVG clinopyroxene (Titanaugite and clinopyroxene 2), aenigmatite kaersutite, spinels, ilmenite, angular apatite
Ferrar Group	Clinopyroxene 1 (augite), orthopyroxene
High grade metamorphic	Andalusite, kyanite, sillimanite
Carbonates	Calcite, dolomite
Granite Harbour Intrusive - Beacon Supergroup	Rounded apatite, zircon, sphene, tourmaline, epidote, rutile, hedenbergite
Low to medium grade metamorphic	Hornblende, garnet, biotite, orthoamphibole

Tab. 7. Source of heavy minerals in the lower part of AND-2A drill core.

McMurdo Volcanic Group (MVG) **-** Basic volcanic rocks of McMurdo Volcanic Group are the source of titanaugite and clinopyroxene 2 (high-Ca augite). The titanaugite compositions clearly fall within the field of MVG clinopyroxene (Fig. 13). This type of clinopyroxene represents the most abundant phenocrysts in the McMurdo Volcanic Group lavas (Gamble *et al*., 1986; George, 1989; Kyle, 1990). Its euhedral shape in the AND-2A sediments indicates that it has not experienced processes of prolonged transport.

Trachytes, hornblende basalts and trachyandesites of MVG are the most likely source for kearsutite (Kyle, 1990; LeMasurier & Thomson, 1990). Moreover, kaersutite is a typical mineral in lava deposits on Minna Bluff (Pompilio *et al*., 2007; Dunbar *et al*., 2008). Spinels and ilmenite are typical accessory constituents of Mt. Erebus phonolite (Kyle & Price, 1975; Kyle, 1990). MVG volcanic rocks are also the source of angular apatite grains. Martin (2009) and Martin *et al.* (2010) have shown that Mount Morning eruptive center is a potential source of aenigmatites and aegirines.

Ferrar Group **-** Jurassic basalts and dolerite of the Ferrar Group in the Transantarctic Mountain are the most likely source for augites (low-Ca augite) as well as for Mg-rich clinopyroxenes and orthopyroxenes (Haban & Elliot, 1985; Armienti *et al*., 1998).

The chemical compositions of augites plot in the field of Ferrar Supergroup clinopyroxenes (Haban & Elliot, 1985; Gamble et al., 1986). The augites with a strong cleavage and subrounded shape (Fig. 14B) have been named "Ferrar type" in many studies (e.g., Cape Roberts Science Team, 1998), and they probably originated from Ferrar Dolerites. Tholeitic igneous rocks from the Ferrar Group are the most likely source for enstatites (Armienti *et al*., 1998; Marsh, 2004; Bedard *et al*., 2007; Zavala *et al*., 2011).

High-grade metamorphic rocks (H-grade metamorphic) **-** The high-grade metamorphic rocks of Koettliz Group located to the north of Koettlitz Glacier could have provided the high-grade metamorphic minerals. Under SEM, it is impossible to discriminate between sillimanite, kyanite and andalusite, hence we decided to put them in the same group called *Al-silicates*. Hauptvogel & Passchier (2012) reported that kyanite, not being a common constituent in these rocks, probably requires a contribution of rocks from the Nimrod Group further south. In addition, Passchier (2001) has found out that large grains of sillimanite occur in the meta-quartzite of Nimrod Group. Nonetheless, due to the low amount of Al-silicate found in the investigated sediments, is likely to infer that these heavy mineral derive from more local sources.

Carbonates **-** Anthill Limestone (Gunn & Warren, 1962; Skinner, 1982), also named Marble Unit by Cook & Craw (2002), which crops out along the margin of the Skelton Glacier (Hauptvogel & Passchier, 2012; Fig. 17), is the most likely source for calcite and dolomite. The Byrd Group (Fig. 17), which crops out further south, is characterized by the

initial deposition of a thick sequence of nearly pure carbonate sediments followed by a thick sequence of clastic sediments (Stump *et al*., 2006). Moreover, Pleistocene tills of lower Byrd Glacier contain detrital carbonate in extremely large abundances (Licht *et al*., 2005). In addition, Passchier (2001) has found limestone-bearing tills in the Queen Maud range in the central Transantarctic Mountains. These tills were probably sourced from the Shackleton Limestone (Goodge *et al*., 2004). Between Ferrar and Koettlitz Glaciers marbles from Ross Supergroup are also present (Warren, 1969; Lopatin, 1972).

Granite Harbour Intrusive (GHI) - Beacon Supergroup – Sedimentary rocks of the Beacon Supergroup are the most likely source of the stable minerals (apatite 2, tourmaline, rutile, zircon, sphene and epidote). They usually occur as sub-rounded to rounded grains and they might indicate a possible recycling and transport from samples of the Beacon Supergroup, which are known to contain both zircon and apatite (Laird & Bradshaw, 1982; La Prade, 1982; Giorgetti et al., 2009). Plutonic rocks and pegmatites of the Granite Harbour Intrusive Complex contain sphene as an accessory constituent (Ghent & Henderson, 1968; Smillie, 1992). Lower Paleozoic dykes and batholiths of the Granite Harbour Intrusive rocks contain tourmaline in higher abundances (Stump, 1995). Hedenbergites have been found in tonalites from Granite Harbour Intrusive rocks (Sandroni & Talarico, 2004).

Low-to medium-grade metamorphic rocks (L-M grade metamorphic rocks)- Transantarctic Mountains, and in particular the amphibolites of the Koettlitz Group are the most likely source for Mg-hornblendes: these amphiboles are characteristic minerals of many metamorphic and intermediate magmatic rocks (Polozek, 2000). We have also to take into account that hornblendes were also described in the granitoids (Granite Harbour Intrusive Complex) of Taylor Valley (Ghent & Henderson, 1968; Smillie, 1992).

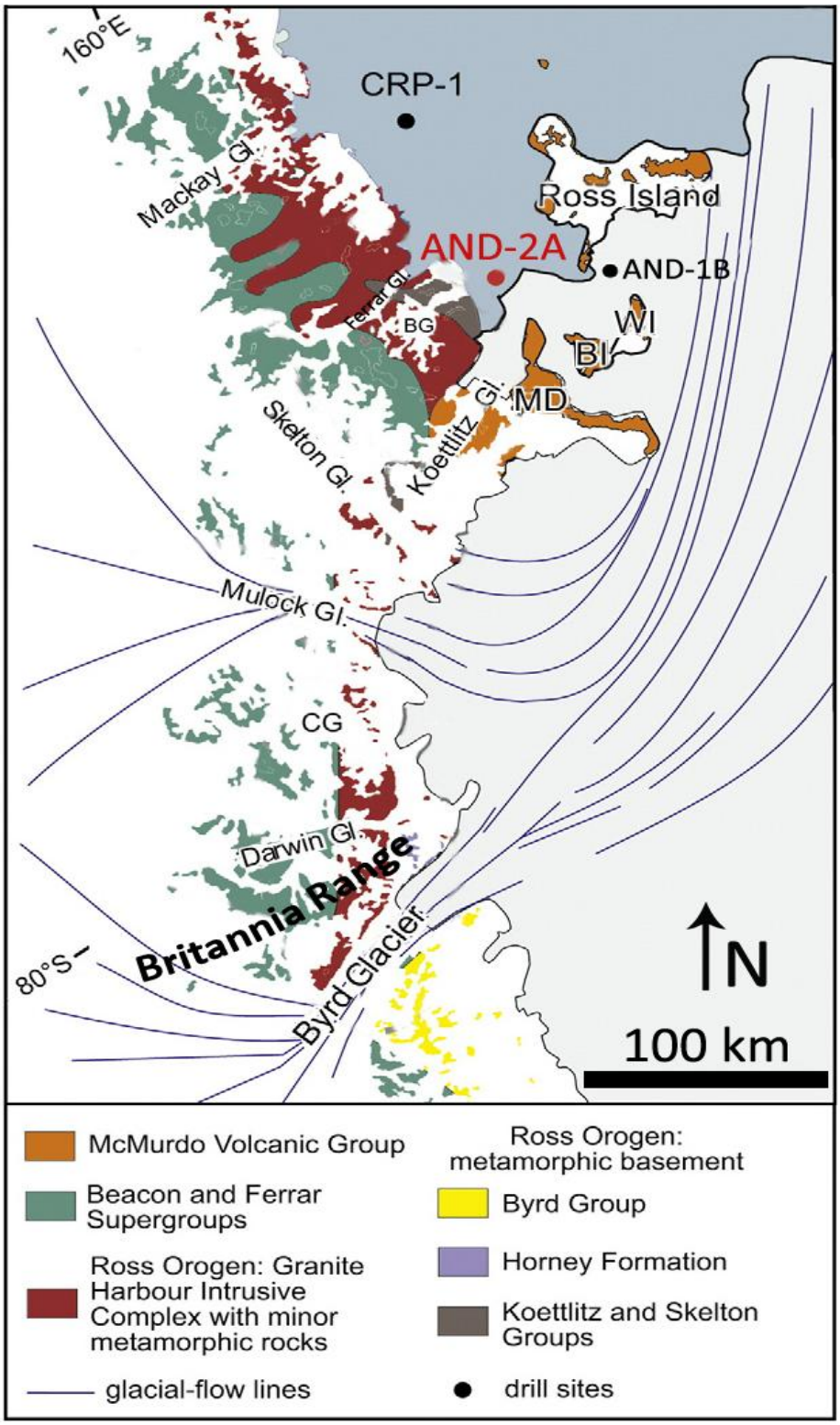

Fig. 17. Geological map (after Gunn & Warren, 1962; Warren, 1969; Talarico & Sandroni, 2011). The present-day glacial-flow directions of major glaciers are also shown (after Fahnestock *et al*., 2000). Abbreviations: BG Blue Glacier, BI Black Island, CG Carlyon Glacier, MD Mount Discovery, WI White Island. The location of ANDRILL McMurdo Sound Project (AND-2A) drill-site, Cape Roberts Project 1 (CRP-1) drill site and ANDRILL McMurdo Ice Shelf Project (AND-1B) drill-site are also shown in the map.

Amphibolites and paragneisses exposed between the Koettlitz and Ferrar Glaciers are the most probable sources for garnets (Fig. 17; Lopatin, 1972) and occur in significant abundances in the Late Miocene and Pliocene tills of the Ferrar, Taylor and Wright Valleys (Ehrmann & Polozek, 1999; Passchier, 2001). Some grains have a sub-rounded to rounded shape. Because garnets are resistant to transport, they also could be recycled from sandy sedimentary rocks, such as those of the Beacon Supergroup, where they occur as accessory minerals (Laird & Bradshaw, 1982; La Prade, 1982). Metasediments and marbles of the Koettlitz Group host pyrope-almandine and grossular garnets. Orthoamphibole gedrite has been reported in Cocks unit of Skelton Group associated with garnet and biotite (Cook & Craw, 2002).

Skelton Group, exposed along the Skelton Glacier, is considered the source of low-grade metasedimentary clasts (Gunn & Warren, 1962; Cook & Craw, 2002). In the portions intruded by granitoid plutons, the metasedimentary rocks are in place characterized by a local contact-metamorphic overprint (Gunn & Warren, 1962; Skinner, 1982), with the development of biotite-spotted and amphibole-bearing varieties.

5.2.2. Heavy mineral distribution

Based on the relative abundance of the heavy mineral assemblage in the core, the lower 650 mbsf of the core can be subdivided into four intervals, numbered 1 to 4 from top to bottom (Fig. 18).

The uppermost interval 1 (650 - 770 mbsf; 17.6 - 18.7 Ma) is characterized by a decrease in Ferrar Group contribution from 650 to 750 mbsf. GHI-Beacon Supergroup, L-M grade metamorphic rocks and Carbonates show a down core decrease. On the contrary, McMurdo Volcanic Group increases in the interval 650 -750 mbsf. Interval 750 - 770 mbsf

displays an increase of Ferrar Group contribution and a McMurdo Volcanic Group decrease. Ferrar Group contribution indicates erosion of dolerites of Ferrar Group located west of the drill-site, followed by an ice advance testified by McMurdo volcanic contribution.

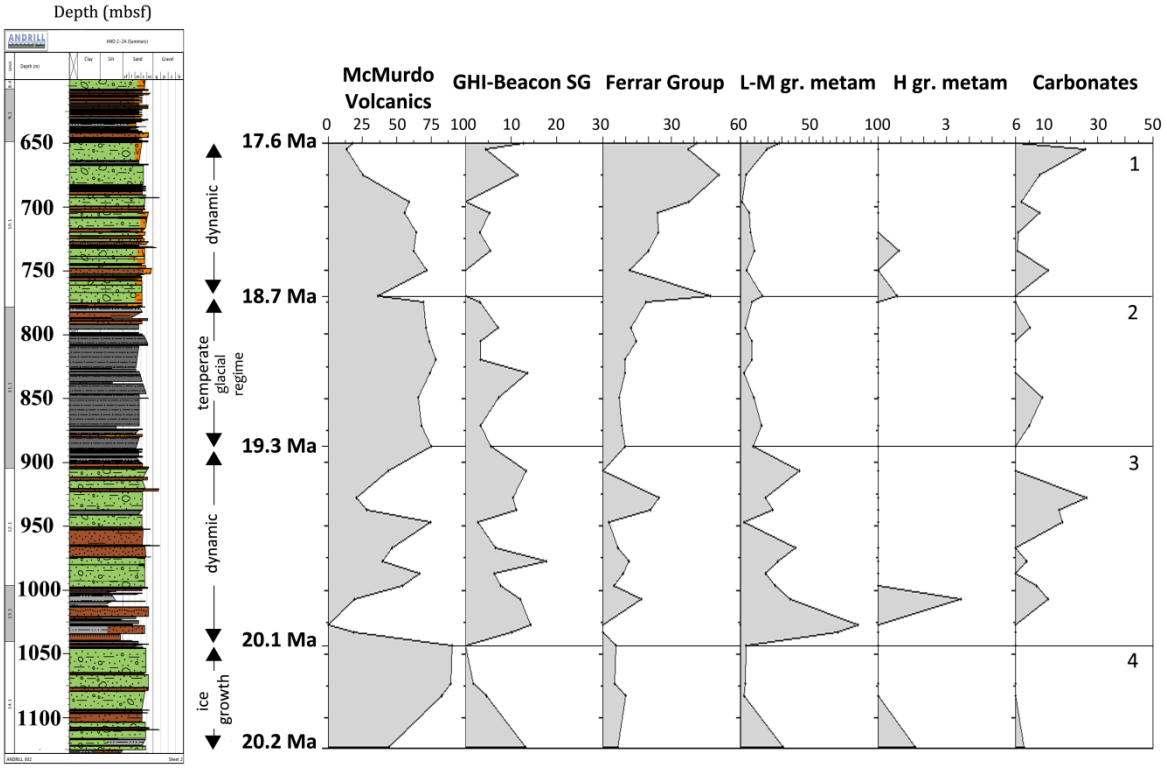

Fig. 18. Summary plot of heavy mineral distribution down-core. On the left, the glacial setting configuration inferred from facies distribution in the core (Passchier *et al.* 2011). The presence of shear fabrics and massive diamictites in core intervals ("ice growth") indicates proximity of the grounding line during glacial maxima, whereas mudstones ("temperate glacial regime") indicate generally open marine conditions with a grounding line at some distance from the drill-site during both glacial maxima and minima (Passchier *et al*. 2011). Ages (^{40}Ar-^{39}Ar geochronology of volcanic material, Acton *et al.*, 2008-2009; Di Vincenzo *et al.*, 2010) are also reported.

A further ice retreat is proved by a renewed increase in Ferrar Group, with a consequent decrease in McMurdo volcanic group contribution.

Interval 2 (770 - 890 mbsf; 18.7 - 19.3 Ma) marks an increase in McMurdo Volcanic Group signal and a decrease in Ferrar Group, GHI-Beacon Supergroup, L-M grade metamorphic rock group as well as Carbonate contribution. For this interval, the heavy minerals assemblages indicate erosion of the basalts of McMurdo Volcanic Group south of

the drill-site, with limited erosion of low- and high-grade metamorphic rocks of basement. A further clue for volcanic origin can be found in the presence of few grains of aenigmatite (Fig. 15), which can be considered a fingerprint heavy mineral for volcanic origin. Clast provenance studies by Talarico & Sandroni (2011) testified a mixed provenance from Royal Society Range area and Skelton-Mulock glacier area, thus helping us to pinpoint a heavy mineral assemblage provenance from an area located south of the drill-site.

Interval 3 (890 - 1043 mbsf; 19.3 - 20.1 Ma) is characterized by large fluctuations of McMurdo Volcanic Group contribution, which point to a source from the south. Oscillations of GHI-Beacon Supergroup, Ferrar and L-M grade metamorphic rocks indicate a local source situated in the Transantarctic Mountains. GHI-Beacon Supergroup, Ferrar Group, L-M grade metamorphic rocks and Carbonates co-vary, and consequently they anti-correlate with McMurdo Volcanic Group. High grade metamorphic group shows very low counts, but seems to correlate with GHI-Beacon Supergroup, Ferrar Group and Carbonates. Nevertheless, the occurrence of minerals of high grade metamorphic group in the lower part of the unit, as suggested by Hauptvogel & Passchier (2012), could indicate either an erosion of Koettlitz Group, where these minerals are present (Lopatin, 1972), or a provenance from the metamorphic rocks of Nimrod Group further south. In addition, Passchier (2001) reported that large amounts of Al-silicate minerals are present within tills that occur in the inland plateau of the central TAM, in correspondence of the outlets of Nimrod glacier. Furhermore, for the same interval, Talarico & Sandroni (2011) reported that the metamorphic clast assemblage suggesting a provenance from Carlyon Glacier and Darwin-Byrd Glacier is constituted by mineral paragenesis like garnet-sillimanite-K-feldspar-biotite, thus indicating medium/high-grade metamorphic conditions which occur only in the Britannia Range. The compositions of iceberg-rafted debris (Talarico & Sandroni, 2011) suggest that the sites of active calving processes changed repetitively in

time from areas located in the present-day Blue - Koettlitz glacier coast to paleo-glacier located further south in the Skelton -Mulock glacier area. Ice sheet most likely experienced a dynamic behavior with time interval of ice advance alternate to period of ice retreat.

Intervals 1 and 3 both indicate a dynamic behavior of the ice sheet, their heavy mineral distribution is very different. Interval 1 is characterized by an up-core decrease of MVG contribution starting from 700 mbsf, linked to a significant enhance of Ferrar Group input, and in particular a high amount of orthopyroxenes. As hypothesized by Hauptvogel & Passchier (2012) for their third interval (308 - 552 mbsf), this would fit a scenario where the grounding lines of outlet glaciers had receded into the valleys of Victoria Land, away from the coast. There, they would have eroded the Ferrar Dolerites in the upper section of the Transantarctic Mountains during glacial times with possibly further retreat. Valleys are eroded into basement rocks near the coast, but do not reach basement further inland (Denton *et al.*, 1993). In addition, further studies conducted in the McMurdo Sound area by Marsh (2004), Bedard *et al*. (2007) and Zavala *et al*. (2011) highlight that there exist four Ferrar sills in the McMurdo Dry Valleys Region of the Trans-Antarctic Mountains. From top to bottom, these are the Mt. Fleming, Asgard, Peneplain and Basement Sills. The upper three sills consist of homogeneous fine- to medium-grained dolerite, whereas the lowermost Basement Sills (Gunn, 1962), which extends from McKay Glacier to the head of Ferrar glacier, has a central cumulate layer or ‘tongue’ consisting of large orthopyroxene and smaller plagioclase crystals, enclosed by fine- to medium-grained dolerite like that of the other sills (Fig. 19A). In the Ferrar Glacier area, Basement Sill is located inland (Fig.19B), and it is the most likely source for the high amounts of orthopyroxenes. These results indicate that the East Antarctic Ice Sheet was reduced in size relative to today's interglacial configuration during the glacial maxima of the Miocene Climatic Optimum.

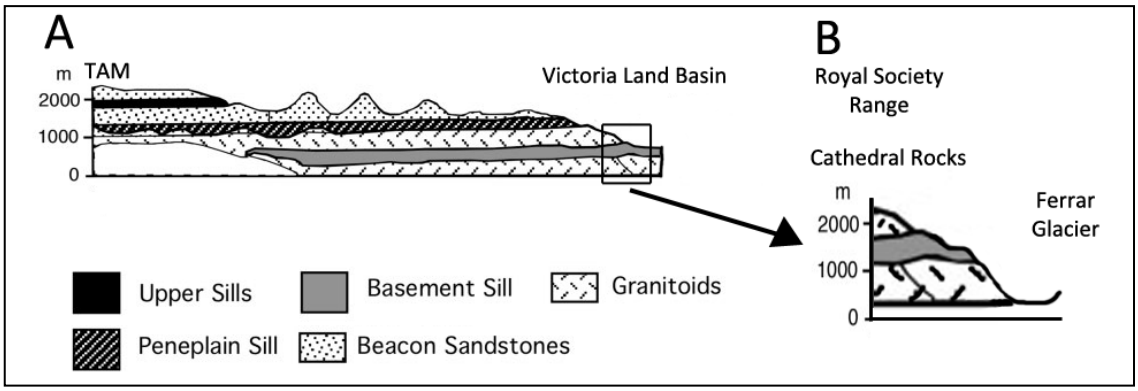

Fig. 19. A) Schematic geological cross-section from the uplands of the Transantarctic Mountains (TAM) to the Victoria Land Basin (VLB) (Modified after Bedard *et al.*, (2007) and Zavala *et al*., (2011). B) Highlight of the Ferrar Glacier area: the Basement sill is located in the upper, inland region of Transantarctic Mountains.

On the other hand interval 3 is characterized by a cyclic McMurdo volcanic Group signal, which indicates a repeated contribution from South, and L-M grade metamorphic, GHI-Beacon Supergroup and Ferrar Group fluctuations, which indicate a heavy mineral assemblage derived from local source. This pattern can be explained as an advance of the grounding lines of EAIS outlet glaciers to the coast in the southern TAM, where they erode largely the Granite Harbour Intrusive-Beacon Supergroup rocks, with minor contribution from Ferrar dolerites.

The lowermost interval 4 (1043 - 1123 mbsf; 20.1 - 20.2 Ma) is characterized by high abundance of heavy minerals derived from McMurdo Volcanic Group, followed by low to medium grade metamorphic rocks and GHI-Beacon Supergroup, as well as Ferrar Group. The heavy mineral assemblage indicates erosion of MVG rocks during ice advance. These results are compatible with ice eroding basalts around the Mount Morning volcanic center to the south of the drill-site.

5.3. Palaeoclimatic interpretation based on an integrated clay and heavy mineral study

On the basis of the integrated clay and heavy mineral variation studies it has been possible to subdivide the entire investigated succession in five intervals, named A to E from top to bottom of the drill core (Fig. 20).

Interval A (36 - 225 mbsf; Pleistocene - 14.3 Ma) is characterized by a constant amount of smectite and illite, with large fluctuations of chlorite. The main source for illite and chlorite is most likely the basement rocks and sedimentary rocks of the Transantarctic Mountains, whereas smectite mainly comes from the McMurdo Volcanic Group rocks located in the area of the present-day Ross Ice Shelf.

The inferred scenario is that of an ice sheet which erodes into the basement of the TAM, with an episodically contribution of McMurdo Volcanic Group from south.

Interval B (225 - 440 mbsf; 14.3 - 16.3 Ma) is dominated by illite; smectite occurs only in minor amounts and chlorite content remains quite stable if compared to the previous interval. This interval shows the highest illite content in the whole AND-2A drill core. The ice-sheet and sea-ice minima at 16.3 - 16.5 (440 mbsf) and 15.6 - 15.7 Ma (300 mbsf) recorded in AND-2A (Passchier *et al.,* 2001) correspond to periods of high global sea-level fluctuations and ice-volume reduction (Miller *et al.*, 1991; Zachos *et al.*, 2008). The high illite content are in agreement with the large amount of Ferrar Group contribution identified by Hauptvogel & Passchier (2012) in the interval 250 - 550 mbsf. High illite contents indicate relatively stable conditions with intensive and persistent physical weathering on the surrounding land masses. This scenario implies that grounding lines of outlet glaciers had receded into the valleys of Victoria Land far from the coast.

Since heavy mineral analyses started from 650 mbsf, we decided to subdivided interval C

(440 - 890 mbsf) into two subsections.

Interval C' (440 - 650 mbsf; 16.3 - 17.6 Ma) shows relatively high illite contents with high smectite fluctuations, with minor contribution of chlorite. The ice retreat at 17.6 Ma, inferred from facies analysis (Passchier *et al*., 2011), presumably marks the onset of the Miocene Climactic Optimum. Facies analysis shows that the large volume of sandy deposits and the intervals of laminated muds as well as diatom content are consistent with colder and drier polythermal glacial conditions. The predominance of illite in the clay mineral assemblage seems to confirm a prevalent physical weathering in cold and dry conditions with polythermal glaciers. Climatic conditions are most likely less stable than those described for interval B.

Interval C" (650 - 890 mbsf; 17.6 - 18.7 Ma) is characterized by an illite-smectite oscillation in relative proportions, like the previous interval C'. Heavy mineral assemblages show a down-core increase in McMurdo Volcanic Group contribution and a contemporary decrease in Ferrar Group contribution down to 890 mbsf (Fig. 20). GHI-Beacon Supergroup, L-M grade metamorphic rocks and Carbonates show lower oscillations. The heavy mineral assemblages dominated by McMurdo Volcanic Group indicate a sediment source located south of the drill site. The most likely scenario implicates advancing ice masses from south capable of eroding volcanic edifices of MVG. The 17.6 - 19.3 Ma period of glacial intensification and ice growth in AND-2A can be tentatively correlated to the Mi-1b glacial event of Miller *et al*. (1991). Although heavy mineral assemblages dominated by McMurdo Volcanic Group contribution in the lower part of interval C"(770 - 890 mbsf) indicate a sediment provenance located south of the drill site, the mudstone-dominated facies at 770 - 890 mbsf (Fig. 18) probably indicates ice sheet in a reduced configuration, with predominantly melt-water plume deposition and minor ice rafting (Passchier *et al.,* 2011). We have therefore to take into account also an

alternative glacial scenario. The probable mechanisms able to transport MVG heavy minerals to the AND-2A drill site in the interval between 770 and 890 mbsf could be the direct fall-out of volcanic material, in an ice-free glacial configuration as well as water plume deposition derived from melt-water with ice sheet in a retreated setting.

Interval D (890 - 1043 mbsf; 18.7 - 20.1 Ma) is characterized by large fluctuation in relative proportions between smectite and illite as well as MVG contribution and L-M grade metamorphic rocks. Smectite and heavy mineral MVG contents show a very good correlation. On the contrary, illite shows a good correlation with L-M grade metamorphic rock heavy mineral group. We can hypothesize that high smectite contents might be related to a high volcanic influx in this section of the drill core. Illite peaks correspond to sediment inputs from TAM, during period of ice retreat. A dynamic glacial configuration is the more likely and it is also supported by facies analysis indicating a scenario characterized by open water to ice-proximal conditions (Passchier *et al.*, 2011). Our clay mineral and heavy mineral data confirm this paleogeographical setting, and they record for the first time this cyclicity in AND-2A drill core.

Interval E (1043 - 1123 mbsf; 20.1 - 20.2 Ma) is characterized by high smectite content and high MVG heavy mineral contribution. Heavy mineral assemblage indicates a sediment source located south of the drill site.

The clay and heavy mineral record of the lower 650 mbsf indicate that the ice sheet similar in size to modern ice sheet was periodically present between 17.6 and 19.3 Ma and between 20.1 and 20.2 Ma.

These data support evidences inferred from isotopic proxy studies. Pekar & DeConto (2006) have highlighted that ice-volume ranged between 50% and 125% of the present day EAIS during most of the early Miocene and maximum ice-volume occurred at each of the early Miocene isotopic events. Furthermore, significant reductions in ice-volume occurred

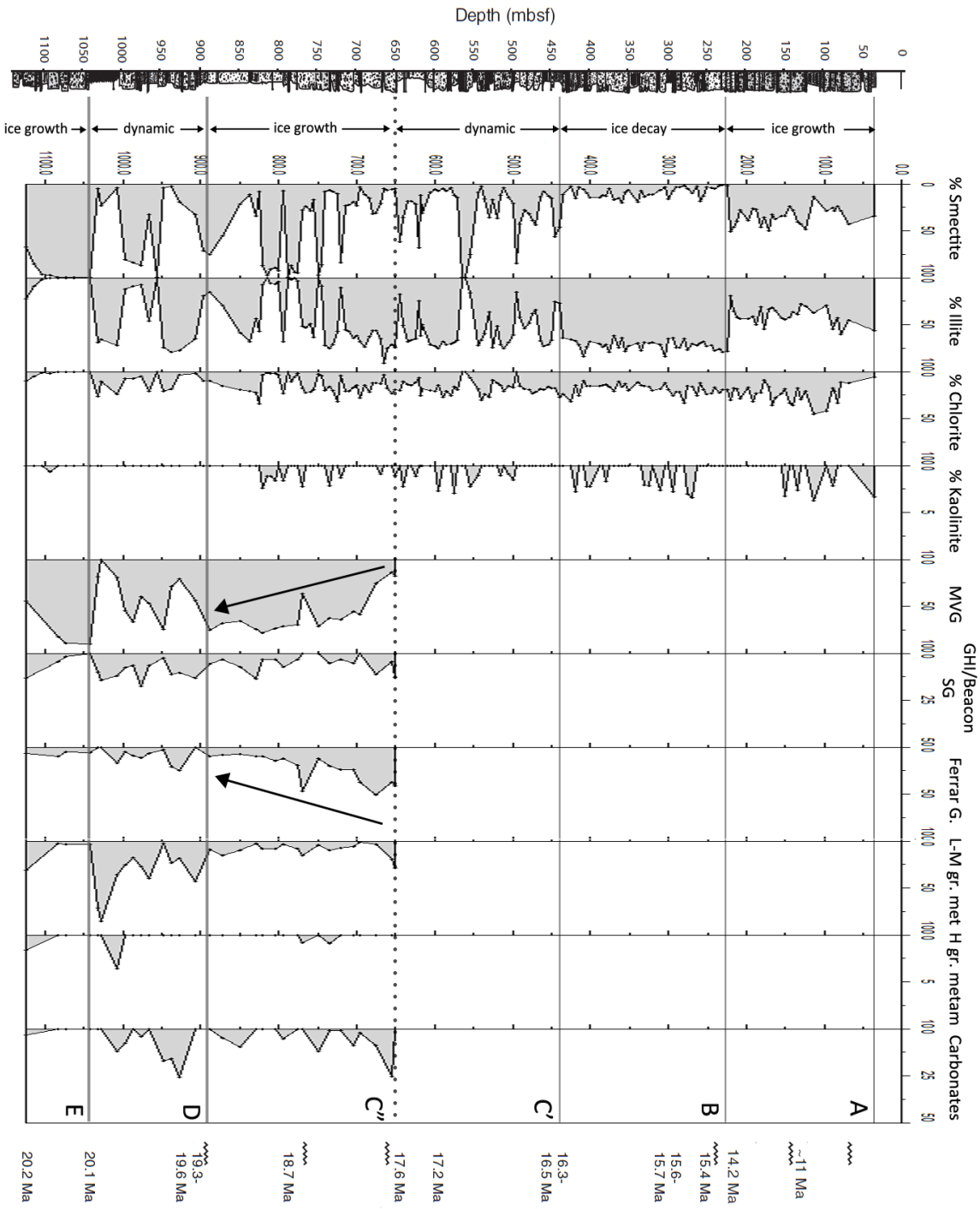

Fig. 20. Integrated clay - heavy mineral variation through AND-2A drill core. Paleoenvironmental interpretation for AND-2A drill core is after Passchier et *al.* (2011). Black arrows indicate increase and decrease trend respectively for McMurdo Volcanic Group and Ferrar Group contribution. Black wavy lines on the right of the image represent grounding line events. Ages (^{40}Ar–^{39}Ar geochronology of volcanic material, Acton *et al.*, 2008-2009; Di Vincenzo *et al.*, 2010) are also reported.

episodically between 22 and 18 Ma and more specifically between 16.7 and 16.0 Ma. In some cases, these large fluctuations occurred in < 100 kyr supporting the view that a dynamic ice sheet existed during the Early Miocene (Pekar & DeConto, 2006).

The clay and heavy mineral record of AND-2A drill core have increased our understanding of the timing and spatial distribution of ice sheet growth and decay in the McMurdo Sound region during Early Miocene (15.9 - 20.2 Ma) and the Miocene Climate Optimum (ca.15 - 17 Ma). The excellent position of AND-2A drill core has been fundamental to record the early onset of ice growth because of its high latitude position and the high elevation of the Transantarctic Mountains: DeConto & Pollard (2003) have found out that the Transantarctic Mountains form a location of ice-sheet inception.

Previous studies have shown that clay minerals are reliable proxies for reconstructing the glacial history of Antarctica. The onset of the continental East Antarctic glaciation is well documented by an important shift in the clay mineralogy that reflects the rapid transition from temperate and humid conditions, with intense chemical weathering during the Eocene, changing to physical weathering conditions under cooler and drier conditions in the Oligocene (Ehrmann & Mackensen, 1992; Ehrmann, 1998a). In AND-2A drill core, the clay mineral assemblages document the dominance of physical weathering especially in the upper part of the investigated succession. As shown above, changes in the relative proportion of illite and smectite were probably not caused by changing weathering conditions and hence climate, but they can be related to changes in the provenance of the sediments and to diagenetic processes.

The present study has demonstrated that the occurrence of authigenic clay minerals may conduct to incorrect paleoclimatic interpretations. Therefore, detailed clay mineral analyses, possibly integrated with heavy mineral study, are necessary for reconstructing sediment provenance and consequently ice-sheet dynamics. The comparison between clay

minerals, heavy minerals and previous clast provenance (Talarico & Sandroni, 2011) and facies analysis (Passchier *et al*., 2011) studies carried on AND-2A drill core allowed us to tentatively reconstruct the paleo-glacial flow directions.

In the future, when new data from other drill cores along the Antarctic continental margin will be available, they will be integrated with the record from AND-2A drill core in order to obtain a more comprehensive representation of the coverage of the Antarctic ice sheet during the Cenozoic.

References

Abad I., Jimenez-Millan J., Molina J.M., Nieto F. & Vera J.A. (2003). Anomalous Reverse Zoning of Saponite and Corrensite Caused by Contact Metamorphism and Hydrothermal Alteration of Marly Rocks Associated with Subvolcanic Bodies. *Clays and Clay Minerals*, **51**(5): 543-554.

Acton G., Crampton J., Di Vincenzo G., Fielding C.R., Florindo F., Hannah M., Harwood D., Ishman S., Johnson K., Jovane L., Levy R., Lum B., Marcano M.C., Mukasa S., Ohneiser C., Olney M., Riesselman C., Sagnotti L., Stefano C., Strada E., Taviani M., Tuzzi E., Verosub K.L., Wilson G.S., Zattin M. & the ANDRILL-SMS Science Team, (2008–2009). Preliminary integrated chronostratigraphy of the AND-2A core, ANDRILL Southern McMurdo Sound project, Antarctica. *Terra Antartica*, **15**, 211–220.

ANDRILL SMS Science Team, (2010). An integrated age model for the ANDRILL-2A drill core. In: ANDRILL Southern McMurdo Sound Project Science Integration Workshop - Program and Abstracts (Kontar K., Harwood D.M., Florindo F., and Fischbein S. editors). ANDRILL Contribution # 16, ANDRILL Science Management Office, University of Nebraska, Lincoln, NE, pp. 113.

Armienti P., Messiga B. & Vannucci R., (1998). Sand provenance from major and trace element analyses of bulk rock and sand grains. *Terra Antartica*, **5**, 598–599.

Bamber J.L., Riva R.E.M., Vermeersen B.L.A. & LeBrocq A.M., (2009). Reassessment of the potential sea-level rise from a collapse of the West Antarctic Ice Sheet. *Science*, **324**, 901–903.

Bardin V.I., (1982). Composition of East Antarctic moraines and some problems of Cenozoic history. In: Craddock, C. (Ed.), Antarctic Geoscience. Univ. Wisconsin Press, Madison, WI, pp. 1069 1076.

Bardin V.I., Bubnova M.I. & Gerasimova V.M., (1979). Clay minerals in unconsolidated deposits of the Prince Charles Mountains. *Inf. Bull. Sov. Antarct. Exped*. **71**, 120-128.

Barrett P., (1979). Proposed drilling in McMurdo Sound. Memoir of the National Institute of Polar Research, Special Issue **13**, 231–239.

Barrett P.J., (2007). Cenozoic climate and sea level history from glacimarine strata off the Victoria Land coast, Cape Roberts Project, Antarctica. In: Hambrey, M.J., Christoffersen, P., Glasser, N.F., Hubbart, B. (Eds.). *Glacial Processes and Products: International Association of Sedimentologists Special Publication*, **39**, 259–287.

Bédard J. H. J., Marsh D. B., Hersum G. T., Naslund H. R. & Mukasa B. S., (2007). Large-scale mechanical redistribution of orthopyroxene and plagioclase in the Basement Sill, Ferrar Dolerites, McMurdo Dry Valleys, Antractica: petrological, mineral-chemical and field evidence for channelized movement of crystals and melt. *Journal of Petrology* , **48**, 2289-2326.

Berner R.A., (1970) Sedimentary pyrite formation. *American Journal of Science*, **268**, 1-23.

Berner R.A., (1980) Early Diagenesis: A Theoretical Approach. Princeton University Press, 256 pp.

Biscaye P.E., (1965). Mineralogy and sedimentation of recent deep-sea clay in the Atlantic Ocean and adjacent seas and oceans. *Geological Society American Bulletin*, **76**, 803-832.

Bradley W.F., (1945). Molecular associations between montmorillonite and some polyfunctional organic liquids. *Journal of the American Chemical Society*, **67**, 975-981.

Brindley G.W. & Brown G. (Editors), (1980). Crystal Structures of Clay Minerals and their X-ray Identification. Mineralogical Society, Monography, London, 5,495 pp.

Brundin N.H. & Bergstrom J., (1977) Regional prospecting for ores based on heavy minerals in glacial till. *Journal of Geochemical Exploration*, **7** (C) , pp. 1-19.

Buatier M.D., Karpoff A.M. & Charpentier D., (2002) Clays and zeolite authigenesis in sediments from the flank of the Juan de Fuca Ridge. *Clay Minerals,* **37** (1), 143-155.

Callahan J., (1987). A non-toxic heavy liquid and inexpensive filters for separation of mineral grains. *Journal of Sedimentary Petrology*, **57**, 765–766.

Cape Roberts Science Team, (1998). Initial report on CRP-1, Cape Roberts Project, Antarctica. *Terra Antartica*, **5**, 1–187.

Carroll D., (1970). Clay minerals in Antarctic ocean sea floor sediments. *Journal of Sedimentary Petrology*, **40**, 814-821.

Chamley H., (1989). Clay sedimentology. Springer, 623 pp.

Claridge G.G.C., (1965). The clay mineralogy and chemistry of some soils from Ross dependency Antarctica. *New Zealand Journal of Geology and Geophysics*, **3**, 186-200.

Claridge G.G.C. & Campbell I.B., (1989). Clay mineralogy. In: Barrett, P.J. (Ed.), Antarctic Cenozoic History from the CIROS-1 DriNhole, McMurdo Sound. *DSIR Bulletin*, **245**, 185 193.

Cook Y.A. & Craw D., (2002). Neoproterozoic structural slices in the Ross Orogen, Skelton Glacier area, South Victoria Land, Antarctica. *New Zealand Journal of Geology and Geophysics*, **45**, 133–143.

Damiani D., Giorgetti G. & Turbanti I. M., (2006). Clay mineral fluctuations and surface textural analysis of quartz grains in Pliocene–Quaternary marine sediments from Wilkes Land continental rise (East-Antarctica): Paleoenvironmental significance. *Marine Geology*, **226**(3-4), 281-295.

Damiani D. & Giorgetti G., (2008). Provenance of glacial–marine sediments under the

McMurdo/Ross Ice Shelf (Windless Bight, Antarctica): Heavy minerals and geochemical data. *Palaeogeography, Palaeoclimatology, Palaeoecology,* **260**(1-2), 262-283. doi:10.1016/j.palaeo.2007.08.010.

Davey F.J., Barrett P.J., Cita M.B., van der Meer J.J.M., Tessensohn F., Thomson M.R.A., Webb P.-N. & Woolfe K.J., (2001). Drilling for Antarctic Cenozoic climate and tectonic history at Cape Roberts, Southwestern Ross Sea, *Eos* Trans. AGU, **82**, 585.

Darby D.A., (1975). Kaolinite and other clay minerals in Antarctic Ocean sediments. *Journal of Sedimentary Petrology*, **45**, 272-279.

Decarreau A. & Bonnin D. (1986). Synthesis and crystallogenesis at low temperature of Fe(III)-smectites by evolution of coprecipitated gels: experiments in partially reducing conditions. *Clay Minerals*, **21**, 861-877.

DeConto R.M. & Pollard D., (2003). Rapid Cenozoic glaciation of Antarctica induced by declining atmospheric CO2. *Nature*, **421**, 245–249.

de la Fuente S., Cuadros J., Fiore S. & Linares J. (2000). Electron microscopy study of the volcanic tuff alteration to illite-smectite under hydrothermal conditions. *Clays and Clay Minerals*, **48** (3), 339-350.

Denton G.H., Sugden D.E., Marchant D.R., Hall B.L. & Wilch T.I., (1993). East Antarctic Ice Sheet sensitivity to Pliocene climatic change from a Dry Valleys perspective. A Special Volume Arising from the Vega Symposium: The Case for a Stable East Antarctic Ice Sheet. *Geografiska Annaler Series A, Physical Geography*, Vol. **75**, No. 4, pp. 155–204.

Diekmann B., Petschick R., Gingele F.X., Fütterer D.K., Abelmann A., Brathauer U., Gersonde R. & Mackensen A. (1996). Clay mineral fluctuations in Late Quaternary sediments of the Southeastern South Atlantic: implications for past changes of deep water advection. In: Wefer G., Berger W.H., Siedler G. & Webb D. (eds): The South Atlantic: Present and Past Circulation. Springer Verlag, Berlin, 621-644.

Diekmann B., Khun G., Mackensen A., Petschick R., Fütterer D.K., Gersonde R., Ruhlemann C., Niebler H.S., (1999). Kaolinite and chlorite as tracers of modern and late Quaternary deep water circulation in the South Atlantic and the adjoining Southern Ocean. In: G. Fischer, G. Wefer (eds). Use of Proxies in Paleoceanography: Examples from the South Atlantic. Springer-Verlag Berlin Heidelberg, 1-29.

Di Vincenzo G., Bracciali L., Del Carlo P., Panter K. & Rocchi S., (2010). 40Ar–39Ar dating of volcanogenic products from the AND-2A core (ANDRILL Southern McMurdo Sound Project, Antarctica): correlations with the Erebus Volcanic Province and implications for the age model of the core. *Bulletin of Volcanology* **72**, 487–505.

Do Campo M., del Papa C., Nieto F., Hongn F. & Petrinovic I. (2010). Integrated analysis for constraining palaeoclimatic and volcanic influences on clay-mineral assemblages in orogenic basins (Palaeogene Andean foreland, Northwestern Argentina). *Sedimentary Geology*, **228**, 98-112.

Dreimanis A. & Vagners U.J., (1972). The effect of lithology upon texture of till. In: Yatsu, E., Falconer, A. (Eds.), Research Methods in Pleistocene Geomorphology, pp. 66–82.

Drief, A., Nieto, F. & Sánchez-Navas, A. (2001). Experimental clay–mineral formation from a subvolcanic rock by interaction with 1 M NaOH solution at room temperature. *Clays and Clay Minerals*, **49**, 92-106.

Dunbar N.W., Panter K., Scanlan M.K., Fargo A., McIntosh W.C. & Wilch T.I., (2008). Evidence for complex mixing processes controlling the composition of a wide range of alkaline volcanic rocks at Minna Bluff, Antarctica. AGU Fall 2008 Meeting, Abstract V13C-2128.

Elliott D.H., (1992). Jurassic magmatism and tectonism associated with Gondwanaland break-up: an Antarctic perspective. In: Storey, B.C., Alabaster, T., Punkhurst, R.J. (Eds.), Magmatism and the causes of continental break-up. : Special Publication, **68**. Geological Society, London, pp. 165–184.

Ehrmann W.U., (1997). Smectite concentrations and crystallinities: Indications for Eocene Age of glaciomarine sediments in the CIROS-1 Drill Hole, McMurdo Sound, Antarctica – In: The Antarctic Region: Geological Evolution and Processes, 771 – 780.

Ehrmann W.U., (1998 a). Implications of Late Eocene to Early Miocene clay mineral assemblages in McMurdo Sound (Ross Sea, Antarctica) on paleoclimate and ice dynamics. *Paleogeography, Paleoclimatology, Paleoecology*, **139**, 213-231.

Ehrmann W.U., (1998 b). Lower Miocene and Quaternary clay mineral assemblages from CRP-1. *Terra Antartica*, **5**(3), 613-619.

Ehrmann W.U., (2000). Smectite content and crystallinity in sediments from CRP-2/2A, Victoria Land Basin, Antarctica. *Terra Antartica*, **7** (4), 575–580.

Ehrmann W.U., (2001). Variations in smectite content and crystallinity in sediments from CRP-3, Victoria Land Basin, Antarctica. *Terra Antartica*, **8** (4), 533-542.

Ehrmann W.U. & Polozek K., (1999). The heavy mineral record in the Pliocene to Quaternary sediments of the CIROS-2 drill core, McMurdo Sound, Antarctica. *Sedimentary Geology*, **128**, 223–244.

Ehrmann W.U., Melles M., Kuhn G. & Grobe H. (1992a). Significance of clay mineral assemblages in the Antarctic Ocean. *Marine Geology*, **107** (4), 249–273.

Ehrmann, W.U., Hambrey, M.J., Baldauf, J.G., Barron, J., Larsen, B., Mackensen, A., Wise, S.W., Jr.. Zachos, J.C., (1992b). History of Antarctic glaciation: an Indian Ocean perspective. In: Duncan, R.A., Rea, D.K., Kidd, R.B., von Rad, U., Weissel. J.K. (Eds.), Synthesis of Results from Scientific Drilling in the Indian Ocean. Geophys. Monogr. 70, 423 446.

Ehrmann W.U & Mackensen A. (1992). Sedimentological evidence for the formation of an East Antarctic ice sheet in Eocene/Oligocene time. *Palaeogeography, Palaeoclimatology, Palaeoecology*, **93**, 85– 112.

Ehrmann W.U., Bloemendal J., Hambrey M.J., McKelvey B. & Whitehead J. (2003). Variations in the composition of the clay fraction of the Cenozoic Pagodroma Group: implications for determining provenance. *Sedimentary Geology*, **161**, 131-152.

Ehrmann W.U., Setti M. & Marinoni L., (2005). Clay minerals in Cenozoic sediments off Cape Roberts (McMurdo Sound, Antarctica) reveal palaeoclimatic history. *Palaeogeography, Palaeoclimatology, Palaeoecology*, **229** (3), 187-211.

Fahnestock M.A., Scambos T.A., Bindschadler R.A. & Kvaran G., (2000). A millennium of variable ice flow recorded by the Ross Ice Shelf, Antarctica. *Journal of Glaciology*, **46**, 652–664.

Fesharaki O., García Romero E., Cuevas-González N. & López-Martinéz N., (2007). Clay mineral genesis and chemical evolution in the Miocene sediments of Somosaguas, Madrid Basin, Spain. *Clay Minerals*, **42**, 173-187.

Fielding C.R., Henrys S.A. & Wilson T.J., (2006). Rift history of the western Victoria Land Basin: a new perspective based on integration of cores with seismic reflection data. In: D. Futterer, D. Damaske, G. Kleinschmidt, H. Miller & F. Tessensohn (Eds.), Antarctica Contributions to Global Earth Sciences, Springer-Verlag, Berlin, 309-318.

Fielding C.R., Atkins C.B., Bassett K.N., Browne G.H., Dunbar G.B., Field B.D., Frank T.D., Krissek L.A., Panter K.S., Passchier S., Pekar S.F., Sandroni S., Talarico F. & ANDRILL-SMS Science Team, (2008–2009). Sedimentology and stratigraphy of the AND-2A core, ANDRILL Southern McMurdo Sound project, Antarctica. *Terra Antartica,* **15**, 77–112.

Fielding C.R., Browne G.H., Field B.D., Florindo F., Harwood D.M., Krissek L.A., Levy R., Panter K.S., Passchier S. & Pekar S.F., (2011). Sequence stratigraphy of the ANDRILL AND-2A drillcore, Antarctica: A long-term, ice-proximal record of Early to Mid-Miocene climate, sea-level and glacial dynamism. *Paleogeography, Paleoclimatology, Paleoecology*, **305**, 337-351.

Fitzgerald P., (2002). Tectonics and landscape evolution of the Antarctic plate since the

breakup of Gondwana, with an emphasis on the West Antarctic Rift System and the Transantarctic Mountains. In: Gamble, J.A., Skinner, D.N.B., Henrys, S. (Eds.), Antarctica at the close of a millennium: Royal Society of New Zealand Bulletin, 35, pp. 453–469.

Franke D. & Ehrmann W., (2010). Neogene clay mineral assemblages in the AND-2A drill core (McMurdo Sound, Antarctica) and their implications for environmental change. *Paleogeography, Paleoclimatology, Paleoecology*, **286**, 55-65.

Gamble J.A., Barrett P.J., & Adams, C.J., (1986). Basaltic clasts from Unit 8. In: Barrett, P.J. (Ed.), Antarctic Cenozoic History from the MSSTS-1 Drillhole, McMurdo Sound. *DSIR Bulletin*, **237**, pp. 145–152.

George A., (1989). Sand provenience. In: Barrett, P.J. (Ed.), Antarctic Cenozoic History from the MSSTS-1 Drillhole, McMurdo Sound. *DSIR Bull*., vol. **237**, pp. 159–167.

Ghent E.D., Henderson R.A., (1968). Geology of the Mt Falconer Pluton, lower Teylor Valley, South Victoria Land, Antarctica. *New Zealand Journal of Geology and Geophysics*, **11**, 851–879.

Giorgetti G., Aghib F.S., Livi K.J.T., Gaillot A.C. & Wilson T.J., (2007) Newly formed phyllosilicates in rock matrices and fractures from CRP-3 core (Antarctica): an electron microscopy study. *Clay Minerals*, **42**, 21-43.

Giorgetti G., Talarico F., Sandroni S., & Zeoli A., (2009). Provenance of Pleistocene sediments in the ANDRILL AND-1B drillcore: Clay and heavy mineral data. *Global and Planetary Change*, **69**(3), 94-102.

Goodge J.W., Williams I.S. & Myrow P., (2004). Provenance of Neoproterozoic and lower Paleozoic siliciclastic rocks of the central Ross orogen, Antarctica: detrital record of rift-, passive- and active-margin sedimentation. *Geological Society of America Bulletin*, **116**, 1253–1279.

Gravenor C.P., (1979). The nature of the Late Paleozoic glaciation in Gondwana as

determined from an analysis of garnets and other heavy minerals. *Canadian Journal of Earth Sciences*, **16**, pp. 1137–1153.

Griffin, J,J., Windom, H. & Goldberg, E.D., (1968). The distribution of clay minerals in the World Ocean. *Deep-Sea Research.*, **15**, 433-459.

Grim R. E., Bray R. H. & Bradley W.F., (1937). The mica in argillaceous sediments: *American Mineralogist*, **22**, 813-829.

Gunn B.M., (1962). Differentiation in Ferrar Dolerites. *New Zealand Journal of Geology and Geophysics,* **5** (5), 820-863.

Gunn B.M. & Warren G., (1962). Geology of Victoria Land between the Mawson and Mulock Glaciers, Antarctica. *New Zealand Geological Survey Bulletin*,**71**, 1–157.

Gwyn Q.H.J. & Dreimanis A., (1979). Heavy mineral assemblages in tills and their use in distinguishing glacial lobes in the Great Lakes region. *Canadian Journal of Earth Sciences,* **16**, 2219–2235.

Haban M.A. & Elliot D.H., (1985). Mineral chemistry of the Kirkpatrick basalt, northern Victoria Land, *Antarctic Journal of the United States*, **19**, 30–31.

Hambrey M.J. & Barrett P.J., (1993). Cenozoic sedimentary and climatic record, Ross Sea region, Antarctica. In: Kennett, J.P., Warnke, D.A. (Eds.), The Antarctic Paleoenvironment: A Perspective on Global Change, 2: *Antarctic Research Series,* **60**, 91–124.

Hanan M.A., Totten M.W., (1996). Analytical techniques for the separation and SEM identification of heavy minerals in mudrocks. *Journal of Sedimentary Research,* **66**, 1027–1030.

Hauptvogel D. W. & Passchier S., (2012). Early–Middle Miocene (17–14Ma) Antarctic ice dynamics reconstructed from the heavy mineral provenance in the AND-2A drill core, Ross Sea, Antarctica. *Global and Planetary Change*, **82-83**, pp. 38-50.

Harwood D.M., & Webb P.N., (1998). Glacial transport of diatoms in the Antarctic Sirius Group: Pliocene refrigerator: *GSA Today*, **8**, no. 4, 1–8.

Harwood D.M., Florindo F., Talarico F.M., Levy R.H., Kuhn G., Naish T., Niessen F., Powell R., Pyne A. & Wilson G., (2009). Antarctic drilling recovers stratigraphic records from the continental margin. *Eos*, **90**, 90–91.

Hillenbrand C.D. & Ehrmann W., (2005). Late Neogene to Quaternary environmental changes in the Antarctic Peninsula region: evidence from drift sediments. *Global and Planetary Change,* **45**, 165–191.

Jiménez-Millán J., Abad I., & Nieto F., (2008). Contrasting Alteration Processes in Hydrothermally Altered Dolerites from the Betic Cordillera, Spain. *Clay Minerals*, **43**, 267-80.

Klug H.P. & Alexander L.E., (1972). X-ray diffraction procedures – Wiley, New York, 966 pp.

Kretz R., (1983). Symbols for rock-forming minerals. *American Mineralogist*, **68**, 277-279.

Kyle P.R., (1981). Mineralogy and Geochemistry of a Basanite to Phonolite Sequence at Hut Point Peninsula, Antarctica, based on Core from Dry Valley Drilling Project Drillholes 1, 2 and 3. *Journal of Petrology*, **22** (4), 451-500.

Kyle P.R., (1990). McMurdo Volcanic Group, western Ross Embayment. Introduction. In: Le Masurier, W.E., Thomson, J.W. (Eds.), Volcanoes of the Antarctic plate and Southern Oceans: *AGU Antarctic Research Series*, **48**, pp. 19–25.

Kyle P.R. & Price R.C., (1975). Occurrence of rhonite in alkali lavas of the McMurdo Volcanic Group, Antarctica, and Dunedin Volcano, New Zealand. *American Mineralogist,* **60**, 722–725.

Laird M.G. & Bradshaw J.D., (1982). Uppermost Proterozoic and Lower Paleozoic geology of the Transantarctic Mountains. In: Craddock, C. (Ed.), Antarctic Geoscience. University Wisconsin Press, Madison, pp. 525–533.

La Prade K.E., (1982). Petrology and petrography of the Beacon Supergroup, Shackleton Glacier area, Queen Maud Range, Transantarctic Mountains, Antarctica. Third Symposium on Antarctic Geology and Geophysics. The University of Wisconsin Press, Madison, Wisconsin, U.S.A, pp. 581–590.

LeMasurier W.E. & Thomson J.W. (Eds.), (1990). Volcanoes of the Antarctic Plate and Southern Oceans. *Antarctic Research Series*., vol. **48** (488 pp.).

Lewis A.R., Marchant D.R., Ashworth A.C., Hemming S.R., & Machlus M.L., (2007). Major middle Miocene global climate change: Evidence from East Antarctica and the Transantarctic Mountains. *Geological Society of America Bulletin*, **119**, p. 1449–1461.

Licht K.J., Lederer J.R., & Swope J., (2005). Provenance of LGM glacial till (sand fraction) across the Ross Embayment, Antarctica. *Quaternary Science Reviews*, **24**, 1499–1520.

Lopatin B. G., (1972). Basement complex of the McMurdo 'oasis', southern Victoria Land. In: Adie, R. J. ed. Antarctic geology and geophysics. Oslo, Universitetsforlaget. Pp. 287-292.

Marsaglia K.M. & Tazaki K., (1992). Diagenetic trends in Leg 126 sandstones. *Proceedings of the Ocean Drilling Program*, Scientific Results, **126**, 125-138.

Marsh B. D., (2004). A magmatic mush column Rosetta Stone: the McMurdo dry valleys of. Antractica. EOS Transactions, *American Geophysical Union*, **85**, 497-502.

Martin A.P., (2009). Mt. Morning, Antarctica: Geochemistry, geochronology, petrology, volcanology, and oxygen fugacity of the rifted Antarctic lithosphere. *PhD thesis*, University of Otago, Dunedin.

Martin A.P., Cooper A.F. & Dunlap W.J., (2010). Geochronology of Mount Morning, Antarctica: two-phase evolution of a long-lived trachyte–basanite–phonolite eruptive center. *Bulletin of Volcanology*, **72**, 357–371.

McClenaghan M.B., Thorleifson L.H., DiLabio R.N.W., (2000). Till geochemical and indicator mineral methods in mineral exploration. *Ore Geology Reviews*, **16**, pp. 145–166.

McClenaghan M.B., (2005). Indicator mineral methods in mineral exploration. *Geochemistry: Exploration, Environment, Analysis*, 5, pp. 233-245. doi: 10.1144/1467-7873/03-066.

McKelvey B.C., Webb P.N., Kohn B.P., (1977). Stratigraphy of the Taylor and lower Victoria Groups (Beacon Supergroup) between Mackay Glacier and Boomerang range, Antarctica. New Zealand Journal of Geology and Geophysics, 20, 813–863.

Miller K.G., Wright J.D., & Fairbanks R.G., (1991). Unlocking the ice house: Oligocene-Miocene oxygen isotopes, eustasy, and margin erosion. *Journal of Geophysical Research*, **96**, 6829–6848.

Miller K.G., Kominz M.A., Browning J.V., Wright J.D., Mountain G.S., Katz M.E., Sugarman P.J., Cramer B.S., Christie-Blick N. & Pekar S.F., (2005). The Phanerozoic record of global sea-level change. *Science*, **312**, 1293–1298.

Moore D. M. & Reynolds R. C., (1997). X-ray Diffraction and the Identification and Analysis of Clay Minerals. Oxford University Press, Oxford. 378 pp.

Moriarty K.C., (1977). Clay minerals in Southeast Indian Ocean sediments, transport mechanisms and depositional environments. *Marine Geology*, **25**, 149-174.

Morton A.C., (1985). Heavy-minerals in provenience studies. In: Zuffa, G.G. (Ed.), Provenance of Arenites. NATO ASI, Ser. C, vol. 148, pp. 249–277.

Morton A. C., & Hallsworth C. R., (1999). Processes controlling the composition of heavy

mineral assemblages in sandstones. *Sedimentary Geology*, **124**(1-4), pp. 3-29.

Neumann M., (2001). Preliminary investigations of heavy mineral record from CRP-3 Drillcore, Victoria Land Basin, Antarctica. *Terra Antartica*, **8**, 517–522.

Novich K. & Martin R.T., (1983). Solvation methods for expandable layers. *Clays & Clay Minerals* **31**,235-238.

Nyland R., Panter K., Del Carlo P., Di Vincenzo G., Rocchi S., Tiepolo M. & Field B., (2011). Evidence for early-phase explosive basaltic volcanism at Mt. Morning from glass-rich sediments in the ANDRILL AND-2A core and possible response to glacial cyclicity. *Abstract. 11th International Symposium on Antarctic Earth Sciences*, 10-15 July 2011, Edinburgh, Scotland.

Panter K.S., Talarico F., Bassett K., Del Carlo P., Field B., Frank T., Hoffmann S., Kuhn G., Reichelt L., Sandroni S., Taviani M., Bracciali L., Cornamusini G., von Eynatten H., Rocchi S. & the ANDRILL-SMS Science Team, (2008-2009). Petrologic and Geochemical composition of the AND-2A Core, ANDRILL Southern McMurdo Sound Project, Antarctica. *Terra Antartica*, **15**(1), 147-192.

Passchier S., (2001). Provenance of the Sirius Group and related Upper Cenozoic glacial deposits from the Transantarctic Mountains, Antarctica: relation to landscape evolution and ice-sheet drainage. *Sedimentary Geology*, **144**(3-4), 263-290.

Passchier S., (2007). Chapter 27. The use of heavy minerals in the reconstruction of ice-sheet drainage patterns: an example from the edge of the east antarctic ice sheet. *Developments in Sedimentology*, Vol. **58**, pp. 677–699. ISSN: 0070-4571/doi:10.1016/S0070-4571(07)58027-1.

Passchier S., Browne G., Field B., Fielding C.R., Krissek L.A., Panter K., Pekar S.F. & ANDRILL-SMS Science Team, (2011). Early and Middle Miocene Antarctic glacial history from the sedimentary facies distribution in AND-2A drill hole, Ross Sea, Antarctica. *Geological Society of America Bulletin*, **123**, n 11/12, pp 2352-2365.

Pekar S.F. & DeConto R.M., (2006). High-resolution ice-volume estimates for the early Miocene: evidence for a dynamic ice sheet in Antarctica. *Palaeogeography, Palaeoclimatology, Palaeoecology*, **231**, 101–109.

Petschick R., Kuhn G. & Gingele F., (1996). Clay mineral distribution in surface sediments of the South Atlantic: sources, transport, and relation to oceanography. *Marine Geology*, **130**, 203-229.

Petschick R., (2001). MacDiff 4.2.5. http://www.geol-pal.uni-frankfurt.de/Staff/Homepages/Petschick/MacDiff/MacDiffInfoE.html.

Peuraniemi V., (1990). Chapter 10—heavy minerals in glacial material. In: Kujansuu, R., Saarnisto, M. (Eds.), Glacial indicator tracing. Balkema, Rotterdam, pp. 165–185.

Pompilio M., Kyle P., Wilch T., Dunbar N. & ANDRILL-MIS Project Science Team, (2007). The volcanic record in the ANDRILL McMurdo Ice Shelf AND-1B drill core. U.S. Geological Survey and The National Academies; USGS OF-2007-1047, Extended Abstract 199. 10th International Symposium on Antarctic Sciences, ANDRILL Research and Publications. Paper 4.

Rebesco M., Camerlenghi A., Geletti R., & Canals M., (2006). Margin architecture reveals the transition to the modern Antarctic ice sheet ca. 3 Ma. *Geology*, **34**, no. 4, 301–304.

Rimington N., Cramp A., Morton A., (2000). Amazon fan sands: implications for provenience. *Marine and Petroleum Geology*, **17**, 267–284.

Sandroni S. & Talarico F., (2004). Petrography and provenance of basement clasts in CIROS-1 core, McMurdo Sound, Antarctica. *Terra Antartica*, **11**, 93–114.

Setti M., Marinoni L., Lòpez-Galindo A. & Ben Aboud A., (1997). XRD, SEM and TEM investigations of smectite of the core CIROS-1 (Ross Sea, Antarctica). *Terra Antartica*, **4**, 119-125.

Setti M. Marinoni L., Lòpez-Galindo A. & Ben Aboud A., (1998). TEM observations and

Rare Earth element analysis on the clay minerals of the CRP-1 Core (Ross-Sea, Antarctica). *Terra Antartica*, **5**, 621-626.

Setti M., Marinoni L., Lòpez-Galindo A., & Delgado-Huertas A., (2000). Compositional and morphological features of the smectite of the sediments of the CRP-2A Core, Victoria Land Basin, Antarctica. *Terra Antartica*, **7**, 581-587.

Setti M., Marinoni L. & Lòpez-Galindo A., (2001). Crystal-chemistry of smectite in sediments of CRP 3 Drillcore (Victoria Land Basin, Antarctica): Preliminary results. *Terra Antartica*, **8** (4), 543-550.

Setti M., Marinoni L. & Lòpez-Galindo A., (2004). Mineralogical and geochemical characteristics (major, minor, trace elements and REE) of detrital and authigenic clay minerals in a Cenozoic sequence from Ross Sea, Antarctica. *Clay Minerals*, **39**, 405-421.

Shilts W.W., (1996). Chapter 15—drift exploration. In: Menzies, J. (Ed.), Past Glacial Envi- ronments; Sediments, Forms and Techniques—Glacial Environments, vol. 2. Butterworth- Heinemann, Oxford, pp. 411–439.

Skinner D. N. B., (1982). Stratigraphy and structure of lower grade metasediments of Skelton Group, McMurdo Sound: Does Teall Greywacke really exist? In: Craddock, C. ed. Antarctic geoscience. Madison, University of Wisconsin Press. Pp. 555-563.

Smellie J.L., (2000). Erosional history of the Transantarctic Mountains deduced from sand grain detrital modes in CRP-2/2A, Victoria Land Basin, Antarctica. *Terra Antartica*, **7**, 545–552.

Smillie R.W., (1992). Suite subdivision and petrological evolution of granitoids from the Taylor Valley and Ferrar Glacier region, south Victoria Land. *Antarctic Science,* **4**, 71–87.

Środoń J., Eberl D.D., (1984). Illite. *Mineral Society of America Reviews in Mineralogy*, **13**, 495–544.

Stokes C.R. & Clark C.D., (2001). Palaeo-ice streams. *Quaternary Science Reviews*, **20**, pp. 1437–1457.

Stump E., (1995). The Ross Orogen of the Transantarctic Mountains. Cambridge University Press, Cambridge U.K.

Stump E., Gotee B. & Talarico F., (2006). Tectonic model for development of the Byrd Glacier Discontinuity and Surroundings regions of the Neoproterozoic-Early Paleozoic. In Fütterer D.K., Damaske D., Kleinschmidt G., Hubert M. & Tessensohn F. (eds.). Antarctica: Contributions to Global Earth Sciences. Springer-Verlag, Berlin Heidelberg New York, pp. 155-162.

Sugden D. & Denton G., (2004). Cenozoic landscape evolution of the Convoy Range to Mackay Glacier area, Transantarctic Mountains: onshore to offshore synthesis. *Geological Society of America Bulletin,* **116** (7–8), 840–857.

Talarico F. M., & Sandroni S., (2011). Early Miocene basement clasts in ANDRILL AND-2A core and their implications for paleoenvironmental changes in the McMurdo Sound region (western Ross Sea, Antarctica). *Global and Planetary Change*, **78**(1-2), 23-35.

Tripati A.K., Roberts C.D., & Eagle R.A., (2009). Coupling of CO2 and ice sheet stability over major climate transitions of the last 20 million years. *Science*, **326**, no. 5958, 1394–1397.

Vitali F., Blanc G., Larqué P., Duplay J. & Morvan G., (1999). Thermal diagenesis of clay minerals within volcanogenic material from the Tonga convergent margin. *Marine Geology*, **157**, 105-125.

Vogt C., Knies J., Spielhagen R.F., & Stein, R., (2001). Detailed mineralogical evidence for two nearly identical glacial/deglacial cycles and Atlantic water advection to the Arctic Ocean during the last 90,000 years. *Global and Planetary Change*, **31(1–4)**, 23–44.

Warren G., (1969). Geology of the Terra Nova Bay–McMurdo Sound area, Victoria Land. Antarctic Map Folio Series 12, Geology, Sheet 14, *American Geographical Society*, New York.

Weaver C.E., (1989). Clays, Muds and Shales, Developments in Sedimentology, vol. 44. Elsevier. 819 pp.

Wilson G.S., Roberts A.P., Verosub K.L., Florindo F. and Sagnotti L., (1998). Magnetobiostratigraphic chronology of the Eocene-Oligocene transition in the CIROS-1 core, Victoria Land margin, Antarctica: Implications for Antarctic glacial history. *Geological Society of America Bulletin*, **110**, 35-47.

Wilson T.J., (1999). Cenozoic structural segmentation of the Transantarctic rift flank in southern Victoria Land. *Global and Planetary Change*, **23**, 105–127.

Wise S.W., Smellie J., Aghib F.S., Jarrad R. & Krissek L., (2001). Authigenic smectite clay coats in CRP-3 Drillcore, Victoria Land Basin, Antarctica, as possible indicators of fluid flow: a progress report. *Terra Antarctica*, **8**, 281-298.

Zachos J.C., Pagani M., Sloan L., Thomas E. & Billups K., (2001). Trends, rhythms, and aberrations in global climate 65 Ma to present. *Science* **292**, 686–693.

Zachos J.C., Dickens G.R., & Zeebe R.E., (2008). An early Cenozoic perspective on greenhouse warming and carbon-cycle dynamics. *Nature*, **451**, 279–283.

Zavala K., Leitch A. M., & Fisher G. W., (2011). Silicic Segregations of the Ferrar Dolerite Sills, Antarctica. *Journal of Petrology*, **52**(10), 1927-1964.

Zeschke G., (1961). Prospecting for ore deposits by panning heavy minerals from river sands. *Economic Geology,* **56**, pp. 1250-1257.

Aknowledgments

This work was carried out at the Earth Sciences Department, University of Siena, during 2008–2012. I would like to express my gratitude to my supervisor, Professor Isabella Memmi and to my co-tutor, Dr. Giovanna Giorgetti for introducing me to marine geology and palaeoclimatology, but most of all for their guidance and support.

I would also like to thank Professor Fernando Nieto, from Granada University (Spain), for hosting me in Granada for mineralogical analysis and for data discussion. I also owe my gratitude to Professor Sandra Passchier, from Montclair State University (United States of America) for hosting me in Montclair State University in order to discuss heavy minerals data.

I owe my gratitude to the staff of the Earth Sciences Department of Siena University, especially to Claudia "La maga" Magrini, for her help with laboratory preparation, and Alessandro "Sandro" Berto for his help with the XRD analysis, to Professor Cecilia Viti for her help with some mineralogical issues I have encountered. I would also like to thank PhD students Ivan Martini, Alessio Casagli, and Dr. Elisabetta Gliozzo for all the coffees they have offered me during these months and for their support and cooperation. My warmest gratitude goes to my parents, Rocco and Lida for their support. Most of all I want to thank my girlfriend, *moja mala* Maja, for tolerating and encouraging me at the same time, in general and especially during the preparation of this manuscript.

Ringraziamenti

Questo lavoro è stato portato avanti presso il Dipartimento di Scienze della Terra dell'Università degli Studi di Siena durante il periodo 2008-2012. Voglio esprimere la mia gratitudine al mio tutor, la Professoressa Isabella Memmi e al mio co-tutor, la dottoressa Giovanna Giorgetti, per avermi introdotto alla geologia marina e alla paleoclimatologia, ma soprattutto per il loro supporto e la loro guida. Vorrei ringraziare anche il Professore Fernando Nieto dell'Università di Granada (Spagna), per avermi ospitato a Granada per effettuare delle analisi mineralogiche e per la discussione dei dati ottenuti. Devo anche la mia gratitudine alla Professoressa Sandra Passchier dell'Università di Montclair State (Stati Uniti d'America) per avermi ospitato all'Università di Montclair State per discutere i dati sui minerali pesanti.

Voglio ringraziare lo staff del Dipartimento di Scienze della Terra dell'Università di Siena, specialmente Claudia "La maga" Magrini, per il suo aiuto nella preparazione dei campioni in laboratorio e Alessandro "Sandro" Berto per il suo aiuto con le analisi XRD, e la Professoressa Cecilia Viti, per l'aiuto che mi ha dato nel superare alcuni problemi di carattere mineralogico. Vorrei ringraziare inoltre i miei colleghi dottorandi Ivan Martini e Alessio Casagli e la Dottoressa Elisabetta Gliozzo per tutti i caffè che mi hanno offerto in questi ultimi mesi ma soprattutto per il loro supporto morale. La mia più calda gratitudine va ai miei genitori, Rocco e Lida, per il loro sostegno. Più di tutti però voglio ringraziare la mia ragazza, *moja mala* Maja, per avermi sopportato ed incoraggiato allo stesso tempo, in generale ed in particolar modo nella stesura di questa tesi di dottorato.

Appendix

N°	Depth (mbsf)	Smectite	Illite	Chlorite	Kaolinite
1	36,88	34	57	6	3
2	68,01	43	45	12	0
3	78,05	29	60	11	0
4	83,50	24	43	34	0
5	88,01	29	48	21	2
6	90,01	26	55	17	2
7	98,00	29	30	42	0
8	114,05	14	37	45	4
9	124,97	49	30	21	0
10	130,05	43	28	29	0
11	135,00	41	39	18	3
12	140,07	28	36	36	0
13	145,00	24	42	33	0
14	150,04	34	44	18	3
15	155,03	34	43	23	0
16	162,00	37	35	28	0
17	167,02	32	32	36	0
18	172,00	50	34	16	0
19	177,02	36	55	9	0
20	181,99	46	31	22	0
21	187,04	27	50	23	0
22	191,98	26	42	32	0
23	197,02	39	44	17	0
24	207,03	28	43	29	0
25	212,00	40	42	18	0
26	216,99	46	36	18	0
27	219,99	50	19	30	0
28	225,00	2	78	19	0
29	230,02	1	79	19	0
30	235,03	2	76	22	0
31	239,98	5	78	17	0
32	245,01	5	72	23	0
33	252,08	3	73	24	0
34	255,00	13	68	20	0
35	260,01	18	69	12	0
36	264,25	3	72	26	0
37	270,01	10	70	17	3
38	275,01	5	77	15	3
39	280,01	2	65	34	0
40	285,04	3	75	22	0
41	289,99	4	75	22	0
42	295,00	8	64	26	3
43	299,50	16	65	19	0
44	305,02	4	84	12	0
45	309,50	7	72	19	3
46	320,00	11	69	20	0
47	325,50	12	70	16	2
48	331,01	14	69	16	2
49	336,00	7	78	15	0

50	340,00	19	70	11	0
51	350,50	7	73	20	0
52	355,00	9	78	13	0
53	359,98	20	64	16	0
54	364,31	15	75	10	0
55	370,00	17	62	21	0
56	375,20	5	79	16	0
57	379,98	13	72	14	2
58	384,96	12	74	14	0
59	388,00	14	70	16	0
60	400,00	15	68	15	2
61	405,01	9	73	15	2
62	409,50	6	84	10	0
63	415,02	3	71	25	0
64	419,99	15	67	15	3
65	425,02	2	66	32	0
66	435,02	11	64	24	0
67	439,52	46	27	27	0
68	445,00	56	26	18	0
69	450,02	16	67	18	0
70	455,00	13	71	16	0
71	459,98	8	73	19	0
72	465,00	14	67	19	0
73	470,00	44	35	22	0
74	475,00	39	38	23	0
75	479,59	32	48	19	0
76	485,00	28	54	18	0
77	490,07	43	42	15	0
78	495,30	85	15	0	0
79	499,98	21	61	17	2
80	505,03	15	69	15	1
81	510,80	4	75	21	0
82	514,98	13	72	15	1
83	520,01	37	51	12	0
84	525,01	17	74	9	0
85	530,68	36	36	27	0
86	535,06	16	60	24	0
87	540,00	3	67	31	0
88	544,97	9	72	18	1
89	554,96	75	16	6	2
90	560,02	100	0	0	0
91	564,99	100	0	0	0
92	570,01	14	66	19	0
93	575,01	12	69	16	3
94	580,04	4	70	26	0
95	585,00	7	72	21	0
96	590,01	5	68	27	0
97	595,02	7	75	15	3
98	600,03	6	73	21	0
99	605,02	9	71	20	0
100	615,01	31	50	19	0
101	618,97	12	62	26	0
102	620,01	68	25	7	0
103	625,01	22	65	12	1

104	630,15	18	67	15	0
105	634,89	18	68	14	0
106	639,99	36	51	11	2
107	644,99	62	18	20	0
108	649,99	5	75	20	1
109	655,45	6	71	23	0
110	660,00	7	75	18	0
111	664,58	5	91	4	0
112	669,98	21	65	13	1
113	674,97	31	56	13	0
114	680,00	32	56	12	0
115	684,54	15	63	22	0
116	690,02	12	74	15	0
117	695,95	4	68	28	0
118	700,00	24	62	14	0
119	705,02	19	64	17	0
120	710,00	22	57	21	0
121	715,00	24	56	21	0
122	719,99	84	11	4	1
123	724,98	11	57	32	0
124	729,80	8	72	20	0
125	735,02	7	75	16	2
126	739,96	8	72	20	0
127	744,96	86	9	4	0
128	749,99	97	0	3	0
129	754,96	17	64	19	0
130	760,01	29	49	22	0
131	765,00	24	53	23	0
132	770,00	28	52	18	2
133	775,00	95	3	2	0
134	779,98	94	0	6	0
135	784,99	87	2	11	0
136	789,00	100	0	0	0
137	794,99	7	68	23	2
138	800,02	92	4	3	0
139	805,00	90	7	2	2
140	810,00	91	6	2	1
141	815,00	97	0	2	1
142	820,02	87	8	3	2
143	825,80	8	57	35	0
144	830,01	35	43	22	0
145	837,00	11	68	21	0
146	849,01	22	59	19	0
147	871,53	55	29	15	0
148	887,57	75	15	10	0
149	897,01	71	19	10	0
150	907,00	33	65	2	0
151	927,28	20	77	3	0
152	937,01	3	79	18	0
153	947,07	5	75	21	0
154	957,05	100	0	0	0
155	967,03	33	46	21	0
156	977,07	87	7	5	0
157	987,13	84	9	8	0

158	996,91	81	12	7	0
159	1007,00	5	72	24	0
160	1027,01	23	66	11	0
161	1033,00	5	69	26	0
162	1043,02	100	0	0	0
163	1063,00	100	0	0	0
164	1073,00	100	0	0	0
165	1083,00	100	0	0	0
166	1093,20	97	0	2	1
167	1103,00	96	2	1	0
168	1113,02	86	9	5	0
169	1123,20	67	23	10	0

Tab.1A. Summary table showing clay mineral percentages of all 169 investigated samples.